

THERMODYNAMIC PHENOMENOLOGY FOR PEROVSKITE
STRUCTURE FERROELECTRIC SOLID SOLUTIONS WITH
MORPHOTROPIC PHASE BOUNDARIES

Period June 1, 2001 to April 30, 2004

FINAL REPORT

Office of Naval Research
Contract No. N00014-01-1-870

L. Eric Cross
Materials Research Laboratory
University Park, PA 16802

DISTRIBUTION STATEMENT A
Approved for Public Release
Distribution Unlimited

20051219 050

REPORT DOCUMENTATION PAGE

Form Approved
OMB No. 0704-0188

The public reporting burden for this collection of information is estimated to average 1 hour per response, including the time for reviewing instructions, searching existing data sources, gathering and maintaining the data needed, and completing and reviewing the collection of information. Send comments regarding this burden estimate or any other aspect of this collection of information, including suggestions for reducing the burden, to Department of Defense, Washington Headquarters Services, Directorate for Information Operations and Reports (0704-0188), 1215 Jefferson Davis Highway, Suite 1204, Arlington, VA 22202-4302. Respondents should be aware that notwithstanding any other provision of law, no person shall be subject to any penalty for failing to comply with a collection of information if it does not display a currently valid OMB control number.

PLEASE DO NOT RETURN YOUR FORM TO THE ABOVE ADDRESS.

1. REPORT DATE (DD-MM-YYYY) Dec 13, 2005		2. REPORT TYPE Written/Final		3. DATES COVERED (From - To) 1 Jun 2001 through 30 Jun 2004	
4. TITLE AND SUBTITLE Thermodynamic Phenomenology for Perovskite Structure Ferroelectric Solid State with Morhpotropic Phase Boundaries				5a. CONTRACT NUMBER N00014-99-1-1011	
				5b. GRANT NUMBER	
				5c. PROGRAM ELEMENT NUMBER	
6. AUTHOR(S) L. Eric Cross 187 Materials Research Laboratory University Park PA 16823				5d. PROJECT NUMBER	
				5e. TASK NUMBER	
				5f. WORK UNIT NUMBER	
7. PERFORMING ORGANIZATION NAME(S) AND ADDRESS(ES) Pennsylvania State University 187 Materials Research Laboratory University Park, PA 16823				8. PERFORMING ORGANIZATION REPORT NUMBER	
9. SPONSORING/MONITORING AGENCY NAME(S) AND ADDRESS(ES) Office of Naval Research 230 South Dearborn, Room 380 Chicago, IL 60604 1595				10. SPONSOR/MONITOR'S ACRONYM(S) Office of Naval Research 800 North Randolph Street Room 648 Arlington, VA 22217-56660	
				11. SPONSOR/MONITOR'S REPORT NUMBER(S)	
12. DISTRIBUTION/AVAILABILITY STATEMENT Approved for Public Release; distribution is Unlimited					
13. SUPPLEMENTARY NOTES					
14. ABSTRACT Topics for study which will be reported include: Lower temperature (down to 12K) studies of the dielectric properties of single crystal lead zinc niobate; lead titanate. Studies of a new two order parameter model for lead zirconate titanate which leads naturally to the occurrence of the lower temperature monoclinic phase interleaving the tetragonal: rhombohedral classical MPB. Application of the flexoelectric measurement technique developed on the ONR US; Japan Global studies program to explore strain gradient drive of ferroelastic domain walls and the development of a new thermodynamic function for BaTiO3 to better describe the high temperature phase transitions evidenced under large epitaxial strains in thin BaTiO3 films on non matching substrates.					
15. SUBJECT TERMS					
16. SECURITY CLASSIFICATION OF:			17. LIMITATION OF ABSTRACT	18. NUMBER OF PAGES	19a. NAME OF RESPONSIBLE PERSON
a. REPORT	b. ABSTRACT	c. THIS PAGE			L. Eric Cross
UU	UU	UU			19b. TELEPHONE NUMBER (Include area code) 814-865-1181

TABLE OF CONTENTS

1.	INTRODUCTION.....	1
2.	TWO ORDER PARAMETER MODEL FOR LEAD ZIRCONATE TITANATE PZT	1
3.	FLEXOELECTRIC STUDIES OF FERROELASTIC: FERROELECTRIC DOMAIN WALL MOTION IN PZT.....	2
4.	STUDIES RELATED TO PZN:PT SINGLE CRYSTALS	3
5.	BARIUM TITANATE PHENOMENOLOGY	4
6.	POLARIZATION SWITCHING IN $\text{Pb}(\text{Yb}_{1/2}\text{Nb}_{1/2})\text{O}_3\text{-PbTiO}_3$ SINGLE CRYSTALS	5
7.	REFERENCES.....	5
8.	GRADUATE STUDENTS	5
9.	HONORS AND AWARDS	5
10.	PAPERS PUBLISHED IN REFEREED JOURNALS	5
11.	INVITED LECTURES	7
12.	PAPERS IN PRESS	10
13.	BOOKS, CHAPTERS PUBLISHED.....	10
14.	BOOKS CHAPTERS IN PRESS.....	10
15.	INVENTION DISCLOSURES.....	10
16.	PATENTS GRANTED	10
17.	PATENTS PENDING.....	10
18.	DEGREES GRANTED.....	10
19.	POST DOCS	11
20.	PERSONNEL.....	11

Thermodynamic Phenomenology for Perovskite Structure Ferroelectric
Solid Solutions with Morphotropic Phase Boundaries

Final Report
Period 06/01/01 – 04/30/04

L. Eric Cross
The Pennsylvania State University
Materials Research Laboratory
University Park, PA 16802
Phone: 814-865-1181 Fax: 814-863-7846
E-mails lec3@psu.edu

Grant Number No. N00014-98-1-0530

ONR Program Officer Wallace A. Smith

Abstract

The report covers the period June 1 2001 to April 30th 2004 on the Office of Naval Research Grant N00014 01-1-870 on the topic "Thermodynamic Phenomenology for Perovskite Structure Ferroelectric Solid Solutions with Morphotropic Phase Boundaries". Topics for study which will be reported include: Lower temperature (down to 12K) studies of the dielectric properties of single crystal lead zinc niobate: lead titanate. Studies of a new two order parameter model for lead zirconate titanate which leads naturally to the occurrence of the lower temperature monoclinic phase interleaving the tetragonal: rhombohedral classical MPB. Application of the flexoelectric measurement technique developed on the ONR US; Japan Global studies program to explore strain gradient drive of ferroelastic domain walls and the development of a new thermodynamic function for BaTiO₃ to better describe the high temperature phase transitions evidenced under large epitaxial strains in thin BaTiO₃ films on non matching substrates.

1. INTRODUCTION

The program on the "Thermodynamic Phenomenology for Perovskite Structure Ferroelectric Solid Solutions with Morphotropic Phase Boundaries" was originally funded under N00014-01-1-870 for the two years 01 June 2001 to 31 May 2003 and to help complete the proposed studies a supplementary period from 01 June 2003 to April 30, 2004 was funded. This final report will cover the whole period, but since much of the earlier work was described in the proposal for supplementary funding, this focus will be upon the completed studies. Following earlier precedent, work already published will be provided as technical appendices from which the important salient features will be discussed in this text.

2. NEW TWO-ORDER PARAMETER MODEL FOR LEAD ZIRCONATE TITANATE (PZT)

The proposed two order parameter thermodynamic function for PZT is discussed in detail in appendices (1, 2, 3). The free energy in this model comprises three sets of terms, two expansions of polarization representing contributions to the total polarization of each end member in the solid solution weighted linearly with respect to composition, plus terms representing the coupling between the two contributors. Employing the coefficients for lead titanate (PbTiO₃) and extrapolated values for a hypothetical lead zirconate (PbZrO₃) taken from the earlier phenomenology of Haun et al (1,2,3,4,5). The function predicts the composition of the Morphotropic ferroelectric tetragonal: rhombohedral phase boundary to lie at 0.55 mole fraction PbZrO₃ independent of the strength of coupling between the two order parameters.

The model also predicts a monoclinic interleaving phase at lower temperature where composition range does depend on the strength of the coupling terms between the order parameters. The model with a suitable choice of coupling gives a good fit to lattice parameters of the Morphotropic $\text{Pb}(\text{Zr}_{0.52}\text{Ti}_{0.48})\text{O}_3$ composition over a wide temperature range. Details are given in the appendices 1, 2, 3.

3. FLEXOELECTRIC STUDIES OF FERROELASTIC: FERROELECTRIC DOMAIN WALL MOTION IN PZT.

During studies of flexoelectric effects in cubic perovskite paraelectrics such as $(\text{Ba}_x\text{Sr}_{1-x})\text{TiO}_3$, (BST) $\text{Pb}(\text{Mg}_{1/3}\text{Nb}_{1/3})\text{TiO}_3$ (PMN) etc., which are in point group $m\bar{3}m$ and cannot show piezoelectricity under uniform elastic stress it was pointed out by Dr. Wenhui Ma that unpoled PZT which is in the Curie group $\infty\infty m$ also cannot show a piezoelectric effect in a uniform stress field so that it could be interesting to explore flexoelectricity i.e. charge separation induced by controlled elastic strain gradient.

Several questions which might be answered by simple transverse gradients of strain which could be generated in a flexing bar of PZT included:

- a. Would the measured values scale with weak field dielectric permittivity as in PMN and BST.
- b. Would the value of the scaling parameter γ be similar to PMN, indicating the importance of the lead chemistry or similar to BST indicating the importance of soft mode behavior as distinct from relaxor ferroelectric response.
- c. Since stress levels could be easily achieved which lead to a remanent curvature of the beam indicating ferroelastic poling of the ferroelastic: ferroelectric domain structure would there be a domain wall contribution to the flexoelectric γ .
- d. Could the higher strain gradient levels lead to a sufficient poling of the ferroelectric component in the domain structure to give a measurable residual piezoelectric response.

Detailed answers to these questions are given in appendices 4 and 5. Briefly: Measured values do scale with permittivity but the scaling factor γ changes with drive

level. Static measurements show a clear onset of domain wall motion in the soft PZT-5H which coincides with a change in elastic stiffness. For low drive levels the scale factor γ is similar to that in PMN not BST showing relation to the chemistry and not the relaxor character. Even for very high static stress levels which clearly evidenced remanent curvature no measurable piezoelectricity was induced.

4. STUDIES RELATED TO PZN:PT SINGLE CRYSTALS

4.1 Orthorhombic Phase Stability

In appendix 6, the question of the orthorhombic phase which can be stabilized in both PZN:PT and PMN:PT single crystals at composition close to the MPB is discussed. It is pointed out that even in the PZT phenomenology the orthorhombic phase comes very close in free energy to the tetragonal and rhombohedral at the MPB composition.

4.2 Dielectric Relaxation in PZN:PT Crystals at Composition 0.955 PZN: 0.45PT

Dielectric studies covering the temperature range from 12 K to 300 K are reported in appendix 7. Two additional dielectric anomalies occurring near 250 K and near 100 K are reported. The lower temperature anomaly has Arrhenius character with $T \sim 10^{11.5}$ and activation energy $E \sim 0.24$ eV, the upper peak is not sensitive to DC bias and appears more intrinsic in character. Unipolar high field studies show that high strain is retaining for the 001 poled crystal into the cryogenic region.

4.3 Dielectric Switching in PZN;PT Crystals

Anisotropy of fatigue behavior between 001 and 111 poled PT:4.5% PZN is striking. In appendix 8 polarization decay after $\frac{1}{2} E_c$ fields was explored in virgin and 10^5 cycled crystals. Relaxation was shown to lengthen markedly in 111 poled crystals but not under 001 poling. It may be noted that in both orientations switching is primarily by domain rotation and not by 180° switching. For 001 poling of the rhombohedral phase this is clearly likely, that is also occurs for 111 poling is clearly evidence by the study described in appendix 9 where the elastic strain associated with reversal clearly indicates that it is not by 180° wall motion.

4.4 Hydrostatic d_n in PZT, PZN:PT and PYN:PT

It has long been realized that ferroelastic ferroelectric domains can not be driven by uniform hydrostatic stress so that for ferroelectric materials where domains can

contribute strongly to direct and converse piezoelectric d_{33} and d_{31} in uniaxial phases, d_n as measured under hydrostatic stress may not be equivalent to $(d_{33} + 2d_{31})$ as measured by resonance methods. It must be remembered also however that in relaxor ferroelectric crystals the nano-polar regions which can persist in both paraelectric and ferroelectric phases do change orientation under electric field and can contribute markedly to dielectric response. It is very clear from these true hydrostatic measurements in Appendix 10 that in all the systems studied there is a discrepancy between d_n and $(d_{33} + 2 d_{31})$. In soft PZT this is most probably a true domains wall contribution. PZN:PT and PYN:PT are however, both embracing relaxor end members. Now there is much more massive disagreement but since nanopolar regions which also will not be driven by hydrostatic stress are strongly associated it is not clear whether this should be classed as an extrinsic effect or not.

5. BARIUM TITANATE PHENOMENOLOGY

To uncover the reason for the disagreement between predicted and observed phase transitions driven by electric field in 111 oriented BaTiO₃ single crystals, it was hoped to make a detailed study of the Fujikura BaTiO₃ crystals used in the 111 high field studies at TIT in Japan. Unfortunately due to personnel changes on the contract this became impossible. It was also clear however, that Bell/Cross free energy function used in the analysis, which was designed primarily to describe dielectric and electric field behavior near the 10° C and -90° C orthorhombic and rhombohedral transitions was becoming unusable at higher temperatures. The need for a modified form is highlighted by recent thin film studies where induced strain associated with epitaxial constraint on a SiTiO₃ substrate is sufficient to raise T_c to more than 950 K. (Appendix 11) To explore this higher temperature region a new energy function embracing up to eighth order terms has been developed (Appendix 12). In spite of the fact that only the second order terms are linearly temperature dependent the function nicely describes the entropy changes at all three ferroelectric transitions and enables prediction of higher temperatures high strain properties. Unfortunately the spread of current values in the measured electrostrictive Q constants still leaves a wide spread in predicted changes of T_c (6) and do clearly highlight the need for more precise measurements which are now well within the capability of modern ultra dilatometers.

6. POLARIZATION SWITCHING IN $\text{Pb}(\text{Yb}_{1/2}\text{Nb}_{1/2})\text{O}_3\text{-PbTiO}_3$ SINGLE CRYSTALS

Evidence of the importance of disorder in the Yb/Nb arrangement in the high temperature grown $\text{Pb}(\text{Yb}_{1/2}\text{Nb}_{1/2})\text{O}_3\text{-PbTiO}_3$ crystals is addressed from the ferroelectric switching behavior discussed in Appendix 13. This important paper highlights the role of random fields and nano-polar direction in the switching process, and the strong role which they play in the single crystal systems which exhibit massive piezoelectric properties.

7. REFERENCES

1. M. J. Huang, E. Furman, S. J. Jang, L. E. Cross, *Ferroelectric,s* 99, 13, 1989
2. M J. Haun, E. Furman, H. A. McKinstry, L. E. Cross, *Ferroelectrics*, 99, 27, 1989.
3. M. J. Haun, Q. Zhuang, E. Furman, S. J. Jang, L.E. Cross, *Ferroelectrics*, 99, 45, 1989
4. M. J. Haun, E. Furman, T. R. Halemane, L. E Cross, *Ferroelectrics*, 99, 55, 1989.
5. M. J. Haun, E. Furman, S. J. Jing, L. E. Cross, *Ferroelectrics*, 99, 63, 1989
6. K. J. Choi, M. Biegalski, Y. L. Li, A. slharan, J Schubert, R. Vecker, R. Reiche, Y. B. Chen, X. Q. Pan, V. Gopalau, L-Q Chen, D. G. Schlom, E. B. Eom, *Science*, 306, 1005, 2004

8. GRAD STUDENTS

None

9. HONORS AND AWARDS

- L. Eric Cross, American Ceramic Society, Honorary Life Member 2001
- L. Eric Cross IEEE Honorary Life Member 2001
- L. Eric Cross, ISI Highly Cited Researcher 2003

10. PAPER PUBLISHED in REFEREED JOURNALS

1. Ma, Wenwui, L. Eric Cross, "Observation of the flexoelectric effect in relaxor $\text{Pb}(\text{Mg}_{1/3}\text{Nb}_{2/3})\text{O}_3$ ceramics", *Applied Physics Letters*, 78 No 19, 2920-2921, (7 May 2001).

2. Viehland, D., J. Powers, L. E. Cross, J. F. Li, "Importance of random fields on the properties and ferroelectric phase stability of <001> oriented 0.7 Pb(Mg_{1/3}Nb_{2/3})O₃-0.3 PbTiO₃ crystals", Applied Physics Letters, **78**, No **22**, 3508-3511, (May 2001).
3. Cross, L. Eric, Petr Hana, "Phenomenology of the Elasto-Dielectric Response in the Field Forced Ferroelectric Phases of Lead Zinc Niobate: Lead Titanate (PZN:PT) Relaxor Ferroelectrics"
4. Newnham, Robert, Eric Cross, "Symmetry and Antisymmetry in Electroceramics", The Art of Ceramics, The Blend of Art and Science in Technology, 205-204, (2001).
5. Fousek, J, L. E. Cross, "Engineering Multidomain Ferroic Samples", Ferroelectrics, **252**, pp. 171-180, (2001).
6. Satoshi Wada, Hirofumi Kakemoto and Takaaki Tsurumi, Seng-Eek Park*, L. Eric Cross*, and Thomas Shrout*, "Enhanced Ferroelectric Related Behaviors of Ferroelectric Single Crystals Using the Domain Engineering", Transactions of the Materials Research Society of Japan, **27** [1] 282-286 (2002)
7. Yu Zhi, Ang Chen, E. Furman, L. E. Cross, "Dielectric relaxation and strain behavior of 95.5% Pb(Zn_{1/3}Nb_{2/3})O₃-4.5% PbTiO₃ single crystals at cryogenic temperatures", Applied Physics Letters, **82** No. 5, 790-793, 3 February 2003
8. Wenhui Ma, L. Eric Cross, "Strain-gradient induced electric polarization in lead zirconate titanate ceramics", Applied Physics Letters, **82** No. 19 3293-3295, May 2003
9. J. Fousek, L. E. Cross, "Open Issues in Application Aspects of Domains in Ferroic Materials", Ferroelectrics, Vol 290, 43-60, 2003
10. L. Eric Cross, Wenyi Zhu, "Direct evidence of ferroelastic participation in 180° polarization switching and fatigue for 111 oriented rhombohedral ferroelectric 0.955 Pb(Zn_{1/3} Nb_{2/3})O₃:0.045 PbTiO₃ single crystals, Applied Physics Letters, **84**, No. 13, 29 March 2004.
11. A. Amin, L.E. Cross, "Intermediate states in Pb(B_{1/3}^I B_{2/3}^{II})O₃-PbTiO₃ ferroelectric single crystals" British Ceramic Transactions, **103** No. 2 , 89-91, 2004,

12. Wenhui Ma, L. Eric Cross, "Flexoelectric effect in ceramic lead zirconate titanate" Applied Physics Letters **86**, 072905, 2005
13. Y.L. Li, L.E. Cross, L.Q. Chen, "A phenomenological thermodynamic potential for BaTiO₃ single crystals" Journ of Appl. Physics **98**, 06401 (2005)

11. INVITED LECTURES

2001

1. L.E. Cross, E. Furman, and P. Hana, "Stability of Lower Symmetry Ferroelectric Phases in Perovskite Structure Solid Solutions", International Meeting on Ferroelectrics IMF-10, Madrid, Spain, September 3, 2001
2. L.E. Cross, Wenhui Ma, "Progress in Flexoelectric Measurements" 10th US Japan Seminar on Dielectric and Piezoelectric ceramics Providence Ceramics Providence Rhode Island, USA, September 26, 2004
3. L. E. Cross "Reflections on 50 years of Ferroelectricity People Places and Phenomena" International Conference on Adaptive Structures and Technologies ICAST 12 University of Maryland, Oct 15-17, 2001
4. L. Eric Cross, "Diverse Behaviors in Relaxor Ferroelectric Materials", Materials Research Society Fall Meeting, Boston, November 27, 2001

2002

1. L. E. Cross, Wenhui Ma, "Mechanisms for high strain in electroactive actuator materials" POLECER Mtg. Piezoelectrics for the End user Interlaken Switzerland 24th Feb, 2002
2. L. E. Cross, "Enhancing Strain Capability and Energy Density in Current and Potential Future Actuator Materials", 9th SPIE meeting on Smart Structures and Materials 17th March, 2002, San Diego, CA
3. L. E. Cross, "An overview of Multiferroic Materials and Dynamics", Am Phy Soc. (APS) March Meeting Indianapolis IN, March 18th, 2002.
4. L. E. Cross, "Complimentary and Conflicting requirements in Perovskite Structure High Strain Piezoelectrics between Single Crystal and Polycrystal Ceramic Systems", Am. Ceram Soc 104th Annual Meeting, St. Louis, MO, April 28th, 2002.

5. L. E. Cross, "Progress in Studies on the Flexoelectric Effect", US Navy Workshop on Acoustic Transduction Materials and devices, Harbor Place Baltimore, 14th May 2002.
6. L. E. Cross, Susan-Troiler-McKinstry, "Tutorial on the Fundamental of Ferroelectricity", International Joint Conference on Applications of Ferroelectrics IFFF 2002, Nara Japan, May 28th 2002.
7. L. E. Cross, "Composites Approaches in High Strain Electro-Active Actuator and Transducer Composites", IUMRS-ICEM Xian China, June 10, 2002.
8. L. E. Cross, "Composite Approaches in High Strain Electro Active Actuator Materials", ICCE/9 San Diego, CA, July 1-6, 2002
9. L. E. Cross, Pan American Advanced Study Institute on Science and Technology of Ferroelectric Materials: Rosario Argentina, September 2002.
 - a. Brief History of Ferroelectrics
 - b. Fundamentals of Piezoelectrics
 - c. Relaxor Ferroelectrics and Phase Change Materials Research Institute
10. L. E. Cross, "Recent Progress in High Strain Active Actuator Materials", 13th ICAST October 7th, Potsdam/Berlin Germany, 2002
11. L. E. Cross, "Recent Progress in Ferroic High Strain Actuators Materials" Optatech 2002, October 28th, Brugge Belgium.
12. L. E. Cross, "Diverse Behavior in Relaxor Ferroelectric Materials", Jinrong Cheng, "High Temperature Dielectric Properties of Sol-Gel Derived Thick PZT thin films with different Zr/Ti ratios" MRS Fall meeting Boston, MA, November 27, 2002.
13. L. E. Cross, "Ferroic High Strain Actuators: Common Mechanisms in Diverse Material Systems", World Congress on Biometrics and Artificial Muscles, Albuquerque, N.M. Dec 9th, 2002.

2003

1. L.E. Cross, "Thermodynamic Phenomenology for Perovskite Structure ferroelectrics with Morphotropic Phase Boundaries" Fundamental Physics of Ferroelectrics, ONR Williamsburg, Feb 2, 2003.

2. L. E. Cross, "Recent Advances in High Strain Actuator Materials Based on Organic Polymers and Inorganic Oxides", Dept of Physics/Chemistry Seminar, University of Akron, February 20, 2003
3. L. E. Cross, "High Strain Piezoelectric Actuators", American Ceramic Society Annual Meeting, Nashville, TN, April 27, 2003
4. L. E. Cross, "Strain Gradient induced Electric Polarization in Lead Zirconate Titanate Ceramics", US Navy Workshop on Transducer Materials and Devices, State College, PA, 6th May, 2003.
5. L. E. Cross, "Flexoelectric Polarization in the Ferroelectric Phase of PZT-5H Ceramic", 11th US:Japan Seminar on Dielectric and Piezoelectric Ceramics, Sapporo Japan, Sept 9th, 2003.
6. L. E. Cross, "Domain and Phase Composites in Single Crystal Ferroelectric Actuators", Composites at Lake Louise, Oct 19, 2003, Lake Louise, Canada
7. L. E. Cross, "Recent Progress in Transducers and Actuators for Smart Materials", Materials Research Society Meeting Boston, November 27, 2003
8. L. E. Cross, "Progress Prospects and Problems in Advanced Materials for Dielectric Piezoelectric and Electro-optic Applications", 2nd International Conference on Materials for Advanced Technologies ICMAT and IUMRS, International Conference in Asia, 29th November Singapore (Keynote Address), 2003
9. L. E. Cross, "Progress in Actuators and Sensors for Smart Structures AMF-4 Bangalore, India, December 12, 2003, (Plenary 1 Address)

2004

1. Jinrong Cheng, L. Eric Cross, "Bismuth Based Perovskite Structure Solid Solution with Morphotropic Phase Boundaries for Piezoelectric Applications", 106th Annual Mtg American Ceramic Society, Indianapolis, Indiana, 18-21, 2004
2. L. Eric Cross, "Ferroelectric Composites: The Flagship for many following Ferroelectric Device Structure", Franklin Institute Awards Week Program, Drexel University, Philadelphia, April 28, 2004

3. A. Amin, L. Eric Cross, "Stress induced Orthorhombic Symmetry in High Coupling Crystals", 2004 US Navy Workshop on Acoustic Transduction Materials and Devices, State College, PA May 11-13 2004
4. W. Zhu, L. Eric Cross, "Direct Evidence of Ferroelastic Participation in 180° Polarization and Fatigue for 111 Oriented Rhombohedral Ferroelectric 0.955 Pb(Zn_{1/3}Nb_{2/3})O₃:0.045PbTiO₃ Single Crystals" 2004 Navy Workshop on Acoustic Transduction Materials and Devices State College PA, May 11-13, 2004
5. L. Eric Cross, "Progress in Studies of the Flexoelectric Effect", ONR Workshop on Future Directions in Materials for Electromechanical Transducers, Washington, D.C., July 12-13, 2004.
6. L. Eric Cross, Wenhui Ma, Wenyi Zhu, "Strain Gradient Induced Electric Polarization in Paraelectric Ferroelectric and Relaxor Ferroelectrics", 7th European Conference on Polar Dielectrics ECAP7, Sept 6-9, 2004 Liberec, Czech Republic.
7. L. Eric Cross, "Recent Progress in Transducers Actuators and Sensors for Smart Systems" MRS Fall Meeting, Symposium D, Boston Nov 30, 2004
8. L. Eric Cross, "Recent Progress in Transduction Materials for Sensing and Actuation", World Congress on Biomimetics Artificial muscles and nano-Bio 2004", Dec 6-8, 2004 Albuquerque, NM

12. PAPERS IN PRESS

None

13. BOOKS, CHAPTERS PUBLISHED

None

14. BOOKS CHAPTERS in PRESS

None

15. INVENTION DISCLOSURES

None

16. PATENTS GRANTED

None

17. PATENTS PENDING

None

18. DEGREES GRANTED

None

19. POST DOCS,

Dr. Ang Chen

Dr. Yi Zhu

Dr. Jinrong Cheng

21. PERSONNEL

Eric Cross, Evan Pugh Professor Emeritus of Electrical Engineering

Dr. Eugene Furman

Paul Moses Technical Assistant

Dee Baumgardner Staff Assistant

Wenyi Zhu, Research Assistant

Nan Li, Research Assistant

APPENDIX 1

A Two-Parameter Thermodynamic Model for PZT

ANDREW J. BELL¹ and EUGENE FURMAN²

¹*Institute of Materials Research, University of Leeds, UK*

²*Materials Research Institute, The Pennsylvania State University, USA*

(Received September 4, 2002; In final form December 15, 2002)

A two-parameter thermodynamic model is proposed for the ferroelectric solid solution system $\text{Pb}(\text{Zr}_{1-x}\text{Ti}_x)\text{O}_3$. The free energy comprises three sets of terms: two expansions of polarization, one representing each of the end-members, weighted linearly with respect to composition, and terms representing the coupling between the two polarization contributions. Employing previously published coefficients for PbTiO_3 and values extrapolated from Zr-rich PZT compositions for PbZrO_3 , calculations predict the morphotropic phase boundary lies at $x = 0.45$ and is independent of the strength of coupling between the two order parameters. A monoclinic phase is predicted, the range of existence of which depends upon the strength of the parameter coupling, but in general, is broadest at low temperature. It is proposed that the two contributions to the polarization have their origins in the two types of cation shifts identified in PZT: the major, homogenous shifts parallel to the polar direction and randomly-oriented, or heterogeneous, minor shifts away from the polar axis. The field-induced ordering of the minor shifts is identified as the origin of the large intrinsic piezoelectric coefficient in PZT.

Keywords: Thermodynamic model; PZT

INTRODUCTION

Lead zirconate-titanate, $\text{Pb}(\text{Zr}_{1-x}\text{Ti}_x)\text{O}_3$ or PZT [1], has been widely studied due to the outstanding piezoelectric properties of compositions close to $x = 0.5$. The peak in the piezoelectric coefficient for these compositions has often been associated with the presence, at $x = 0.48$, of a morphotropic phase boundary between the zirconium-rich rhombohedral perovskite and the titanium-rich tetragonal perovskite phases. Haun [2–6] successfully modelled the PZT phase diagram, as it had been known for 30 years, using the thermodynamic approach of Devonshire [7], in which the free energy associated with the polar order parameter is expressed in terms of a power series of the pseudo-cubic components of the polarization. A sufficiently accurate fit to experimental data has usually been achieved with expressions expanded up to the 6th power of polarization.

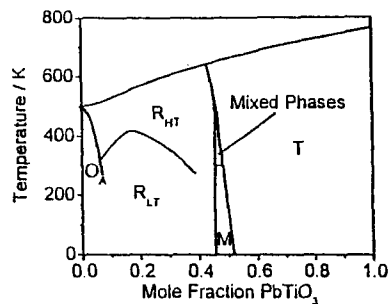


Figure 1. Revised phase diagram of PZT, by combining those of Jaffe [1] and Noheda [8].

The recent discovery of a monoclinic phase at the morphotropic phase boundary in PZT [8] (Fig. 1) and the confirmation that other systems with morphotropic phase boundaries that exhibit very large piezoelectric effects [9] also exhibit other phases close to the phase boundary [10, 11], has led to renewed interest in how best to represent ferroelectrics with morphotropic phase boundaries in the context of the Landau-Devonshire model. The monoclinic phase in PZT was the first known phase in a ferroelectric perovskite in which the non-zero components of the polarization with respect to the cubic axes are not equal under conditions of zero applied field and stress. Such phases are not solutions of the conventional 6th power Devonshire model, however Vanderbilt [12] has shown that the inclusion of 8th power terms in the perovskite free energy expansion can lead to the possibility of monoclinic phases, whilst the inclusion of 12th power terms allows triclinic solutions. The suggestion is that due to the implicit disorder in solid solutions such as PZT, the 8th order terms may assume a greater importance than in single component perovskite ferroelectrics. However, the 8th power equations do not explicitly address the disordered nature.

In such treatments, the composition dependence of the free energy coefficients is not implicit in the model, the locus of the morphotropic phase boundary therefore being an input to, rather than output from, the exercise. Neither are the mesoscopic features of solid solutions represented, an example being the local cation displacements in PZT. It would appear that the "local symmetry" of the lead cation is monoclinic in both the rhombohedral and tetragonal phases. For the rhombohedral phase, it has been proposed that the displacement of the Pb cations from their cubic position comprises a homogeneous [111] displacement superimposed with minor, random (001) shifts [13]. In the tetragonal phase, the homogeneous [001] displacements

are augmented with minor $\langle 110 \rangle$ (or equivalent $\langle 111 \rangle$) random shifts [14]. In both cases, the random shifts average to zero so that the macroscopic symmetries remain rhombohedral and tetragonal respectively. The random Pb displacements might be considered as either static shifts or dynamic fluctuations about the homogeneous displacement. It is not known whether they are distributed totally randomly, or whether their directions are partially correlated in clusters and whether their magnitudes are equal on all sites. Nevertheless, it seems clear that the influence of PbTiO_3 exists well into the rhombohedral phase field and that of PbZrO_3 into the tetragonal phase. Moreover, in general, the Ti and Zr ions do not have equal displacements in either phase [13, 14].

The minor displacements can be assumed to be of some significance in the appearance of the monoclinic phase. For example, it might be postulated that the transition from the tetragonal to monoclinic phase in PZT occurs due to the condensation of the random $\langle 111 \rangle / \langle 110 \rangle$ displacements, which combined with the homogeneous $[001]$ shifts give rise to a macroscopic monoclinic symmetry. As the Pb cation shifts are often cited as being the main component of dipole moment in Pb perovskite ferroelectrics, it may be possible to construct thermodynamic expressions to reflect this postulate, in which both the homogeneous and random contributions to the polarization are represented, or in which the symmetry of the two end members is allowed to influence the stable state well inside the solid solution.

Investigations of the composition dependence of the optical phonon frequencies in $\text{PbZr}_{1-x}\text{Ti}_x\text{O}_3$ tend to support the concept of their being two contributions to the polarization in the solid solution. Infra-red measurements by Sivasubramanian [15], on the tetragonal side of the phase diagram $0.475 < x < 1$, show that the $E(\text{1TO})$ mode softens with increasing Zr concentration. In PbTiO_3 , this mode corresponds to the motion of the Ti ion against the oxygen octahedra and has been identified as the soft mode responsible for the ferroelectric transition [16]. Its decrease in frequency with increasing Zr concentration suggests that the transition from the tetragonal to the rhombohedral (or monoclinic) phase is also driven by an instability in this mode. However, Raman measurements [17] on a similar set of compositions at low temperatures (4.2 to 300 K) reveal that for $x < 1$ there is a splitting of the three lowest $E(\text{TO})$ modes, not observed in PbTiO_3 . The frequency difference due to the splitting increases with increasing Zr concentration and, in the case of the $E(\text{1TO})$ mode, both branches decrease in frequency with increasing Zr concentration towards the phase boundary region. The experimental data appear to indicate that the splitting is present at least up to room temperature and that both branches soften with increasing Zr content,

but there is no data above room temperature to show whether both branches soften through T_c . The more recent Raman study by Lima [18] at 7 K concentrates less on the lowest frequency mode due to problems of resolving the spectra, but shows how the higher modes vary in frequency as the morphotropic region is traversed. Although a full experimental survey has yet to be completed, the implication is that the splitting of the low-lying TO modes may contribute to the polarization in a less than straightforward manner.

Here a thermodynamic model is presented in which the free energy of PZT is expressed as an expansion in terms of two polarization contributions, representing the different influences of the two end members of the solution series. It is based upon a linear combination of the free energy expansions of the end-members of the solid solution, together with linear and quadratic coupling terms. The total polarization is a function of the two end member contributions and the composition variable.

THEORY

In general, the free energy, ΔG , of an infinite, homogeneous, single domain ferroelectric with a cubic prototype structure, as in the perovskites, is given as an expansion of the orthogonal components of the polarization \mathbf{P} in which only the coefficient α_{200} is necessarily temperature dependent, with the form $\alpha_{200} = \alpha'_{200}(T - T_0)$:

$$\begin{aligned} \Delta G(\alpha_{mnp}, \mathbf{P}) = & \alpha_{200}(P_1^2 + P_2^2 + P_3^2) + \alpha_{400}(P_1^4 + P_2^4 + P_3^4) \\ & + \alpha_{220}(P_1^2 P_2^2 + P_2^2 P_3^2 + P_3^2 P_1^2) + \alpha_{600}(P_1^6 + P_2^6 + P_3^6) \\ & + \alpha_{420}[P_1^4(P_2^2 + P_3^2) + P_2^4(P_3^2 + P_1^2) + P_3^4(P_1^2 + P_2^2)] \\ & + \alpha_{222}P_1^2 P_2^2 P_3^2 \dots \dots \dots - E_1 P_1 - E_2 P_2 - E_3 P_3, \quad (1) \end{aligned}$$

where \mathbf{E} is the applied electric field. Expansions terminated at the 6th power of polarization have generally been found sufficient to provide an accurate description of most ferroelectric perovskite systems. However, to encapsulate the features of solid solutions discussed above, a solid solution energy function is proposed of the form:

$$\Delta G_{ss}(x) = xG_{PT}(\alpha_{mnp}, \mathbf{p}) + (1 - x)G_{PZ}(\beta_{mnp}, \mathbf{q}) + G_C(\gamma_{mnp}, \mathbf{p}, \mathbf{q}) \quad (2)$$

where x is the mole fraction of PbTiO_3 . The vectors \mathbf{p} and \mathbf{q} represent the contribution to the polarization from the two end-members, PbTiO_3

and PbZrO_3 , respectively. The forms of $G_{\text{PT}}(\alpha_{\text{mnp}}, \mathbf{p})$ and $G_{\text{PZ}}(\beta_{\text{mnp}}, \mathbf{q})$ are identical to that of Eq. 1, hence the symmetry requirements of the cubic prototype are maintained. The sets of coefficients, α_{mnp} and β_{mnp} , are those of the end members of the solid solution, in which only T_0 is a function of composition and is common to both sets, in the form:

$$T_0(x) = x(T_{\text{PT}} - T_{\text{PZ}}) + T_{\text{PZ}} \quad (3)$$

where T_{PT} and T_{PZ} represent the Curie temperatures of PbTiO_3 and PbZrO_3 respectively.

The coupling energy, for terms up to the 4th power of polarization, is of the form:

$$G_{\text{C}}(\gamma_{\text{mnp}}, \mathbf{p}, \mathbf{q}) = \gamma_{100}(p_1q_1 + p_2q_2 + p_3q_3) + \gamma_{200}(p_1^2q_1^2 + p_2^2q_2^2 + p_3^2q_3^2) \\ + \gamma_{220}(p_1^2(q_2^2 + q_3^2) + p_2^2(q_3^2 + q_1^2) + p_3^2(q_1^2 + q_2^2)) \quad (4)$$

Terms in p_iq_j , where $i \neq j$, are disallowed by symmetry, as the free energy should be independent of the sign of p_iq_j . However, terms in p_iq_i are necessary to differentiate between the parallel and anti-parallel states of p_i and q_i . Table I lists the non-degenerate states resulting from combination of the components of \mathbf{p} and \mathbf{q} , using the notation of Vanderbilt [12] for the resulting phases. Due to the coupling energy G_{C} , the components of \mathbf{p} and \mathbf{q} are

TABLE I Classification of phases for non-degenerate combinations of p_i and q_i . Only components constrained to be zero are shown as such. If p_i and q_i are both shown as non-zero, either, but not both, may assume a zero value

p_1	p_2	p_3	q_1	q_2	q_3	Phase
0	0	0	0	0	0	Cubic - C
0	0	p_3	0	0	q_3	Tetragonal - T
0	p_3	p_3	0	q_3	q_3	Orthorhombic - O
p_3	p_3	p_3	q_3	q_3	q_3	Rhombohedral - R
p_1	p_1	p_3	q_1	q_1	q_3	Monoclinic - M_A
p_1	p_1	$-p_3$	q_1	q_1	q_3	Monoclinic - M_B
p_1	p_3	$-p_3$	q_1	q_3	q_3	Triclinic - Tr
p_1	$-p_3$	$-p_3$	q_1	q_3	q_3	Monoclinic - M_A
0	p_2	p_3	0	q_2	q_3	Monoclinic - M_C
0	p_2	$-p_3$	0	q_2	q_3	Monoclinic - M_C
p_1	p_2	p_3	q_1	q_2	q_3	Triclinic - Tr
p_1	p_2	$-p_3$	q_1	q_2	q_3	Triclinic - Tr

not constrained to the 6th power solutions of the end-member contributions. For directions in which the component of the total polarization, P_i , is not constrained by symmetry to be zero, either of the contributions, p_i or q_i , is allowed to be zero as long as $p_i + q_i \neq 0$. It should be noted that all of the phases identified by Vanderbilt [12] for the conventional 12th power Devonshire model are possible solutions of the current approach, including three non-degenerate triclinic phases.

For comparison with quantitative available data, it is necessary to evaluate the total polarization \mathbf{P} , which is a function of \mathbf{p} and \mathbf{q} . For this purpose, it is assumed here that the relationship is of the simple form:

$$\mathbf{P} = k_p(x) \mathbf{p} + k_q(x) \mathbf{q}. \quad (5)$$

Two possible assumptions are (i) $k_p = k_q = 1$ or (ii) $k_p = x$ and $k_q = 1 - x$. The first assumption implies that \mathbf{p} and \mathbf{q} are assigned homogeneously across all unit cells, independent of B-site occupation, i.e. the dipole moment of all unit cells is equal. However, it is clear from the structure data of Corker [13] and Frantti [14] that this is unlikely, as the Zr and Ti displacements are often different within a single composition. Assumption (ii) implies that \mathbf{p} and \mathbf{q} are distributed according to the B-site occupancy of the unit cell. This would mean that in the example addressed below, the dipole associated with, say, Zr cells in the tetragonal phase, would be zero. This is also not supported by the structure data [13, 14]. Hence, the evaluation of k_p and k_q must at present be undertaken by comparison with experimental data.

CALCULATIONS FOR PZT

The model presented here is aimed at the correct prediction of the morphotropic phase boundary and the appearance of perovskite ferroelectric states with non-equal polarization components i.e. monoclinic and triclinic phases. Hence, the orthorhombic antiferroelectric phase in PZT is ignored, and for the purpose of these calculations, lead zirconate is assumed to be a rhombohedral ferroelectric. Similarly, the octahedral tilt transition, which differentiates the high and low temperature rhombohedral phases of PZT, is not addressed here.

Calculations of the temperature and composition dependence of \mathbf{p} and \mathbf{q} and hence the phase boundaries were carried out using the above model for zero applied field. Choosing the A end-member in Eq. 2 to be PbTiO_3 , the solution for $x = 1$ should yield, for $T < T_A$, $p_1 = 0$, $p_2 = 0$, $p_3 \neq 0$, $\mathbf{q} = 0$, i.e. a tetragonal ferroelectric, whereas $x = 0$ should yield solutions for a

TABLE II Free energy coefficients for PbTiO_3 (α_{mnp}) and hypothetically ferroelectric PbZrO_3 (β_{mnp})

mnp	α_{mnp}	β_{mnp}
200	$3.74 \times 10^5 (T - T_0)$	$2.82 \times 10^5 (T - T_0)$
400	-7.9×10^7	5.12×10^8
220	7.5×10^8	-6.5×10^8
600	2.61×10^8	5.93×10^8
420	6.3×10^8	2×10^9
222	-3.66×10^9	-9.5×10^9

rhombohedral ferroelectric, i.e. for $T < T_B$, $\mathbf{p} = 0$, $q_1 = q_2 = q_3 \neq 0$. The α_{mnp} coefficients for PbTiO_3 used for these calculations are those given by Haun [4] and are shown in Table II. The β_{mnp} coefficients for a hypothetically ferroelectric PbZrO_3 have been estimated by extrapolating the Haun coefficients for compositions with $x > 0$ back to $x = 0$. In some cases, notably β_{200} and β_{400} , the extrapolated value is identical to that of the original Haun coefficient, whereas the remaining coefficients tend to a linear dependence on x except close to $x = 0$ and $x = 0.5$.

The calculations were carried out by numerical minimization of $\Delta G_{ss}(x)$ with respect to \mathbf{p} and \mathbf{q} using the **FindMinimum** function of *Mathematica* 4.0. Only positive values of p_i and q_i were considered, hence in this context the γ_{100} term is redundant and for simplicity its value was set to zero, leaving only γ_{200} and γ_{220} as the unknown parameters.

The problems of identifying the absolute free energy minimum in six dimensional polarization space are not trivial, hence solutions were sought which corresponded to the most likely phases in Table I. For each temperature and PbTiO_3 molar fraction, the local minima in $\Delta G_{ss}(x)$ were systematically identified for $p_i > 0$ and $q_i > 0$, with the constraints shown in Table I, for the cubic, tetragonal, orthorhombic, rhombohedral, monoclinic M_A and monoclinic M_C phases. The energies of the minima were then compared to define the stable state.

The strain matrix, σ , is calculated according to:

$$\sigma_{ij} = Q_{ijkl} P_k P_l \quad (6)$$

For reasons of symmetry, there are only three independent components of the electrostriction coefficient tensor \mathbf{Q} , which in reduced notation are Q_{11} , Q_{12} and Q_{44} . Their values as a function of x were derived by linear interpolation from those of the end-members, published by Haun [4].

Calculation of the angular dependence of the piezoelectric coefficient, which is of relevance to understanding the properties of polycrystalline bodies, has been carried out using the current model. The electric field, \mathbf{E} , is applied at angle θ to the [001] axis and ϕ to the [100] axis in the (001) plane. The components of the field parallel to the three principle axes may then be calculated and included in the free energy (Equation 2) as terms in $E_i p_i$ and $E_i q_i$. The values of $\mathbf{p}(\mathbf{E})$ and $\mathbf{q}(\mathbf{E})$ under applied field can thus be found, as may the strain components, σ_{ij} (Equation 6), with the assumption that $\mathbf{P}(\mathbf{E}) = k_p \mathbf{p}(\mathbf{E}) + k_q \mathbf{q}(\mathbf{E})$. Transformation of the strain tensor to calculate the strain parallel to the applied field, $\sigma_{\theta\phi}$, is accomplished via:

$$\sigma_{\theta\phi} = \sigma_3 \cos^2 \theta - \cos \theta \sin \theta (\sigma_6 \cos \phi + \sigma_5 \sin \phi) + \sin^2 \theta (\sigma_1 \cos^2 \phi + \sigma_4 \cos \phi \sin \phi + \sigma_2 \sin^2 \phi), \quad (7)$$

from which the piezoelectric coefficient can be calculated from the difference between the zero-field and field-induced strains.

RESULTS AND DISCUSSION

The stabilities of the phases were determined as a function of γ_{200} and γ_{220} . In the examples discussed, only stable phases corresponding to cubic, tetragonal, rhombohedral and monoclinic M_A were found. Phase diagrams as a function of x and T are shown for various combinations of γ_{200} and γ_{220} in Figs. 2, 3, and 4.

For $\gamma_{200} = \gamma_{220} \leq 0$, there is only a single phase boundary at $T_0(x)$, between cubic and monoclinic M_A , for all PbTiO_3 concentrations except the

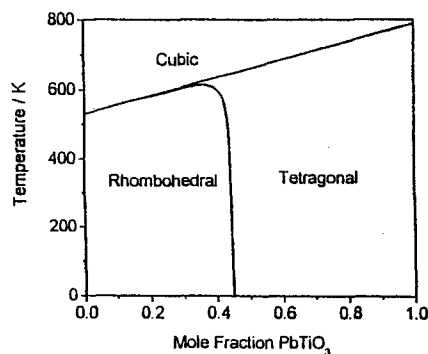


Figure 2. Phase diagram for $\gamma_{200} = \gamma_{220} \rightarrow \infty$.

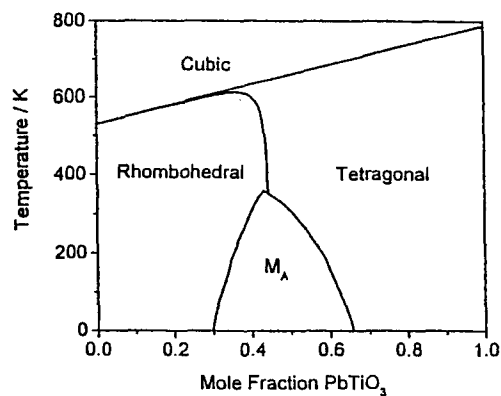


Figure 3. Phase diagram for $\gamma_{200} = \gamma_{220} = 10^8$.

end-members. For non-zero values, γ_{200} and γ_{220} must exceed a threshold value to avoid discontinuities as $x \rightarrow 0$ and $x \rightarrow 1$.

When both γ_{200} and γ_{220} exceed 2×10^8 the appearance of the monoclinic phase is completely inhibited see (Fig. 2). The locus of the morphotropic boundary is independent of γ_{200} and γ_{220} and, well below T_0 , it is also almost independent of temperature, moving to slightly higher values of x with decreasing temperature, and extrapolating to $x = 0.45$ at 0 K. On approaching T_0 , the boundary curves sharply towards lower values of x ; the point at which the morphotropic phase boundary finally coincides with the cubic phase boundary is at $x = 0$. Hence a cubic-tetragonal transition occurs on cooling

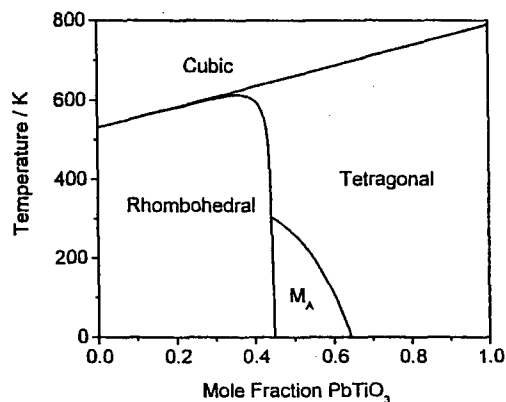


Figure 4. Phase diagram for $\gamma_{200} = 6 \times 10^8$, $\gamma_{220} = 10^8$.

for all compositions with $x > 0$, however for compositions up to $x = 0.35$ the tetragonal phase is only stable for up to 5 K below T_0 , before transforming to the rhombohedral phase. The paraelectric-ferroelectric phase transition is 1st order for all values of x .

For intermediate values of the coupling coefficients, the M_A phase appears in the centre of the phase diagram. On increasing the γ values from zero, there is an almost symmetrical reduction in the width of the monoclinic phase field, yielding to the rhombohedral phase at low x and the tetragonal phase at high x values. There is also a reduction in the maximum temperature of monoclinic stability which occurs close to $x = 0.5$. Thus as the coupling energy is increased, the morphotropic phase boundary between the rhombohedral and tetragonal phases is revealed, with the M_A phase appearing as a wedge, with its apex close to the morphotropic phase boundary. The example shown in Fig. 3 is for $\gamma_{200} = \gamma_{220} = 10^8$, whilst that of Fig. 4 is for $\gamma_{200} = 6 \times 10^8$ and $\gamma_{220} = 10^8$, where the inequality in the coupling coefficients results in the monoclinic phase favouring the "tetragonal" side of the morphotropic phase boundary.

In the absence of any reliable measurements of polarization on single crystals of PZT, the values of k_p and k_q may be estimated by comparison of the values of p_1 and q_1 calculated here with the values of P_1 calculated from the Haun model, which are thought to be an accurate representation of the single crystal polarization. Figure 5 shows the ratio of P_3 from the Haun model to $p_3 + q_3$ from the two-parameter model as a function of composition, both calculated at 300 K. Only points in the rhombohedral and tetragonal fields

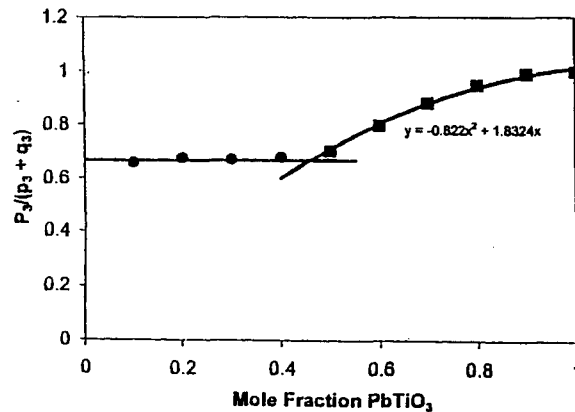


Figure 5. Ratio of the polarization along [001] from the Haun model to that calculated from the current model.

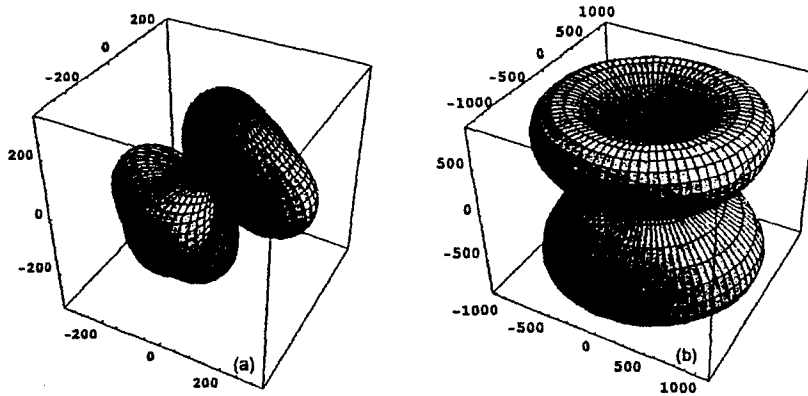


Figure 6. Calculated piezoelectric coefficient as a function of the applied field at 250 K in units of pm V^{-1} for (a) $\text{Pb}(\text{Zr}_{0.6}\text{Ti}_{0.4})\text{O}_3$ and (b) $\text{Pb}(\text{Zr}_{0.4}\text{Ti}_{0.6})\text{O}_3$; the [001] axis is vertical.

were considered so that p_3 and q_3 were never simultaneously non-zero. In the rhombohedral phase, the ratio $P_3/q_3 (= k_q)$ is seen to be constant with a value of 0.67. In the tetragonal phase the ratio $P_3/p_3 (= k_p)$ falls from a maximum of 1 at $x = 1$ to a value of approximately 0.7 at $x = 0.5$. The trend line is quadratic with $k_p = -0.822x^2 + 1.8324x$ and coincides with the value 0.67 at $x = 0.46$, which might be interpreted as the phase boundary composition.

Examples of the angular dependence of the piezoelectric coefficient for $\text{Pb}(\text{Zr}_{0.4}\text{Ti}_{0.6})\text{O}_3$ and $\text{Pb}(\text{Zr}_{0.6}\text{Ti}_{0.4})\text{O}_3$ are shown in Fig. 6 and are similar to those calculated by Du et al. [16] from the Haun model. It is possible to determine which of the two parameters, \mathbf{p} and \mathbf{q} , contributes most to the piezoelectric coefficient as their contributions to the induced strain can be examined separately. In general terms, the induced strain is proportional to $P(\mathbf{E})^2 - P(0)^2$, which, assuming that $P(\mathbf{E}) = k_p p(\mathbf{E}) + k_q q(\mathbf{E})$, expands to:

$$k_p^2 p(\mathbf{E})^2 + 2k_p k_q p(\mathbf{E})q(\mathbf{E}) + k_q^2 q(\mathbf{E})^2 - k_p^2 p(0)^2 - 2k_p k_q p(0)q(0) - k_q^2 q(0)^2. \quad (8)$$

However, in the tetragonal phase, $q(0) = 0$, hence there are only three terms: (i) $p(\mathbf{E})^2 - p(0)^2$, (ii) $q(\mathbf{E})^2$, and (iii) $p(\mathbf{E})q(\mathbf{E})$. A corresponding argument applies to the rhombohedral phase, with $p(0) = 0$. Interestingly, for all the compositions and temperatures examined numerically, it is the term in $p(\mathbf{E})q(\mathbf{E})$, which dominates the value of the piezoelectric coefficient. This implies that the large piezoelectric coefficients found in the MPB region are due to the field-ordering of the random components of the polarization,

"amplified" by the homogeneous component. A similar argument may also be applied to the permittivity. As the morphotropic boundary is approached, the random components of polarization (or cation displacement) assume greater importance, culminating in the well-reported peak in permittivity and piezoelectric coefficient at the boundary. According to the model proposed here, the phenomenon is therefore essentially due to the local random nature of the PZT solid solution.

CONCLUSIONS

A novel thermodynamic model has been proposed to describe the properties of $\text{Pb}(\text{Zr},\text{Ti})\text{O}_3$ solid solutions, particularly in the region of the morphotropic phase boundary. Based on an expression which sums the two end member contributions to the free energy in proportion to their concentration, the model predicts the position of the morphotropic phase boundary at $x = 0.45$. This should be compared to the experimental locus of $x = 0.48$. The morphotropic phase boundary is independent of any of the adjustable parameters in the model and hence the good agreement with experimental data appears to confirm the suitability of the approach taken. The range of existence of the monoclinic phase is controlled by the coupling energy between the two end-member contributions to the polarization, \mathbf{p} and \mathbf{q} . At zero-field, \mathbf{p} and \mathbf{q} coexist only in the monoclinic phase. Although the model allows for the appearance of the three possible perovskite monoclinic phases, only the M_A phase was predicted by the model for PZT, again in keeping with experiment. In the examples here, only two coefficients were used to describe the coupling energy. By increasing the coupling between the parallel components of \mathbf{p} and \mathbf{q} , whilst keeping the orthogonal coupling energy at moderate levels, the M_A phase is restricted to the PbTiO_3 -rich side of the morphotropic phase boundary, as suggested by experimental data [19].

Examination of the contributions to the piezoelectric coefficient from the two polarization parameters reveals that the cross term between the two parameters is dominant, implying that the field stabilization of the random fluctuations is the origin of the large intrinsic piezoelectric coefficients in PZT.

REFERENCES

- [1] B. Jaffe, Cook, W. R., and Jaffe, H., *Piezoelectric Ceramics*: (Academic Press, London) 1971.
- [2] M. J. Haun, E. Furman, S. J. Jang, and L. E. Cross, *Ferroelectrics* **99**, 13 (1989).
- [3] M. J. Haun, E. Furman, H. A. McKinstry, and L. E. Cross, *Ferroelectrics* **99**, 27 (1989).

- [4] M. J. Haun, Z. Q. Zhuang, E. Furman, S. J. Jang, and L. E. Cross, *Ferroelectrics* **99**, 45 (1989).
- [5] M. J. Haun, E. Furman, T. R. Halemane, and L. E. Cross, *Ferroelectrics* **99**, 55 (1989).
- [6] M. J. Haun, E. Furman, S. J. Jang, and L. E. Cross, *Ferroelectrics* **99**, 63 (1989).
- [7] A. F. Devonshire, *Adv. Phys.* **3**, 85 (1954).
- [8] B. Noheda, D. E. Cox, G. Shirane, J. A. Gonzalo, L. E. Cross, and S. E. Park, *Appl. Phys. Lett.* **74**, 2059 (1999).
- [9] S. E. Park and T. R. Shrout, *J. Appl. Phys.* **82**, 1804 (1997).
- [10] Z. G. Ye, B. Noheda, M. Dong, D. Cox, and G. Shirane, *Phys. Rev. B* **64**, 184114 (2001).
- [11] D. La-Orauttapong, B. Noheda, Z. G. Ye, P. M. Gehring, J. Toulouse, D. E. Cox, and G. Shirane, *Phys. Rev. B* **65**, 144101 (2002).
- [12] D. Vanderbilt and M. H. Cohen, *Phys. Rev. B* **63**, 4108 (2001).
- [13] D. L. Corker, A. M. Glazer, R. W. Whatmore, A. Stallard, and F. Fauth, *J. Phys. Cond. Matter* **10**, 6251 (1998).
- [14] J. Frantti, J. Lappalainen, S. Eriksson, V. Lantto, S. Nishio, M. Kakihana, S. Ivanov, and H. Rundlof, *Jpn. J. Appl. Phys.* **39**, 5697 (2000).
- [15] V. Sivasubramanian, V. R. K. Murthy, B. Viswanathan, and M. Sieskind, *J. Phys.: Condens. Matter* **8**, 2447 (1996).
- [16] G. Burns and B. A. Scott, *Phys. Rev. B* **7**, 3088 (1973).
- [17] J. Frantti, J. Lappalainen, V. Lantto, S. Nishio, and M. Kakihana, *Jpn. J. Appl. Phys.* **38**, 5679 (1999).
- [18] K. C. V. Lima, A. G. Souza Filho, A. P. Ayala, J. Mendes Filho, P. T. C. Freire, F. E. A. Melo, E. B. Araujo, and J. A. Eiras, *Phys. Rev. B* **63**, 184105 (2001).
- [19] B. Noheda, D. E. Cox, G. Shirane, R. Guo, B. Jones, and L. E. Cross, *Phys. Rev. B* **63**, 14103 (2000).

APPENDIX 2

An Alternative Thermodynamic Model for PZT

Andrew J. Bell¹ and Eugene Furman²

¹Institute of Materials Research, University of Leeds, UK

²Materials Research Institute, The Pennsylvania State University, US

Abstract - A thermodynamic model is proposed to account for the monoclinic phase observed in the solid solution system $Pb(Zr_{1-x}Ti_x)O_3$. The free energy comprises three sets of terms: two expansions of polarization, one representing each of the end-members, weighted linearly with respect to composition, and terms representing the coupling between the two contributions. Employing previously published coefficients for $PbTiO_3$, and values extrapolated from Zr-rich PZT compositions for $PbZrO_3$, calculations predict the composition of the morphotropic phase boundary between the rhombohedral and tetragonal phases lies at $x=0.45$ and is virtually independent of temperature and the strength of coupling between the two order parameters. The range of existence of the monoclinic phase depends upon the strength of the coupling, but in general, is broadest at low temperature.

INTRODUCTION

Lead zirconate-titanate, $Pb(Zr_{1-x}Ti_x)O_3$ or PZT [1], has been widely studied due to the outstanding piezoelectric properties of compositions close to $x = 0.5$. The peak in the piezoelectric coefficient for these compositions has often been associated with the presence, at $x = 0.48$, of a morphotropic phase boundary between the zirconium-rich rhombohedral perovskite and the titanium-rich tetragonal perovskite phases. Haun [2 - 6] successfully modelled the PZT phase diagram, as it had been known for 30 years, using the thermodynamic approach of Devonshire [7], in which the free energy associated with the polar order

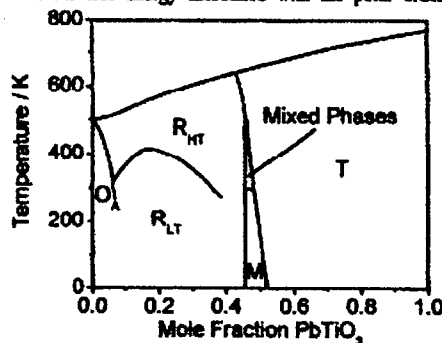


Fig. 1. Revised phase diagram of PZT, by combining those of Jaffe [1] and Noheda [8].

parameter is expressed in terms of a power series of the pseudo-cubic components of the polarization. A sufficiently accurate fit to experimental data has usually been achieved with expressions expanded up to the 6th power of polarization.

The recent discovery of a monoclinic phase at the morphotropic phase boundary in PZT [8] (Figure 1) and the confirmation that other systems with morphotropic phase boundaries that exhibit very large piezoelectric effects [9] also exhibit other phases close to the phase boundary [10 & 11], has led to renewed interest in how best to represent ferroelectrics with morphotropic phase boundaries in the context of the Landau-Devonshire model. The monoclinic phase in PZT was the first known phase in a ferroelectric perovskite in which the non-zero components of the polarization with respect to the cubic axes are not equal under conditions of zero applied field and stress. Such phases are not solutions of the conventional 6th power Devonshire model, however Vanderbilt [12] has shown that the inclusion of 8th power terms in the perovskite free energy expansion can lead to the possibility of monoclinic phases, whilst the inclusion of 12th power terms allows triclinic solutions. The suggestion is that due to the implicit disorder in solid solutions such as PZT, the 8th order terms may assume a greater importance than in single component perovskite ferroelectrics. However, the 8th power equations do not explicitly address the disordered nature.

In such treatments, the composition dependence of the free energy coefficients is not implicit in the model, the locus of the morphotropic phase boundary therefore being an input to, rather than output from, the exercise. Neither are the mesoscopic features of solid solutions represented. In PZT, close to the morphotropic phase boundary, there may be expected to be local competition between tetragonal and rhombohedral polar shifts, producing additional strain contributions to the free energy.

Moreover, the conventional approach does not explicitly take account of the details of local cation displacements in this system. It would appear that the local symmetry of the lead cation is monoclinic in both the rhombohedral and tetragonal phases. For the rhombohedral phase, it has been proposed that the displacement of the Pb cations from their cubic position comprises a homogeneous $[111]$ displacement superimposed with minor, random $\langle 001 \rangle$ shifts [13]. In the tetragonal phase, the homogeneous $[001]$ displacements are augmented with minor $\langle 110 \rangle$ (or equivalent $\langle 111 \rangle$) random shifts [14]. In both cases, the random shifts average to zero so that the macroscopic

symmetries remain rhombohedral and tetragonal respectively. The random Pb displacements might be considered as either static shifts or dynamic fluctuations about the homogeneous displacement. It is not known whether they are distributed totally randomly, or whether their directions are partially correlated in clusters and whether their magnitudes are equal on all sites. Nevertheless, it seems clear that the influence of PbTiO₃ exists well into the rhombohedral phase field and that of PbZrO₃ into the tetragonal phase. Moreover, in general, the Ti and Zr ions do not have equal displacements in either phase [13 & 14].

The minor displacements can be assumed to be of some significance in the appearance of the monoclinic phase. For example, it might be postulated that the transition from the tetragonal to monoclinic phase in PZT occurs due to the condensation of the random <111><110> displacements, which combined with the homogeneous [001] shifts give rise to a macroscopic monoclinic symmetry. As the Pb cation shifts are often cited as being the main component of dipole moment in Pb perovskite ferroelectrics, it may be possible to construct thermodynamic expressions to reflect this postulate, in which both the homogeneous and random

contributions to the polarization are represented, or in which the symmetry of the two end members is allowed to influence the stable state well inside the solid solution.

The example explored here is one in which the free energy is expressed as an expansion in terms of two polarization contributions, representing the different influences of the two end members of the solution series. It is based upon a linear combination of the free energy expansions of the end-members of the solid solution, together with linear and quadratic coupling terms. The total polarization is a function of the two end member contributions and the composition variable.

THEORY

In general, the free energy, ΔG , of an infinite, homogeneous, single domain ferroelectric with a cubic prototype structure, as in the perovskites, is given as an expansion of the orthogonal components of the polarization P in which only the coefficient α_{200} is necessarily temperature dependent, with the form $\alpha_{200} = \alpha'_{200}(T-T_0)$:

$$\Delta G(\alpha_{mp}, P) = \alpha_{200} (P_1^2 + P_2^2 + P_3^2) + \alpha_{400} (P_1^4 + P_2^4 + P_3^4) + \alpha_{220} (P_1^2 P_2^2 + P_2^2 P_3^2 + P_3^2 P_1^2) + \alpha_{600} (P_1^6 + P_2^6 + P_3^6) + \alpha_{420} [P_1^4 (P_2^2 + P_3^2) + P_2^4 (P_3^2 + P_1^2) + P_3^4 (P_1^2 + P_2^2)] + \alpha_{222} P_1^2 P_2^2 P_3^2 \dots - E_1 P_1 - E_2 P_2 - E_3 P_3, \quad (1)$$

where E is the applied electric field. Expansions terminated at the 6th power of polarization have generally been found sufficient to provide an accurate description of most ferroelectric perovskite systems. However, to

encapsulate the features of solid solutions discussed above, a solid solution energy function is proposed of the form:

$$\Delta G_{ss}(x) = x G_{PT}(\alpha_{mp}, p) + (1-x) G_{PZ}(\beta_{mp}, q) + G_C(\gamma_{mp}, p, q) \quad (2)$$

where x is the mole fraction of PbTiO₃. The vectors p and q represent the dissimilar polarizing tendencies of the two end-members, PbTiO₃ and PbZrO₃, respectively. The forms of $G_{PT}(\alpha_{mp}, p)$ and $G_{PZ}(\beta_{mp}, q)$ are identical to that of Equation 1, hence the symmetry requirements of the cubic prototype are maintained. The sets of coefficients, α_{mp} and β_{mp} , are those of the end members of the solid solution, in which only T_0 is a function of composition

and is common to both sets, in the form:

$$T_0(x) = x (T_{PT} - T_{PZ}) + T_{PZ} \quad (3)$$

where T_{PT} and T_{PZ} represent the Curie temperatures of PbTiO₃ and PbZrO₃ respectively.

The coupling energy, for terms up to the 4th power of polarization, is of the form:

$$G_C(\gamma_{mp}, p, q) = \gamma_{100} (p_1 q_1 + p_2 q_2 + p_3 q_3) + \gamma_{200} (p_1^2 q_1^2 + p_2^2 q_2^2 + p_3^2 q_3^2) + \gamma_{220} (p_1^2 (q_2^2 + q_3^2) + p_2^2 (q_3^2 + q_1^2) + p_3^2 (q_1^2 + q_2^2)) \quad (4)$$

Terms in $p_i q_j$, where $i \neq j$, are disallowed by symmetry, as the free energy should be independent of the sign of $p_i q_j$. However, terms in $p_i q_i$ are necessary to differentiate between the parallel and anti-parallel states of p_i and q_i . Table I lists the non-degenerate states resulting from combination of the components of p and q , using the notation of Vanderbilt [12] for the resulting phases. Due to the coupling energy G_C , the components of p and q are not constrained to the 6th power solutions of the end-

member contributions. For directions in which the component of the total polarization, P_i , is not constrained by symmetry to be zero, either of the contributions, p_i or q_i , is allowed to be zero as long as $p_i + q_i \neq 0$. It should be noted that all of the phases identified by Vanderbilt [12] for the conventional 12th power Devonshire model are possible solutions of the current approach, including three non-degenerate triclinic phases.

TABLE I. Classification of phases for non-degenerate combinations of p_i and q_i . Only components constrained to be zero are shown as such. If p_i and q_i are both shown as non-zero, either, but not both, may assume a zero value.

P_1	P_2	P_3	q_1	q_2	q_3	Phase
0	0	0	0	0	0	Cubic - C
0	0	p_3	0	0	q_3	Tetragonal - T
0	p_3	p_3	0	q_3	q_3	Orthorhombic - O
p_3	p_3	p_3	q_3	q_3	q_3	Rhombohedral - R
p_1	p_1	p_3	q_1	q_1	q_3	Monoclinic - M_A
p_1	p_1	$-p_3$	q_1	q_1	q_3	Monoclinic - M_B
p_1	p_3	$-p_3$	q_1	q_3	q_3	Triclinic - Tr
p_1	$-p_3$	$-p_3$	q_1	q_3	q_3	Monoclinic - M_A
0	p_2	p_3	0	q_2	q_3	Monoclinic - M_C
0	p_2	$-p_3$	0	q_2	q_3	Monoclinic - M_C
p_1	p_2	p_3	q_1	q_2	q_3	Triclinic - Tr
p_1	p_2	$-p_3$	q_1	q_2	q_3	Triclinic - Tr

For comparison with quantitative available data, it is necessary to evaluate the total polarization P , which is a function of p and q . For this purpose, it is assumed here that the relationship is of the simple form:

$$P = k_p(x) p + k_q(x) q. \quad (5)$$

The simplest assumptions are that either (i) $k_p = k_q = 1$ or (ii) $k_p = x$ and $k_q = 1-x$. The first assumption implies that p and q are assigned homogeneously across all unit cells, independent of B-site occupation, i.e. the dipole moment of all unit cells is equal. However, it is clear from the structure data of Corker [13] and Frantti [14] that this is unlikely as the Zr and Ti displacements are often different within a single composition. Assumption (ii) implies that p and q are distributed according to the B-site occupancy of the unit cell. This would mean that in the example addressed below, the dipole associated with, say, Zr cells in the tetragonal phase, would be zero. This is also not supported by the structure data [13 & 14]. The evaluation of k_p and k_q will therefore be undertaken by comparison with experimental data.

CALCULATIONS FOR PZT

The model presented here is aimed at the correct prediction of the morphotropic phase boundary and the appearance of perovskite ferroelectric states with non-equal polarization components i.e. monoclinic and triclinic phases. Hence, the orthorhombic antiferroelectric phase in PZT is ignored, and for the purpose of these calculations, lead zirconate is assumed to be a rhombohedral ferroelectric. Similarly, the octahedral tilt transition, which differentiates the high and low temperature rhombohedral phases of PZT, is not addressed here.

Calculations of the temperature and composition dependence of p and q and hence the phase boundaries were carried out using the above model for zero applied field. Choosing the A end-member Equation 2 to be $PbTiO_3$, the solution for $x = 1$ should yield, for $T < T_A$, $p_1 = 0$, $p_2 = 0$, $p_3 \neq 0$, $q = 0$, i.e. a tetragonal ferroelectric,

whereas $x = 0$ should yield solutions for a rhombohedral ferroelectric, i.e. for $T < T_B$, $p=0$, $q_1 = q_2 = q_3 \neq 0$. The α_{mnp} coefficients for $PbTiO_3$ used for these calculations are those given by Haun [4] and are shown in Table II. The β_{mnp} coefficients for a hypothetically ferroelectric $PbZrO_3$ have been estimated by extrapolating the Haun coefficients for compositions with $x > 0$ back to $x = 0$. In some cases, notably β_{200} and β_{400} , the extrapolated value is identical to that of the original Haun coefficient, whereas the remaining coefficients tend to a linear dependence on x except close to $x = 0$ and $x = 0.5$.

The calculations were carried out by numerical minimization of $\Delta G_m(x)$ with respect to p and q using the FindMinimum function of *Mathematica 4.0*. Only positive values of p_i and q_i were considered, hence in this context the γ_{100} term is redundant and for simplicity its value was set to zero, leaving only γ_{200} and γ_{220} as the unknown parameters.

The problems of identifying the absolute free energy minimum in six dimensional polarization space are not trivial, hence solutions were sought which corresponded to the most likely phases in Table II. For each temperature and $PbTiO_3$ molar fraction, the local minima in $\Delta G_m(x)$ were systematically identified for $p_i > 0$ and $q_i > 0$, with the constraints shown in Table I, for the following phases: cubic, tetragonal, orthorhombic, rhombohedral, monoclinic M_A and monoclinic M_C . The energies of the minima were then compared to define the stable state.

TABLE II. Free energy coefficients for $PbTiO_3$ (α_{mnp}) and hypothetically ferroelectric $PbZrO_3$ (β_{mnp})

mnp	α_{mnp}	β_{mnp}
200	$3.74 \times 10^5 (T - T_0)$	$2.82 \times 10^5 (T - T_0)$
400	-7.9×10^7	5.12×10^8
220	7.5×10^8	-6.5×10^8
600	2.61×10^8	5.93×10^8
420	6.3×10^8	2×10^9
222	-3.66×10^9	-9.5×10^9

Lattice parameters and permittivity were calculated for the case of $\text{PbZr}_{0.52}\text{Ti}_{0.48}\text{O}_3$. The spontaneous strain matrix, σ , is calculated according to:

$$\sigma_{ij} = Q_{ijl} P_k P_l \quad (6)$$

For reasons of symmetry, there are only three independent components of the electrostriction coefficient tensor Q , which in reduced notation are Q_{11} , Q_{12} and Q_{44} . Their values for $\text{PbZr}_{0.52}\text{Ti}_{0.48}\text{O}_3$ were derived by linear interpolation from those of the end-members, published by Haun [4]: $Q_{11} = 0.0667$, $Q_{12} = -0.0197$ and $Q_{44} = 0.0567$. These were used in preference to values interpolated from the full set of coefficients given at intervals of $\Delta x = 0.1$ in the same reference. The adopted procedure assumes that the electrostriction coefficients are "well-behaved" on passing through the morphotropic phase boundary with no anomalous values.

The spontaneous strains are converted to the lattice parameters referenced to the pseudo-cubic axes, again using reduced notation, as follows:

$$\begin{aligned} a_p &= b_p = a_0(\sigma_1 + 1), & c_p &= a_0(\sigma_3 + 1), \\ \gamma_p &= \pi/2 - \tan^{-1}\sigma_4, & \beta_p &= \pi/2 + \tan^{-1}\sigma_5 \end{aligned} \quad (7)$$

where a_p , b_p , and c_p are the unit cell lengths, γ_p is the angle between the a - and b -axes, and β_p is the angle between the c -axis and the x - y plane. a_0 is the equivalent cubic lattice parameter extrapolated for the full temperature range from the data of Noheda [8] in the paraelectric phase, giving:

$$a_0 = 4.0584 + 2.9156 \times 10^{-5} T \text{ \AA} \quad (8)$$

For the monoclinic phase ($T < 300$ K), the transformation to the monoclinic lattice parameters (denoted by subscript m) is given by:

$$\begin{aligned} a_m &= 2a_p \sqrt{2 \left(1 + \tan^2 \left(\frac{\gamma_p}{2} \right) \right)}, \\ b_m &= a_p \tan \left(\frac{\gamma_p}{2} \right), & c_m &= c_p \cos \left(\beta_p - \frac{\pi}{2} \right), \\ \beta_m &= \arccos \left[\frac{\cos(\beta_p)}{\cos \left(\frac{\gamma_p}{2} \right)} \right] \end{aligned} \quad (9)$$

The small signal permittivities, ϵ_{33} and ϵ_{11} , were calculated from the increment in the polarization, P_i , on applying a field E_i of 1 kV m^{-1} , for $i = 3$ and 1 respectively.

RESULTS

The stabilities of the phases were determined as a function of γ_{200} and γ_{220} . In the examples discussed, only stable phases corresponding to cubic, tetragonal, rhombohedral and monoclinic M_A were found. Phase diagrams as a function of x and T are shown for various combinations of γ_{200} and γ_{220} in Figs. 2, 3, and 4.

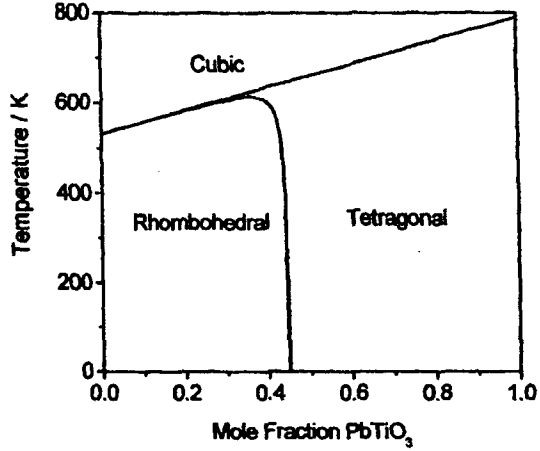


Fig. 2. Phase diagram for $\gamma_{200} = \gamma_{220} \rightarrow \infty$.

For $\gamma_{200} = \gamma_{220} \leq 0$, there is only a single phase boundary at $T_0(x)$, between cubic and monoclinic M_A , for all PbTiO_3 concentrations except the end-members. For non-zero values, γ_{200} and γ_{220} must exceed a threshold value to avoid discontinuities as $x \rightarrow 0$ and $x \rightarrow 1$.

When both γ_{200} and γ_{220} exceed 2×10^8 the appearance of the monoclinic phase is completely inhibited see (Fig. 2). The locus of the morphotropic boundary is independent of γ_{200} and γ_{220} and, well below T_0 , it is also almost independent of temperature, moving to slightly higher values of x with decreasing temperature, and extrapolating to $x = 0.45$ at 0 K. On approaching T_0 , the boundary curves sharply towards lower values of x ; the point at which the morphotropic phase boundary finally coincides with the cubic phase boundary is at $x = 0$. Hence a cubic-tetragonal transition occurs on cooling for all compositions with $x > 0$, however for compositions up to $x = 0.35$ the tetragonal phase is only stable for up to 5 K below T_0 , before transforming to the rhombohedral phase. The paraelectric-ferroelectric phase transition is 1^{st} order for all values of x .

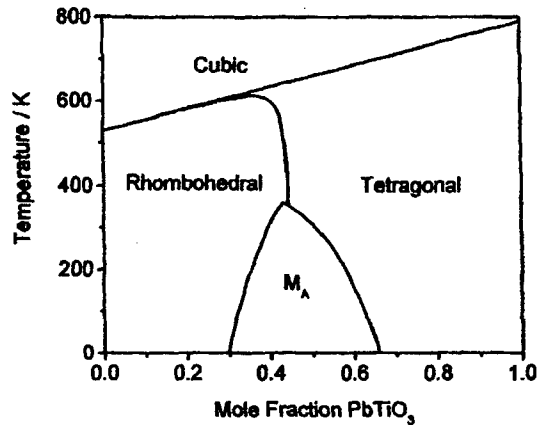


Fig. 3. Phase diagram for $\gamma_{200} = \gamma_{220} = 10^8$.

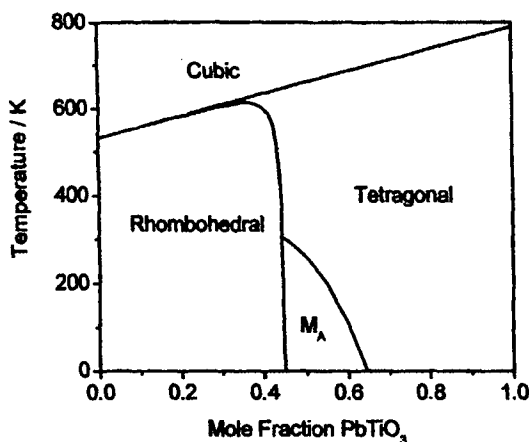


Fig. 4. Phase diagram for $\gamma_{200} = 6 \times 10^8$, $\gamma_{220} = 10^8$.

For intermediate values of the coupling coefficients, the M_A phase appears in the centre of the phase diagram. On increasing the γ values from zero, there is an almost symmetrical reduction in the width of the monoclinic phase field, yielding to the rhombohedral phase at low x and the tetragonal phase at high x values. There is also a reduction in the maximum temperature of monoclinic stability which occurs close to $x = 0.5$. Thus as the coupling energy is increased, the morphotropic phase boundary between the rhombohedral and tetragonal phases is revealed, with the M_A phase appearing as a wedge, with its apex close to the morphotropic phase boundary. The example shown in Figure 3 is for $\gamma_{200} = \gamma_{220} = 10^8$, whilst that of Figure 4 is for $\gamma_{200} = 6 \times 10^8$ and $\gamma_{220} = 10^8$, where the inequality in the coupling coefficients results in the monoclinic phase favouring the "tetragonal" side of the morphotropic phase boundary.

The lattice parameters were calculated for $\text{PbZr}_{0.52}\text{Ti}_{0.48}\text{O}_3$. In keeping with Figure 4 the value of γ_{200} was fixed at 6×10^8 to ensure that the M_A phase existed only on the Ti-rich side of the MPB. The value of γ_{220} was adjusted so that the transition temperature for the tetragonal monoclinic transition was 300 K, as in the data of Noheda [8]. The values of k_p and k_q in Equation 5 were then adjusted to fit the magnitude of the calculated lattice parameters to the measured values [8]. An acceptable fit was obtained for $k_p = 0.73$, $k_q = 0.77$. A comparison of the calculated and measured values is shown in Figure 5.

The above values of k_p and k_q were then used to calculate the relative permittivities, ϵ_{33} and ϵ_{11} (Figure 6).

DISCUSSION AND CONCLUSIONS

A novel thermodynamic model has been proposed to describe the properties of $\text{Pb}(\text{Zr,Ti})\text{O}_3$ solid solutions, particularly in the region of the morphotropic phase boundary. Based on an expression which sums the two end member contributions to the free energy in proportion to their concentration, the model predicts the position of the morphotropic phase boundary at $x = 0.45$. This should

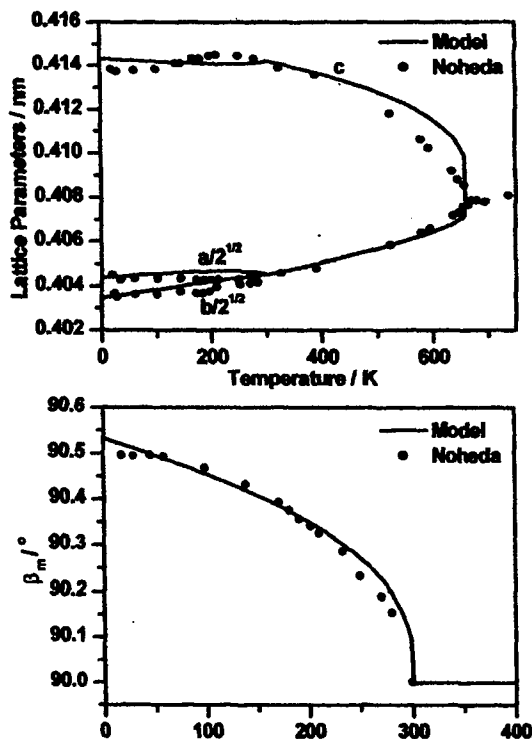


Fig. 5. Comparison of calculated and measured lattice parameters for $\text{PbZr}_{0.52}\text{Ti}_{0.48}\text{O}_3$.

be compared to the experimental locus of $x = 0.48$. The morphotropic phase boundary is independent of any of the adjustable parameters in the model and hence the good agreement with experimental data appears to confirm the suitability of the approach taken. The range of existence of the monoclinic phase is controlled by the coupling energy between the two end-member contributions to the polarization, p and q . At zero-field, p and q coexist only in the monoclinic phase. Although the model allows for the appearance of the three possible perovskite monoclinic phases, only the M_A phase was predicted by the model for PZT, again in keeping with experiment. In the examples here, only two coefficients were used to describe the coupling energy. By increasing the coupling between the parallel components of p and q , whilst keeping the orthogonal coupling energy at moderate levels, the M_A phase is restricted to the PbTiO_3 -rich side of the morphotropic phase boundary, as suggested by experimental data [15].

The comparison of the predicted and measured lattice parameters for the specific case of $\text{PbZr}_{0.52}\text{Ti}_{0.48}\text{O}_3$ is generally good. Parameters within the model have been adjusted to achieve a tetragonal monoclinic transition temperature of 300 K (γ_{220}) and to scale the data correctly (k_p and k_q). Clearly, there is some discrepancy between the detailed behaviour below 300 K, which is most apparent in the c_m parameter.

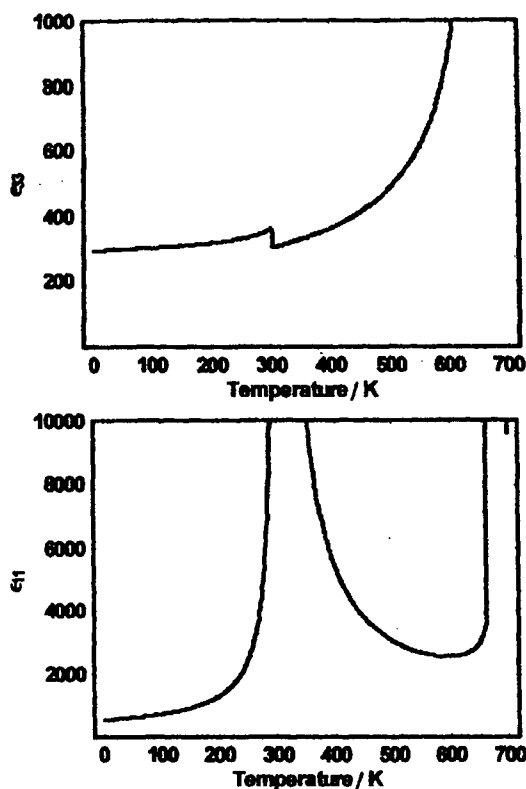


Fig. 6. Relative permittivities, ϵ_{33} and ϵ_{11} , for $\text{PbZr}_{0.52}\text{Ti}_{0.48}\text{O}_3$ calculated as function of temperature.

The calculated permittivity for the same composition shows a small anomaly in ϵ_{33} at the tetragonal monoclinic transition, but a peak of over 10,000 is apparent for ϵ_{11} . This is not too surprising given that in the monoclinic phase, the P_3 component is only slightly different from the saturated component in the tetragonal form, whereas there is far greater compliance in the minor components, P_1 and P_2 .

A feature of the current model is that the paraelectric-ferroelectric transition is always predicted to be first order and the transition always passes through the tetragonal phase, independent of composition. When $T_0 - T$ is small, the α_{400} and β_{400} terms dominate G_{PT} and G_{PZ} respectively, hence $x G_{PT}(T \rightarrow T_0)$ will always be less than $(1-x) G_{PZ}(T \rightarrow T_0)$, even for small x . This aspect is not reflected in the experimental data where the morphotropic phase boundary exhibits minimal curvature towards lower x with increasing temperature and the paraelectric-ferroelectric transition has only been confirmed as first order for compositions in which x is substantially greater than 0.5.

A second difficulty concerns the significance of p and q . Here they are interpreted as the contributions to the macroscopic polarization, P , from the two end members of the solid solution. However, as outlined above, the mathematical relationship between p , q and P is not

obvious. A simple relationship has been assumed here (Equation 5), which on comparison of the calculated lattice parameters with experimental data, shows that around $x = 0.5$, $P \approx 0.75(p + q)$. However, it must be assumed that for $x = 0$, $P = q$ and for $x = 1$, $P = p$. Hence, the form of $k_p(x)$ and $k_q(x)$ is unlikely to be linear in x . Both this problem and that of the first-order nature of the paraelectric-ferroelectric phase transition might be alleviated by taking an approach that is more directly analogous to the *ab initio* method of Bellaiche [16], in which the Hamiltonian includes a term for the average structure and a summation of terms representing the local environment.

The above difficulties clearly reflect the rather empirical nature of the proposed model. However, bearing in mind that the true structure of PZT does not yield to a conventional treatment, based on a rigorous group theoretical approach, the alternative model perhaps provides some directions towards a more comprehensive model.

REFERENCES

- [1] Jaffe B. Jaffe, Cook, W.R., Jaffe, H., *Piezoelectric Ceramics* London: Academic Press Ltd, 1971.
- [2] M. J. Haun, E. Furman, S. J. Jang and L. E. Cross, *Ferroelectrics*, vol. 99, p. 13, 1989
- [3] M. J. Haun, E. Furman, H. A. McKinstry and L. E. Cross, *Ferroelectrics* vol. 99, p. 27, 1989
- [4] M. J. Haun, Z. Q. Zhuang, E. Furman, S. J. Jang and L. E. Cross, *Ferroelectrics* vol. 99, p. 45, 1989
- [5] M. J. Haun, E. Furman, T. R. Halemane and L. E. Cross, *Ferroelectrics* vol. 99, p. 55, 1989
- [6] M. J. Haun, E. Furman, S. J. Jang and L. E. Cross, *Ferroelectrics* 99, p. 63, 1989
- [7] A.F. Devonshire, *Adv. Phys.* vol. 3, p. 85, 1954
- [8] B. Noheda, D. E. Cox, G. Shirane, J. A. Gonzalo, L. E. Cross and S. E. Park, *Appl. Phys. Lett.* vol. 74, p. 2059, 1999.
- [9] S. E. Park and T. R. ShROUT, *J. Appl. Phys.* vol. 82, p. 1804, 1997.
- [10] Z. G. Ye, B. Noheda, M. Dong, D. Cox and G. Shirane, *Phys. Rev. B*, vol. 64, p. 184114, 2001
- [11] D. La-Orauttapong, B. Noheda, Z.G. Ye, P.M. Gehring, J. Toulouse, D.E. Cox and G. Shirane, *Phys. Rev. B*, vol. 65, 144101, 2002
- [12] D. Vanderbilt and M. H. Cohen, *Phys. Rev. B*, vol. 63, p. 4108, 2001
- [13] D. L. Corker, A. M. Glazer, R. W. Whatmore, A. Stallard and F. Fauth, *J. Phys.- Cond. Matter*, vol. 10, p. 6251 1998.
- [14] J. Frantti, J. Lappalainen, S. Eriksson, V. Lantto, S. Nishio, M. Kakihana, S. Ivanov and H. Rundlof, *Jpn. J. Appl. Phys.*, vol. 39, p. 5697, 2000.
- [15] B. Noheda, D. E. Cox, G. Shirane, R. Guo, B. Jones, and L. E. Cross, *Phys. Rev. B*, vol. 63, p.14103, 2000
- [16] L. Bellaiche, A. Garcia and D. Vanderbilt, *Phys. Rev. Lett.* vol. 84, p. 5427, 2000.

APPENDIX 3

A Two Order Parameter Thermodynamic Model for $\text{Pb}(\text{Zr}_{1-x}\text{Ti}_x)\text{O}_3$

Andrew J. BELL and Eugene FURMAN¹

¹Institute for Materials Research, The University of Leeds, Leeds, LS2 9JT, UK

¹Materials Research Institute, The Pennsylvania State University, University Park, Pennsylvania 16802, USA

(Received July 7, 2003; accepted July 11, 2003; published December 10, 2003)

A two order parameter thermodynamic model is proposed which accounts for a number of features of the solid solution system $\text{Pb}(\text{Zr}_{1-x}\text{Ti}_x)\text{O}_3$ not predicted by the conventional 6th order model. The free energy comprises three sets of terms: two expansions of polarization, representing contributions to the polarization of each of the solid solution end-members, weighted linearly with respect to composition, plus terms representing the coupling between the two contributions. Employing previously published coefficients for PbTiO_3 and values extrapolated from Zr-rich PZT compositions for PbZrO_3 , calculations predict that the composition of the morphotropic phase boundary between the rhombohedral and tetragonal phases lies at $x = 0.45$ and is independent of the strength of coupling between the two order parameters. The model allows for the existence of a monoclinic phase, the composition range of which depends upon the strength of the coupling terms. A satisfactory fit to the lattice parameters of $\text{Pb}(\text{Zr}_{0.52}\text{Ti}_{0.48})\text{O}_3$ is obtained over a wide range of temperature. [DOI: 10.1143/JJAP.42.7418]

KEYWORDS: ferroelectricity, PZT, thermodynamic theory

1. Introduction

Lead zirconate-titanate,¹⁾ $\text{Pb}(\text{Zr}_{1-x}\text{Ti}_x)\text{O}_3$ or PZT, is a solid solution between the two compounds lead titanate (PbTiO_3) and lead zirconate (PbZrO_3). Both are of the perovskite structure at room temperature, with PbTiO_3 being tetragonal and ferroelectric, whilst PbZrO_3 is of orthorhombic symmetry and is antiferroelectric. The compounds form a complete perovskite solid solution (Fig. 1), with no discernible ordering of the Ti and Zr on the B-site. The system has been widely studied due to the outstanding piezoelectric properties of compositions close to $x = 0.5$. The peak in the piezoelectric coefficient for these compositions has often been associated with the presence, at $x = 0.48$, of a morphotropic phase boundary (MPB) between the zirconium-rich rhombohedral perovskite and the titanium-rich tetragonal perovskite phases.

Haun²⁻⁶⁾ successfully modelled the PZT phase diagram using the thermodynamic approach of the Landau-Devonshire model⁷⁾ in which the free energy associated with the polar order parameter is expanded in terms of a power series of the pseudo-cubic components of the polarization. Haun determined the coefficients of the free-energy expansion

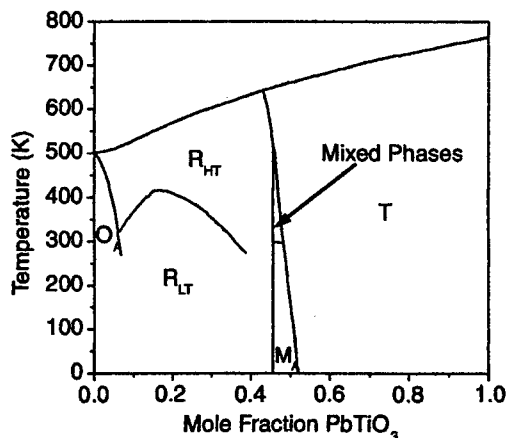


Fig. 1. Revised phase diagram of PZT, by combining those of Jaffe¹⁾ and Noheda.²⁾

experimentally for each of 11 discrete compositions across the phase diagram from the temperature dependence of the first and higher order dielectric stiffnesses. Determination of the electrostriction coefficients allowed a calculation of the intrinsic piezoelectric coefficients, which were shown to peak at the morphotropic phase boundary in keeping with experiment. The locus of the morphotropic phase boundary was an input to, rather than output of, the treatment, which is not predictive in terms of phase stability as function of composition.

The $\text{Pb}(\text{Zn}_{1/3}\text{Nb}_{2/3})\text{O}_3$ - PbTiO_3 system, which exhibits a similar morphotropic phase boundary at around $0.9\text{Pb}(\text{Zn}_{1/3}\text{Nb}_{2/3})\text{O}_3$ - 0.1PbTiO_3 , has also been modelled with some success by assuming a linear mixing of the free energy coefficients of the end-members according to composition.^{8,9)}

Within recent years, three factors have prompted a reassessment of the mechanisms of piezoelectricity in PZT; these are: (i) the detection of a monoclinic phase at the morphotropic phase boundary;¹⁰⁾ (ii) experimental and theoretical evidence for local structures in the rhombohedral and tetragonal phases in which the polar displacement of the lead ion comprises a homogeneous component corresponding to the macroscopic symmetry and local random “off-axis” components which average to zero,¹¹⁻¹³⁾ and (iii) the splitting of low-lying transverse optic phonon modes as a function of the solid solution composition.^{14,15)} The existing thermodynamic theory for PZT is not consistent with these observations.

The monoclinic phase in PZT is one of the few phases in ferroelectric perovskites in which the non-zero components of the polarization with respect to the cubic axes are not equal under conditions of zero applied field and stress. The most common ferroelectric phases in perovskites, as exemplified by barium titanate, are tetragonal, orthorhombic and rhombohedral, with the polarization vector parallel to [001], [011] and [111] respectively. The orthogonal components of polarization for these phases have values that are either zero or equal to each other (see Table I). These phases, plus the paraelectric (cubic) phase, are the only solutions of the conventional Devonshire model expanded up to the 6th power of polarization, which has generally proved sufficient

Table I. Possible symmetries in perovskite ferroelectrics; phases above the dotted line are solutions to the 6th power Devonshire theory.

Reference	Crystal Class	Symmetry	Polarization state	Polar Direction
C	Cubic	m3m	$P_1 = P_2 = P_3 = 0$	paraelectric
T	Tetragonal	4mm	$P_1 = P_2 = 0, P_3 \neq 0$	(001)
O	Orthorhombic	mm2	$P_2 = 0, P_1^2 = P_3^2 \neq 0$	(101)
R	Rhombohedral	3m	$P_1^2 = P_2^2 = P_3^2 \neq 0$	(111)
M _A	Monoclinic	m	$P_1^2 = P_2^2 \neq 0, P_3 \neq 0$ $P_3^2 > P_1^2$	
M _B	Monoclinic	m	$P_1^2 = P_2^2 \neq 0, P_3 \neq 0$ $P_3^2 < P_1^2$	
M _C	Monoclinic	m	$P_1^2 \neq P_2^2 \neq 0, P_3 = 0$	
Tr	Triclinic	1	$P_1^2 \neq P_2^2 \neq P_3^2 \neq 0$	

for a satisfactory fit to experimental data. In the monoclinic phase of PZT, the pseudo-cubic components of polarization along [100] and [010] are non-zero and equal, but are somewhat smaller than that along [001]. Hence, the polarization vector lies in the (110) plane at an arbitrary angle to the [001] direction. The transition from tetragonal to monoclinic is of 2nd order, with the angle of the polarization deviation from the [001] axis increasing continuously from zero. The polarization in the monoclinic phase might therefore be considered as the homogeneous superposition of a small rhombohedral component upon the existing tetragonal one.

Although monoclinic phases are not solutions of the 6th power Devonshire theory, Vanderbilt¹⁶⁾ has shown that the inclusion of 8th power terms in the perovskite free energy expansion does lead to the possibility of monoclinic phases. However, the form of the 8th power equations does not account for the observed splitting of the soft-mode nor does it explicitly address the disordered nature of PZT as does, for example, the first-principles model of Bellaiche.¹⁷⁾

The question addressed by this paper is as follows: is it possible to construct a thermodynamic theory for PZT, (i) in which the composition dependence of the free energy is implicit, with reference only to the end-members, (ii) which is consistent with the observation of soft mode splitting and (iii) which can account for the monoclinic phase as a superposition of the tetragonal and rhombohedral distortions?

The first principles model of Grinberg¹³⁾ supports the view that Pb ion shifts are the main contribution to the macroscopic polarization in PZT. The local deviations of the Pb ion displacements from the macroscopic polar direction are shown to encompass a range in magnitude and direction which are dependent upon the local Zr and Ti configurations. However, as an approximation, the spectrum could be reduced to two types of perturbation, depending on whether the local environment is Ti- or Zr-rich, i.e. predominantly PbTiO₃ or PbZrO₃. Hence the thermodynamic model proposed here is based upon two polarization order-parameters. Each parameter is related to the polarization contribution of one of the two end-members of the solution series. The model comprises a summation of the free energy expansions of the end-members of the solid solution, weighted with respect to composition, together with linear

and quadratic coupling between the two polarization terms.

It is shown here that this model results in an almost temperature independent rhombohedral-tetragonal phase boundary, close to the composition seen experimentally.¹⁾ The range of existence of the neighbouring monoclinic phase is dependent upon the strength of coupling between the two order parameters.

2. Theory

In the conventional Landau-Devonshire model,⁷⁾ the elastic Gibbs free energy, ΔG , of an infinite, homogeneous, single domain ferroelectric with a cubic prototype structure, as in the perovskites, is given as an expansion of the orthogonal components of the polarization, P , in which only the coefficient α_{200} is necessarily temperature dependent, with the form $\alpha_{200} = \alpha'_{200}(T - T_0)$:

$$\begin{aligned} \Delta G(\alpha_{mnp}, P) = & \alpha_{200}(P_1^2 + P_2^2 + P_3^2) \\ & + \alpha_{400}(P_1^4 + P_2^4 + P_3^4) \\ & + \alpha_{220}(P_1^2 P_2^2 + P_2^2 P_3^2 + P_3^2 P_1^2) \\ & + \alpha_{600}(P_1^6 + P_2^6 + P_3^6) \\ & + \alpha_{420}[P_1^4(P_2^2 + P_3^2) + P_2^4(P_3^2 + P_1^2) \\ & + P_3^4(P_1^2 + P_2^2)] \\ & + \alpha_{222}P_1^2 P_2^2 P_3^2 \dots \dots \dots \\ & - E_1 P_1 - E_2 P_2 - E_3 P_3, \end{aligned} \quad (1)$$

where E is the applied electric field. To encapsulate the features of solid solutions discussed above, an energy function for the solution between end-members A and B is proposed, of the form:

$$\begin{aligned} \Delta G_{ss}(x) = & xG_A(\alpha_{mnp}, p) + (1-x)G_B(\beta_{mnp}, q) \\ & + G_C(\gamma_{mnp}, p, q) \end{aligned} \quad (2)$$

where x is the mole fraction of end-member A. The forms of $G_A(\alpha_{mnp}, p)$ and $G_B(\beta_{mnp}, q)$ are identical to that of eq. (1), hence the symmetry requirements of the cubic prototype are maintained. The sets of coefficients, α_{mnp} and β_{mnp} , are those of the end members of the solid solution, in which only T_0 is a function of composition and is common to both sets, in the form:

$$T_0(x) = x(T_A - T_B) + T_B \quad (3)$$

where T_A and T_B represent the Curie temperatures of the two end-members.

The coupling energy, for terms up to the 4th power of polarization, is of the form:

$$\begin{aligned} G_C(\gamma_{mnp}, p, q) = & \gamma_{100}(p_1 q_1 + p_2 q_2 + p_3 q_3) \\ & + \gamma_{200}(p_1^2 q_1^2 + p_2^2 q_2^2 + p_3^2 q_3^2) \\ & + \gamma_{220}(p_1^2(q_2^2 + q_3^2) + p_2^2(q_3^2 + q_1^2) \\ & + p_3^2(q_1^2 + q_2^2)) \end{aligned} \quad (4)$$

This is consistent with the treatment by Salje¹⁸⁾ for ferroelastic materials with two order-parameters, in which bi-linear and bi-quadratic coupling terms appear to be the most important. Higher order coupling terms are only excluded here for a reduction in complexity. However, terms in $p_i q_j$, where $i \neq j$, are disallowed by symmetry, as the free energy should be independent of the sign of $p_i q_j$, but

Table II. Classification of phases for non-degenerate combinations of p_i and q_i . Only components constrained to be zero are shown as such. If p_i and q_i are both shown as non-zero, either, but not both, may assume a zero value.

p_1	p_2	p_3	q_1	q_2	q_3	Phase
0	0	0	0	0	0	Cubic - C
0	0	p_3	0	0	q_3	Tetragonal - T
0	p_3	p_3	0	q_3	q_3	Orthorhombic - O
p_3	p_3	p_3	q_3	q_3	q_3	Rhombohedral - R
p_1	p_1	p_3	q_1	q_1	q_3	Monoclinic - M_A
p_1	p_1	$-p_3$	q_1	q_1	q_3	Monoclinic - M_B
p_1	p_3	$-p_3$	q_1	q_3	q_3	Triclinic - Tr
p_1	$-p_3$	$-p_3$	q_1	q_3	q_3	Monoclinic - M_A
0	p_2	p_3	0	q_2	q_3	Monoclinic - M_C
0	p_2	$-p_3$	0	q_2	q_3	Monoclinic - M_C
p_1	p_2	p_3	q_1	q_2	q_3	Triclinic - Tr
p_1	p_2	$-p_3$	q_1	q_2	q_3	Triclinic - Tr

terms in $p_i q_i$ are necessary to differentiate between the parallel and anti-parallel states of p_i and q_i .

Table II lists the non-degenerate states resulting from combination of the components of p and q , using the notation of Vanderbilt¹⁶⁾ for the resulting phases. Due to the presence of the coupling energy G_C , the components of p and q are not constrained to the 6th power solutions of the end-member contributions. For directions in which the component of the total polarization, P_i , is not constrained by symmetry to be zero, either of the contributions, p_i or q_i , is allowed to be zero as long as $p_i + q_i \neq 0$. It should be noted that all of the phases identified by Vanderbilt¹⁶⁾ for the conventional 12th power Devonshire model are possible solutions of the current approach, including three non-degenerate triclinic phases.

The relationship between the total polarization, P , and p and q is not explicit in the model, but is assumed here to be of the simple form:

$$P = h(x)p + k(x)q, \quad (5)$$

two possible examples of which are (i) $h(x) = k(x) = 1$ and (ii) $h(x) = x$ and $k(x) = (1 - x)$. The first assumption implies that p and q are summed homogeneously in all unit cells, independent of B-site occupation, i.e. the dipole moment of all unit cells is identical. However, it is clear from the structure data^{11,12)} and first principles calculations¹³⁾ that this is unlikely for PZT. Assumption (ii) implies that p and q are distributed according to the B-site occupancy of the unit cell. This would imply that the dipole associated with, say, Zr-rich regions in the tetragonal phase, is zero. Again, this is not supported by the structure refinements and calculations, therefore the approach taken here is to attempt to discern the values of $h(x)$ and $k(x)$ by comparison with previous data for the system.

3. Calculations for PZT

The model is aimed at determining the states of PZT close to the morphotropic phase boundary, therefore the orthorhombic antiferroelectric phase in PZT is ignored, and for the purpose of these calculations, lead zirconate is assumed to be a rhombohedral ferroelectric. Similarly, the octahedral

Table III. Free energy coefficients for PbTiO_3 (α_{mnp}) and hypothetically ferroelectric PbZrO_3 (β_{mnp}).

mnp	α_{mnp}	β_{mnp}
200	$3.74 \times 10^5 (T - T_0)$	$2.82 \times 10^5 (T - T_0)$
400	-7.9×10^7	5.12×10^8
220	7.5×10^8	-6.5×10^8
600	2.61×10^8	5.93×10^8
420	6.3×10^8	2×10^9
222	-3.66×10^9	-9.5×10^9

tilt transition, which differentiates the high and low temperature rhombohedral phases of PZT, is not addressed.

Calculations of the temperature and composition dependence of p and q and hence the phase boundaries were carried out using the above model for zero applied field. Choosing the 'A' end-member in eq. (2) to be PbTiO_3 , the solution for $x = 1$ should yield, for $T < T_A$, $p_1 = p_2 = 0$, $p_3 \neq 0$, $q = 0$, i.e. a tetragonal ferroelectric, whereas $x = 0$ should yield solutions for a rhombohedral ferroelectric, i.e. for $T < T_B$, $p = 0$, $q_1 = q_2 = q_3 \neq 0$. The α_{mnp} coefficients for PbTiO_3 used for these calculations are those given by Haun⁴⁾ and are shown in Table III. The β_{mnp} coefficients for a hypothetically ferroelectric PbZrO_3 have been estimated by extrapolating the Haun coefficients for compositions with $x > 0$ back to $x = 0$. In some cases, notably β_{200} and β_{400} , the extrapolated value is identical to that of the original Haun coefficient, whereas the remaining coefficients tend to a linear dependence on x except close to $x = 0$ and $x = 0.5$.

The calculations were carried out by numerical minimization of $\Delta G_{ss}(x)$ with respect to p and q using the FindMinimum function of Mathematica 4.0. Only positive values of p_i and q_i were considered, hence in this context the γ_{100} term is redundant and for simplicity its value was set to zero, leaving only γ_{200} and γ_{220} as the unknown coefficients.

The problems of identifying the absolute free energy minimum in six dimensional polarization space are not trivial, hence solutions were sought which corresponded to the most likely phases in Table II. For each temperature and PbTiO_3 molar fraction, the local minima in $\Delta G_{ss}(x)$ were systematically identified for $p_i > 0$ and $q_i > 0$, with the constraints shown in Table I, for the following phases: cubic, tetragonal, orthorhombic, rhombohedral, monoclinic M_A and monoclinic M_C . The energies of the minima were then compared to define the stable state.

Lattice parameters were calculated for the case of $\text{PbZr}_{0.52}\text{Ti}_{0.48}\text{O}_3$. The spontaneous strain matrix, σ , is calculated according to:

$$\sigma_{ij} = Q_{ijkl} P_k P_l \quad (6)$$

For reasons of symmetry, there are only three independent components of the electrostriction coefficient tensor Q , which in reduced notation are Q_{11} , Q_{12} and Q_{44} . Their values for $\text{PbZr}_{0.52}\text{Ti}_{0.48}\text{O}_3$, $Q_{11} = 0.0667$, $Q_{12} = -0.0197$ and $Q_{44} = 0.0567$, were derived by linear interpolation from those of the end-members, published by Haun.⁴⁾ These were used in preference to values interpolated from the full set of coefficients in the same reference. The adopted procedure assumes that the "true" electrostriction coefficients are "well-behaved" on passing through the morphotropic phase

boundary with no anomalous values.

The spontaneous strains are converted to the lattice parameters referenced to the pseudo-cubic axes, again using reduced notation, as follows:

$$a_p = b_p = a_0(\sigma_1 + 1), \quad c_p = a_0(\sigma_3 + 1), \quad (7)$$

$$\gamma_p = \pi/2 - \tan^{-1} \sigma_4, \quad \beta_p = \pi/2 + \tan^{-1} \sigma_5$$

where a_p , b_p , and c_p are the unit cell lengths, γ_p is the angle between the a - and b -axes, and β_p is the angle between the c -axis and the a - b plane. a_0 is the equivalent cubic lattice parameter extrapolated for the full temperature range from the data of Noheda¹⁰ in the paraelectric phase, giving:

$$a_0 = 4.0584 + T \times 2.9156 \times 10^{-5} \text{ \AA} \quad (8)$$

where T is temperature.

For the monoclinic phase, the transformation to the monoclinic lattice parameters (denoted by subscript m) is given by:

$$a_m = 2a_p / \sqrt{2(1 + \tan^2(\gamma_p/2))},$$

$$b_m = a_m \tan(\gamma_p/2), \quad c_m = c_p \cos(\beta_p - \pi/2), \quad (9)$$

$$\beta_m = \arccos[\cos(\beta_p) / \cos(\gamma_p/2)]$$

4. Results

Phase stabilities were determined as a function of γ_{200} and γ_{220} . In the examples discussed, only phases corresponding to cubic, tetragonal, rhombohedral and monoclinic M_A were found. Phase diagrams as a function of x and T are shown for various combinations of γ_{200} and γ_{220} in Figs. 2, 3, and 4.

For $\gamma_{200} = \gamma_{220} \leq 0$, there is only a single phase boundary at $T_0(x)$, between the cubic and monoclinic M_A phases, for all PbTiO_3 concentrations except the end-members. γ_{200} and γ_{220} must be in a certain range to avoid discontinuities as $x \rightarrow 0$ and $x \rightarrow 1$.

When both γ_{200} and γ_{220} exceed 2×10^8 , the appearance of the monoclinic phase is completely inhibited (see Fig. 2). The locus of the morphotropic boundary is independent of γ_{200} and γ_{220} and, well below T_0 , it is also almost independent of temperature, moving to slightly higher values of x with decreasing temperature, and extrapolating

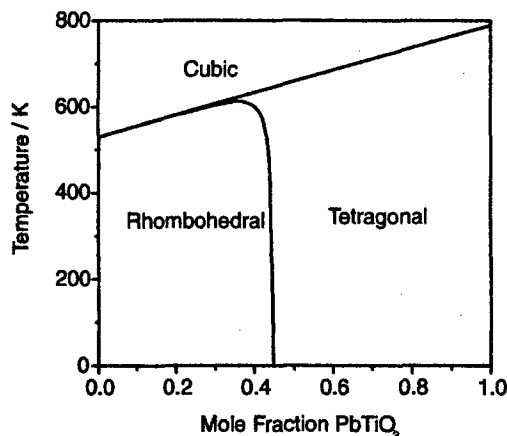


Fig. 2. Calculated PZT phase diagram for $\gamma_{200} = \gamma_{220} \rightarrow \infty$.

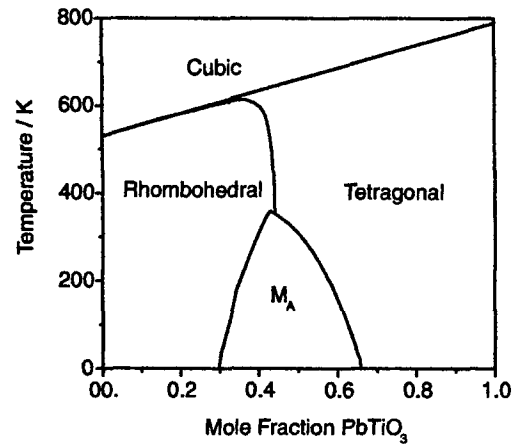


Fig. 3. Calculated PZT phase diagram for $\gamma_{200} = \gamma_{220} = 10^8$.

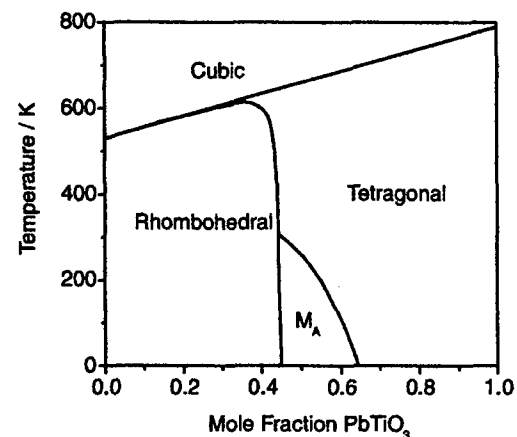


Fig. 4. Calculated PZT phase diagram for $\gamma_{200} = 6 \times 10^8$, $\gamma_{220} = 10^8$.

to $x = 0.45$ at 0 K. On approaching T_0 , the boundary curves sharply towards lower values of x ; the point at which the morphotropic phase boundary finally coincides with the cubic phase boundary is at $x = 0$. Hence a cubic-tetragonal transition occurs on cooling for all compositions with $x > 0$, however for compositions up to $x = 0.35$ the tetragonal phase is only stable for up to 5 K below T_0 , before transforming to the rhombohedral phase. The paraelectric-ferroelectric phase transition is 1st order for all values of x .

For intermediate values of the coupling coefficients, the M_A phase appears in the centre of the phase diagram. On increasing the γ values equally from zero, there is an almost symmetrical reduction in the width of the monoclinic phase field, yielding to the rhombohedral phase at low x and to the tetragonal phase at high x values. There is also a reduction in the maximum temperature of monoclinic stability, which occurs close to $x = 0.5$. Thus as the coupling energy is increased, the morphotropic phase boundary between the rhombohedral and tetragonal phases is revealed, with the M_A phase appearing as a wedge, with its apex close to the morphotropic phase boundary. The example shown in Fig. 3 is for $\gamma_{200} = \gamma_{220} = 10^8$, whilst that of Fig. 4 is for $\gamma_{200} = 6 \times 10^8$ and $\gamma_{220} = 10^8$, where the inequality in the coupling

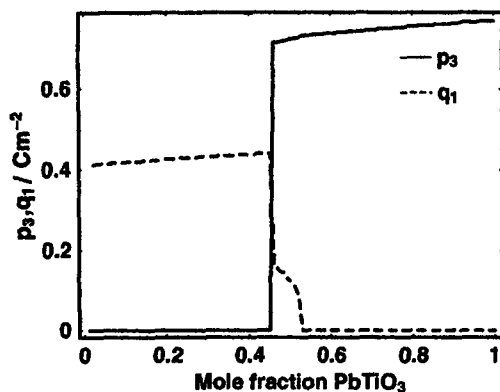


Fig. 5. Calculated values of p_3 and q_1 as a function of composition at 250 K for $\gamma_{200} = 6 \times 10^8$, $\gamma_{220} = 10^8$.

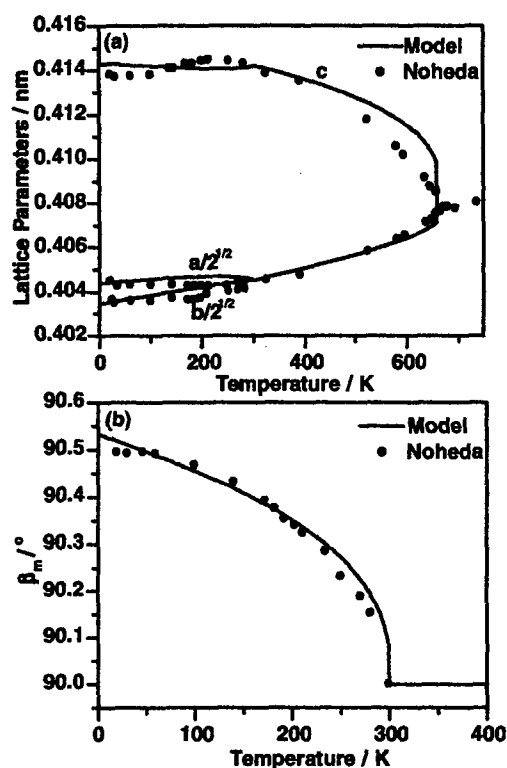


Fig. 6. Comparison of calculated and measured lattice parameters for $\text{PbZr}_{0.52}\text{Ti}_{0.48}\text{O}_3$.

coefficients results in the monoclinic phase favouring the "tetragonal" side of the morphotropic phase boundary. The corresponding values of p_3 and q_1 as a function of composition at 250 K are shown in Fig. 5.

The lattice parameters were calculated for $\text{PbZr}_{0.52}\text{Ti}_{0.48}\text{O}_3$. In keeping with Fig. 4 the value of γ_{200} was fixed at 6×10^8 to ensure that the M_A phase existed only on the Ti-rich side of the MPB. The value of γ_{220} was adjusted so that the tetragonal to monoclinic transition temperature was 300 K, as in the data of Noheda.¹⁹⁾ The values of $h(x)$ and $k(x)$ in eq. (5) were then adjusted to fit the magnitude of the calculated lattice parameters to the measured values. An acceptable fit was obtained for $h(x) = 0.73$, $k(x) = 0.77$. A

comparison of the calculated and measured lattice parameters is shown in Fig. 6.

5. Discussion

The model presented can reproduce some aspects of the PZT system with reasonable accuracy. It predicts the position of the morphotropic phase boundary, independent of any of the adjustable parameters, at $x = 0.45$, whereas the consensus of experimental data suggests the MPB lies at $x = 0.48$.

The range of existence of the monoclinic phase is controlled by the coupling energy between the two contributions to the polarization, p and q . At zero-field, p and q coexist only in the monoclinic phase. Although the model allows for the appearance of the three possible perovskite monoclinic phases, only the M_A phase was predicted by the model for PZT. In the examples here, only two coefficients were used to describe the coupling energy. By increasing the positive coupling energy between the parallel components of p and q (i.e. reducing the tolerance of the system to large values of p_i and q_i), whilst keeping the orthogonal coupling energy at moderate levels, the M_A phase is restricted to the PbTiO_3 -rich side of the morphotropic phase boundary. This is illustrated by the example of Fig. 4 in which the non-zero components of p and q in the monoclinic phase were p_3 , q_1 and $q_2 (= q_1)$.

The values of p and q obtained from the free energy minimization should be interpreted as macroscopic average values. In the tetragonal phase, whilst p is non-zero, q is zero and vice-versa in the rhombohedral phase. Only in the monoclinic phase are they simultaneously non-zero. It may be postulated that in the tetragonal and rhombohedral phases the non-zero parameter represents the polarization due to the major, homogeneous cation shifts whilst the parameter with zero value represents the average of the minor, random shifts. Thus the transition into the monoclinic state might be regarded as an order-disorder transition, in which either the p or q parameter passes from the disordered to the ordered state.

6. Conclusions

A thermodynamic model has been proposed to describe the properties of $\text{Pb}(\text{Zr},\text{Ti})\text{O}_3$ solid solutions, particularly in the region of the morphotropic phase boundary. The model is based on an expression in terms of two coupled polarization contributions, p and q , representing the preferred symmetries of compositions towards the two extremes of the solid solution. The model not only locates the composition of the morphotropic phase boundary with acceptable accuracy, but it also predicts the presence of a monoclinic phase around the morphotropic phase boundary and, with a limited number of adjustable parameters, agrees well with experiment. The comparison of the predicted and measured lattice parameters for the specific case of $\text{PbZr}_{0.52}\text{Ti}_{0.48}\text{O}_3$ is generally good. However, the relationship between the macroscopic polarization, P , and the parameters p and q has only been determined empirically for this composition.

Only in the monoclinic phase are both p and q non-zero; in the tetragonal and rhombohedral phases the equilibrium value of one of the parameters is always zero. It has been postulated that in the tetragonal and rhombohedral phases

the two polarization contributions correspond to the homogeneous and local random components of the cation displacements.

Acknowledgements

The authors wish to thank Professor L.E. Cross of The Pennsylvania State University for enlightening discussions and invaluable encouragement.

- 1) B. Jaffe, W. R. Cook and H. Jaffe: *Piezoelectric Ceramics* (Academic Press, London, 1971).
- 2) M. J. Haun, E. Furman, S. J. Jang and L. E. Cross: *Ferroelectrics* **99** (1989) 13.
- 3) M. J. Haun, E. Furman, H. A. McKinstry and L. E. Cross: *Ferroelectrics* **99** (1989) 27.
- 4) M. J. Haun, Z. Q. Zhuang, E. Furman, S. J. Jang and L. E. Cross: *Ferroelectrics* **99** (1989) 45.
- 5) M. J. Haun, E. Furman, T. R. Halemane and L. E. Cross: *Ferroelectrics* **99** (1989) 55.
- 6) M. J. Haun, E. Furman, S. J. Jang and L. E. Cross: *Ferroelectrics* **99** (1989) 63.
- 7) A. F. Devonshire: *Adv. Phys.* **3** (1954) 85.
- 8) K. Abe, O. Furukawa and H. Imagawa: *Ferroelectrics* **87** (1988) 55.
- 9) T. Yamamoto and Y. Terashima: *Jpn. J. Appl. Phys.* **31** (1992) 3252.
- 10) B. Noheda, D. E. Cox, G. Shirane, J. A. Gonzalo, L. E. Cross and S. E. Park: *Appl. Phys. Lett.* **74** (1999) 2059.
- 11) D. L. Corker, A. M. Glazer, R. W. Whatmore, A. Stallard and F. Fauth: *J. Phys.: Condens. Matter* **10** (1998) 6251.
- 12) J. Frantti, J. Lappalainen, S. Eriksson, V. Lantto, S. Nishio, M. Kakihana, S. Ivanov and H. Rundlof: *Jpn. J. Appl. Phys.* **39** (2000) 5697.
- 13) I. Grinberg, V. R. Cooper and A. M. Rappe: *Nature* **419** (2002) 909.
- 14) J. Frantti, J. Lappalainen, V. Lantto, S. Nishio and M. Kakihana: *Jpn. J. Appl. Phys.* **38** (1999) 5679.
- 15) K. C. V. Lima, A. G. Souza Filho, A. P. Ayala, J. Mendes Filho, P. T. C. Freire, F. E. A. Melo, E. B. Araujo and J. A. Eiras: *Phys. Rev. B* **63** (2001) 184105.
- 16) D. Vanderbilt and M. H. Cohen: *Phys. Rev. B* **63** (2001) 094108.
- 17) L. Bellaiche, A. Garcia and D. Vanderbilt: *Phys. Rev. Lett.* **84** (2000) 5427.
- 18) E. K. H. Salje: *Acta. Cryst. A* **47** (1991) 452.
- 19) B. Noheda, J. A. Gonzalo, L. E. Cross, R. Guo, S.-E. Park, D. E. Cox and G. Shirane: *Phys. Rev. B* **61** (2000) 8687.

APPENDIX 4

Strain-gradient-induced electric polarization in lead zirconate titanate ceramics

Wenhui Ma^{a)}

Max-Planck-Institute of Microstructure Physics, Weinberg 2, D-06120 Halle, Germany

L. Eric Cross

Materials Research Laboratory, The Pennsylvania State University, University Park, Pennsylvania 16802

(Received 27 September 2002; accepted 4 March 2003)

Strain-gradient-induced polarization or flexoelectricity was investigated in unpoled soft lead zirconate titanate (PZT) ceramic where the texture symmetry ∞m forbids macropiezoelectricity. Even under high strain gradient (1 m^{-1}) the induced polarization is small ($1.6 \mu\text{C}/\text{m}^2$) at 20°C . Higher strain gradients induce ferroelastic poling and an additional extrinsic contribution to the flexoelectric coefficient μ_{12} raising the value from 0.5 to $2.0 \mu\text{C}/\text{m}$. Cooling through the Curie point (T_C) under maximum stress (80 MPa) where the peak permittivity ($\sim 20\,000$) could raise μ_{12} to $20 \mu\text{C}/\text{m}$, the equivalent electric field is still only $\sim 1 \text{ kV}/\text{m}$, inadequate to achieve significant ferroelectric poling. The situation may be different in thin PZT films where much larger strain gradients can occur. © 2003 American Institute of Physics. [DOI: 10.1063/1.1570517]

The well-known elastoelectric coupling effects include piezoelectric effect, electrostrictive effect, and Maxwell stress effect. Piezoelectric ceramics¹ and more recently single crystals² have demonstrated the capability for broad applications in sensor, actuator, and transducer devices. In soft polymers, it is shown recently that Maxwell stress effect (attractive forces between opposite charges on the electrodes) can generate ultrahigh strain responses and exhibit great potential for a variety of electromechanical device applications.³ All the earlier-mentioned physical effects, however, generally assume the situations of uniform stress or strain. In nature, there is elastoelectric coupling caused by inhomogeneous deformation where stress or strain gradient associated polarization effects (flexoelectric effects) need to be considered. Overall, mechanical stress or strain can generate electric polarization in a deformable dielectric material through the following two mechanisms:

$$P_i = d_{ijk}\sigma_{jk} + \mu_{ijkl} \frac{\partial \epsilon_{jk}}{\partial x_l}. \quad (1)$$

In Eq. (1) and thereafter Einstein summation convention is assumed ($i, j, k, l = 1, 2, 3$). The first term on the right-hand side refers to the well-known direct piezoelectric effect, where σ_{jk} is the stress uniformly distributed across the sample and d_{ijk} is the piezoelectric coefficient, a third-rank polar tensor. The second term on the right-hand side refers to the strain gradient ($\partial \epsilon_{jk} / \partial x_l$) induced polarization and μ_{ijkl} is the flexoelectric coefficient, a fourth-rank polar tensor. In centrosymmetric materials, $d_{ijk} = 0$, so the piezoelectric term in Eq. (1) can be eliminated, therefore

$$P_i = \mu_{ijkl} \frac{\partial \epsilon_{jk}}{\partial x_l}, \quad (2)$$

where P_i is the electric polarization induced solely by strain gradient.

When reviewing the history of flexoelectric investigations, it is noted that while the concept was originally formed in early 1960s,^{4,5} not until 1981 was such effect in crystalline solids given the name "flexoelectric."⁶ Based upon an ionic model,⁷ Tagantsev analyzed the flexoelectric effect and suggested possible larger effects in ferroelectrics. In soft polymers Marvan *et al.*⁸ observed flexoelectric coefficients of the order of 10^{-11} – $10^{-10} \text{ C}/\text{m}$. Up to now very little attention has been paid to test the magnitude of flexoelectric coefficients and the mechanism remains unclear. Recently we measured the flexoelectric coefficients (μ_{12}) in lead magnesium niobate (PMN)^{9,10} (a well-known relaxor ferroelectric material) and barium strontium titanate (BST)^{11,12} (a normal ferroelectric material). Both materials were tested in the phase region with macroscopic cubic symmetry, moreover the samples were measured in the form of a cantilevered beam so that any remnant piezoelectric contributions from the top and bottom halves of the beam would cancel. In this letter, we investigate the flexoelectric effect in a well-known lead zirconate titanate (PZT) piezoelectric ceramic in the ferroelectric phase by using a four-point bend fixture to generate a uniform strain gradient.

In this work several interesting questions were explored: (i) using a four point bending fixture is it possible to induce and measure a quasistatic flexoelectric polarization generated by μ_{12} ; (ii) is the flexoelectric polarization enhanced or inhibited by the onset of ferroelastic domain wall motion which will be evidenced by change of the flexural stiffness and the development of remnant curvature in the sample; and (iii) is it possible in soft PZT to reach levels of flexoelectric induced field sufficient to pole the ceramic into a piezoelectric form.

The samples used were unpoled PZT-5H ceramics (doped with La and Sn) fabricated by TRS Ceramics Company, State College, Pennsylvania. Dielectric measurements performed using an HP4284A LCR meter show a weak field permittivity of 2200 at 20°C and a strong but rounded dielectric maximum ($\epsilon_3 \approx 20\,000$) without little dispersion

^{a)}Electronic mail: mawenhui@mpi-halle.de

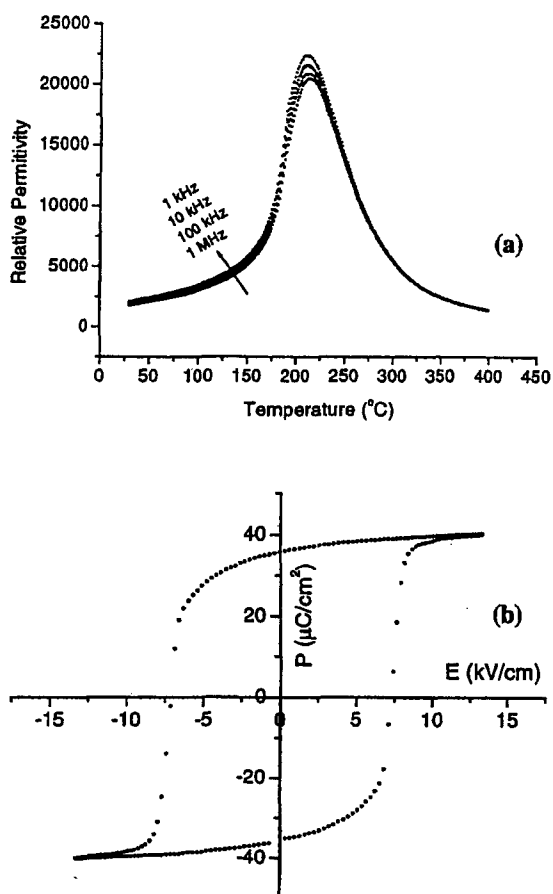


FIG. 1. (a) Weak field dielectric permittivity ($E \sim 10$ V/cm) as a function of frequency and temperature in the soft PZT-5H sample measured; (b) dielectric hysteresis (P vs E) in the soft PZT-5H composition.

over the frequency range of 1 kHz–1 MHz [Fig. 1(a)], suggesting a diffuse phase transition without strong relaxor character. Polarization hysteresis loops measured using a modified Sawyer–Tower circuit show remnant polarization of 35 $\mu\text{C}/\text{cm}^2$ and coercive field of 7 kV/cm [Fig. 1(b)] with no discernable bias. Young's modulus was measured to be 70 GPa by a dynamic resonance method.

A uniform strain gradient was generated using a four-point bend fixture schematically illustrated in Fig. 2(a). Samples for measurement had dimensions 60 mm long, 7 mm wide, and 3 mm thick. Surfaces were carefully polished and the samples were annealed at 700 °C to relieve surface stresses. Sputtered gold electrodes with dimensions 10×7 mm² were applied to upper and lower surfaces in the center of the beam. No residual piezoelectricity could be detected by Berlincourt d_{33} meter, and the impedance trajectory from 1 kHz to 1 MHz was free from evidence of piezoelectric resonance. The bend test was carried out according to the ASTM C-1161-94 by using an Instron machine model 4202 with a 10 kN load cell. Outer and inner spans of the fixture are 40 and 20 mm, respectively. The generated electric charge was detected by a Keithley 6517 electrometer that can resolve 10 fC and will measure up to 2.1 μC . Before measurement the electrometer was carefully calibrated for voltage burden and input offset current.

The stress distribution along the sample length direction

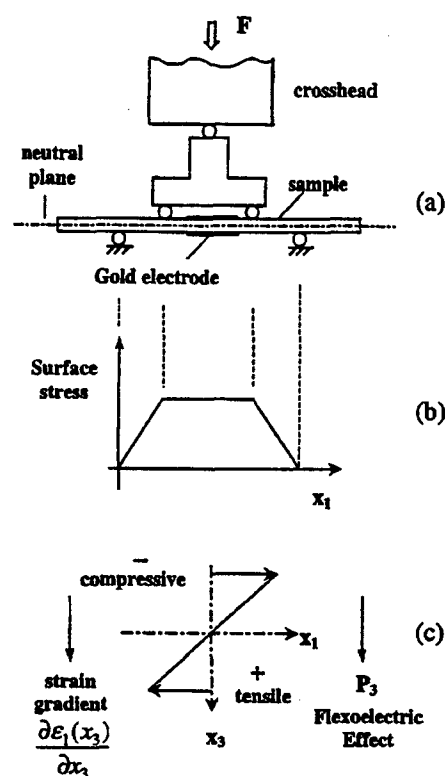


FIG. 2. Schematic illustration of strain gradient induced quasi-static polarization measurement, (a) typical four-point bending fixture; (b) stress distribution; (c) schematic of strain gradient and the induced polarization along the thickness of the sample.

(x_1) is shown in Fig. 2(b). Within the inner span the stress $\sigma_{11}(x_1)$ is uniform along the length, while along the thickness direction (x_3) the stress $\sigma_{11}(x_3)$ varies and there is a stress or strain gradient as shown by Fig. 2(c), which can generate electric polarization through the flexoelectric effect. Because the bar length is much greater than the bar thickness, we omit the shear stress and strain and only consider the principal stress and strain. Therefore, for simplification here only one suffix was used for describing the stress and strain tensors. The absolute value of surface stress was calculated using the following equation:

$$\sigma_1(x_3)|_{x_3=\pm d/2} = \frac{3FL}{4wd^2}, \quad (3)$$

where F is the load, w is the width, d is the thickness, and L is the outer span of the bend fixture.

The strain gradient in the thickness direction is given by

$$\frac{\partial \epsilon_1(x_3)}{\partial x_3} = \frac{12st}{L^2}, \quad (4)$$

where s is the crosshead speed and t the time gone by.

Figure 3 presents data on the surface stress versus strain curves for tests carried out at 1 and 0.2 mm/min crosshead speed. As shown in Fig. 3(a), the flexure strength is measured to be 85 MPa. The softening of the samples at certain stress/speed levels (e.g., around 30 MPa for 1 mm/min crosshead speed) we believe corresponds to the onset of ferroelastic domain motion. As expected in PZT the sample becomes softer at lower loading rates due to the relaxational nature of

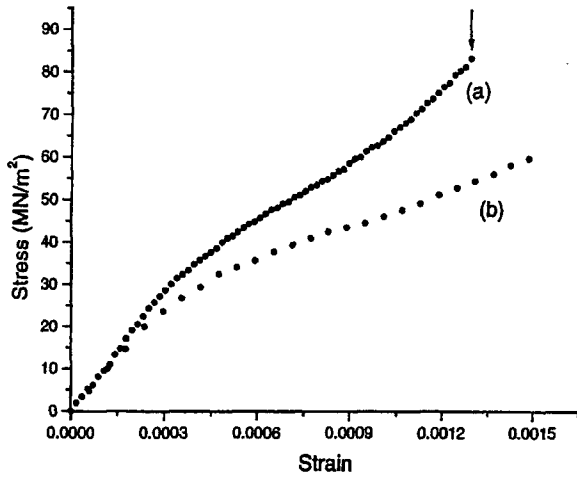


FIG. 3. Surface stress as a function of strain measured at two different crosshead speeds on PZT-5H bar, (a) 1 mm/min crosshead speed (the arrow indicates the level of stress at which the sample broke); (b) 0.2 mm/min crosshead speed.

ferroelastic domain switching. That ferroelastic switching has occurred at the higher loading levels is evident by a static remnant curvature in the sample after testing.

Flexoelectric polarization versus strain gradient is displayed in Fig. 4. It is clear that the behavior is not linear, showing a low-gradient and high-gradient linear behavior but of different slope. The changeover occurs at the gradient $\sim 0.3 \text{ m}^{-1}$ corresponding to the onset of ferroelastic switching. At very small strain level, the sample is only subjected to elastic deformation, so the measured electric polarization response represents the intrinsic flexoelectric effect. The low-gradient slope corresponds to a flexoelectric coefficient $\mu_{12} \approx 0.5 \mu\text{C/m}$, and the high-gradient slope takes $\mu_{12} \approx 2.0 \mu\text{C/m}$ showing that ferroelastic domain wall motion aids the response.

The measured flexoelectric polarization is very small compared to the remnant polarization, only $1.6 \mu\text{C/m}^2$ at a strain gradient of 1 m^{-1} . By using a relative permittivity value of $\epsilon_r = 2200$ (at 1 kHz), we figure out that a strain gradient of 1 m^{-1} is equivalent to an electric field of 100 V/m, which is obviously too small compared to the coercive field. In high-permittivity ferroelectrics we may expect from elementary theory of flexoelectricity⁷ that μ_{ij} be proportional to dielectric susceptibility χ_{ij} following a relation:¹¹

$$\mu_{ij} = \gamma \chi_{ij} \frac{e}{a}, \quad (5)$$

where γ is a constant of value close to unity. For the PZT unpoled ceramic at low gradient levels the normalized flexoelectric coefficients μ_{12}/χ_{22} at 20°C is 0.23 nC/m giving $\gamma \approx 0.57$. In PMN from our earlier study,^{9,10} μ_{12}/χ_{22} is 0.26 nC/m giving $\gamma \approx 0.65$, both in reasonable accord with the elementary theory. For BST ceramic at 25°C , however, $\mu_{12}/\chi_{22} \approx 3.72 \text{ nC/m}$ yielding a value $\gamma = 9.3$ ¹¹ much higher than those in the lead-based systems.

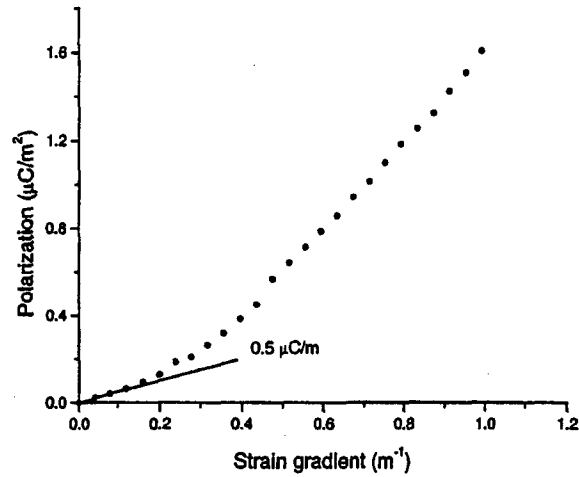


FIG. 4. Polarization vs strain gradient for an unpoled PZT-5H sample induced during a four-point bend test carried out at a crosshead speed of 0.2 mm/min.

It may be noted that in earlier investigations of the thermopolarization effects Strukov *et al.*¹³ found exceedingly high values for the normalized thermopolarization coefficient (b_{ij}^0) in triglycine sulfate which they attributed to the order-disorder nature of the ferroelectric phase change in this compound. We note that in $\text{Ba}_x\text{Sr}_{1-x}\text{TiO}_3$,¹³ there is strong evidence of a local order-disorder component between polarization vectors in the unit cell. It will be interesting to measure μ_{12} in potassium niobate tantalate, where again order-disorder has been identified,¹⁴ to see if the coefficients are again anomalously large.

In conclusion, the PZT ceramic does exhibit modest flexoelectricity and ferroelastic domain wall motion enhances the response, but it is not possible in our samples using stress levels up to the full fracture strength to induce ferroelectric poling, although ferroelastic poling was patently obvious.

In the PZT thin films epitaxially grown on lattice-mismatched substrates the strain gradient between surfaces and strain-relieving dislocations can be exceedingly large and the flexoelectric effects could be of major importance in these systems.

¹B. Jaffe, W. Cook, and H. Jaffe, *Piezoelectric Ceramics* (Academic, New York, 1971).

²S. Park and T. R. ShROUT, *J. Appl. Phys.* **82**, 1804 (1997).

³R. Pelrine, R. Kornbluh, Q. Pei, and J. Joseph, *Science* **287**, 836 (2000).

⁴V. S. Mashkevich and K. B. Tolpygo, *Sov. Phys. JETP* **5**, 435 (1957).

⁵Sh. M. Kogan, *Sov. Phys. Solid State* **5**, 2069 (1964).

⁶V. L. Indenbom, E. B. Loginov, and M. A. Osipov, *Sov. Phys. Crystallogr.* **26**, 656 (1981).

⁷A. K. Tagantsev, *Sov. Phys. JETP* **61**, 1246 (1985).

⁸M. Marvan and A. Havránek, *Prog. Colloid Polym. Sci.* **78**, 33 (1988).

⁹W. Ma and L. E. Cross, *Appl. Phys. Lett.* **78**, 2920 (2001).

¹⁰W. Ma and L. E. Cross, *Appl. Phys. Lett.* **79**, 4420 (2001).

¹¹W. Ma and L. E. Cross, *Appl. Phys. Lett.* **81**, 3440 (2002).

¹²B. H. Strukov, A. V. Dautyan, E. L. Sorkin, and K. A. Minaeva, *Bull. Acad. Sci. USSR, Phys. Ser.* **49**, 276 (1985).

¹³O. Tikhomirov, H. Jiang, and J. Levy, *Appl. Phys. Lett.* **77**, 2048 (2000).

¹⁴G. A. Samara and L. A. Boatner, *Phys. Rev. B* **61**, 3889 (2000).

APPENDIX 5

Flexoelectric effect in ceramic lead zirconate titanate

Wenhui Ma^{a)}

Department of Physics, Shantou University, Shantou, Guangdong 515063, People's Republic of China

L. Eric Cross

Materials Research Laboratory, Pennsylvania State University, University Park, Pennsylvania 16802

(Received 7 September 2004; accepted 30 December 2004; published online 11 February 2005)

Mechanical strain gradient generated electric polarization or flexoelectric effect was investigated in unpoled lead zirconate titanate (PZT) ceramics in the ferroelectric state by using a cantilevered beam based approach. Flexoelectric coefficient μ_{12} at room temperature was measured to be $1.4 \mu\text{C}/\text{m}$ in the PZT ceramic at small level of strain gradient. Temperature-dependent experimental investigations clearly showed that high dielectric permittivity in the ferroelectrics enhanced flexoelectric polarization: essentially a linear relation was found to exist between μ_{12} and dielectric susceptibility χ at lower permittivity level (2100–2800), while μ_{12} versus χ curve started to deviate from the straight line at the $\chi \sim 2800$ and nonlinear enhancement of μ_{12} with χ was observed, with μ_{12} value reaching 9.5 at $\chi \sim 11\,000$. The nonlinearity in the flexoelectric effect was associated with domain-related processes. It is suggested that flexoelectric effect can have a significant impact on epitaxial ferroelectric thin films and mesoscopic structures. © 2005 American Institute of Physics. [DOI: 10.1063/1.1868078]

Flexoelectric effect is the coupling between mechanical strain gradient and electric polarization and can be described by

$$P_i = \mu_{ijkl} \frac{\partial \varepsilon_{ij}}{\partial x_k}, \quad (1)$$

where P_i is the flexoelectric polarization, μ_{ijkl} the flexoelectric coefficient, ε_{ij} the elastic strain, and x_k the position coordinate. μ_{ijkl} is a fourth-rank polar tensor and therefore has nonzero components in dielectric solids of any crystal symmetry. Theoretical estimations predicted that flexoelectric coefficients in simple dielectrics are generally small (of the order e/a or $\sim 10^{-10} \text{ C}/\text{m}$, where e is the electron charge and a the dimension of unit cell).^{1–3} Earlier experimental work on polymers⁴ supported the theoretical predictions. Recently we developed a cantilevered beam based approach⁵ to perform reliable measurements of flexoelectric effect. Experimental investigations using the approach showed that flexoelectric coefficients in the ferroelectric materials are many orders of magnitude higher (10^{-6} to $10^{-4} \text{ C}/\text{m}$).^{6,7} The cantilevered beam based approach is generally used for dynamic flexoelectric measurements at lower level of strain gradient. To investigate the flexoelectric effect at higher strain gradient we developed another approach based on four-point bending and used the approach in static measurements of the flexoelectric coefficients in ferroelectric materials.⁸

Based on flexoelectric effect, ideas for developing new types of piezoelectric composites⁹ were proposed, where none of the components is piezoelectric. If we understood flexoelectric effect well and there were database of flexoelectric coefficients available, a range of properly engineered flexoelectric composite structures could provide completely new piezoelectric capability.

Ferroelectric thin films and mesoscopic structures have exhibited a lot of potential for device applications such as

FERAM and MEMS.¹⁰ Misfit strain certainly exists at the interface between the epitaxially grown thin film ferroelectric and the substrate or electrode material. Nonuniform relaxation of the misfit strain in the thin films can lead to strain gradient,¹¹ which can then influence the dielectric and polarization behaviors of the ferroelectrics. Experimentally, some new phenomena recently observed in the thin film ferroelectrics were suggested to be due to the consequences of flexoelectric effect, such as the mechanical stress induced imprint in PZT capacitor structures¹² and pyroelectricity in highly stressed quasiamorphous BaTiO_3 films.¹³ Recently a phenomenological model¹⁴ of flexoelectricity was also proposed, showing that flexoelectric effect could play an important role in reducing the dielectric maximum in ferroelectric thin films. Ferroelectric PZT based ceramics and thin films are a family of technologically important functional materials.¹⁵ In this letter, we report experimental investigations of the flexoelectric effect in ceramic PZT.

The PZT samples are the same as those used before,⁸ with dimensions 60 mm long, 7 mm wide, and 3 mm thick. Flexoelectric effect was investigated using the cantilevered beam based approach and the system used for the flexoelectric measurement is identical to that used in earlier studies of barium strontium titanate (BST) and lead magnesium niobate (PMN).^{5–7} A series of 3-mm-diam thin sputtered gold electrodes were prepared on the sample surface along the bar length. The ceramic bar sample is rigidly clamped at one end and driven into transverse vibration at 1 Hz by a small moving coil loudspeaker. The ac mechanical strain as a function of position along the bar was measured using a Microstrain™ DVRT (differential variable reluctance transducer) and the generated current was measured using an SR830 DSP Lock-in amplifier. The measured mode shape was then used to calculate the strain gradient at positions of the electrodes using the free bar model.⁵

For an unpoled PZT ferroelectric ceramic at the morphotropic phase boundary, although individual grains may have lower symmetry (tetragonal or rhombohedral) which permits

^{a)}Electronic mail: mawenhui_usa@yahoo.com

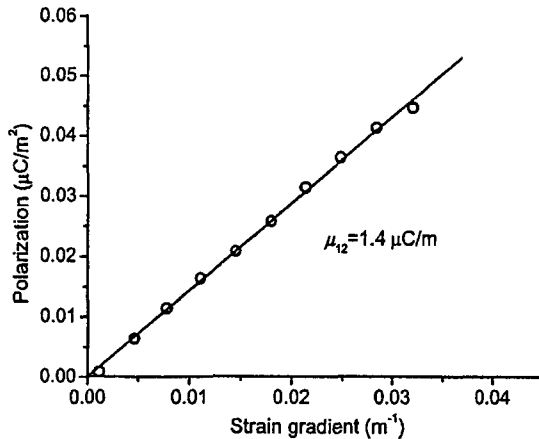


FIG. 1. Room temperature flexoelectric polarization vs strain gradient for unpoled PZT ceramic measured at 1 Hz near the clamped end ($x_1/L=0.18$) of the cantilevered beam.

piezoelectricity, in the volume of the ceramic one may expect a macroscopic symmetry of $\infty\infty m$, so the nonzero components for the flexoelectric tensor μ_{ijkl} should be μ_{1111} , μ_{1122} , and μ_{1212} , or in matrix notation μ_{11} , μ_{12} , and μ_{44} . In the unpoled PZT ceramic, no residual piezoelectricity could be detected by Berlincourt d_{33} meter and no evidence of piezoelectric resonance could be found in the impedance trajectory from 1 kHz to 1 MHz. By using the cantilevered beam based approach, any remnant piezoelectricity from the top and bottom halves of the sample bar is well balanced during the flexoelectric measurements. That some unbalance was affecting the measured value was however ruled out by the simple experiment of inverting the sample and noting that the measured signal did not change either in amplitude or phase. Clearly in ferroelectrics the free surface breaks the symmetry of the bulk and may affect the polarization behavior, however, in the present studies the effect of surface ferroelectricity¹⁶ is unlikely due to the highly conductive metal electrodes on both free surfaces. Thus we believe that the measured electric polarization P_3 is solely due to the strain gradient in the x_3 thickness direction and can be written as

$$P_3 = \mu_{12} \frac{\partial \epsilon_{13}}{\partial x_1}. \quad (2)$$

Figure 1 presents the room temperature (24 °C) flexoelectric polarization as a function of the transverse strain gradient obtained near the clamped end ($x_1/L=0.18$) of the bar by using the cantilevered beam based dynamic approach. It is clear that the generated electric polarization is linearly proportional to the elastic strain gradient and the slope of the line gives a magnitude of μ_{12} of 1.4 $\mu\text{C}/\text{m}$, close to the early data of 0.5 $\mu\text{C}/\text{m}$ ⁸ obtained by static measurements using a four-point bend fixture. Figure 2 presents the measurements of μ_{12} in the PZT ceramic as a function of temperature (24–180 °C). When heating up from room temperature (24 °C), unexpectedly the μ_{12} initially drops before it becomes stabilized at 40 °C, then flexoelectric polarization basically keeps flat at the temperature range of 40–70 °C but starts to rise prominently at 70 °C.

Clearly high dielectric permittivity in the ferroelectric materials can enhance flexoelectric coefficients^{6,7} and μ_{12} can be related to dielectric susceptibility χ by

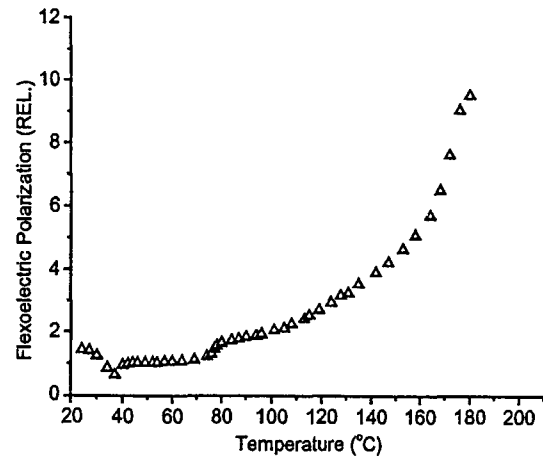


FIG. 2. Flexoelectric polarization (arbitrary unit) measured as a function of temperature in the ferroelectric state for the unpoled PZT ceramic.

$$\mu_{12} = \gamma \chi \frac{e}{a}, \quad (3)$$

where γ is a scaling factor. In order to evaluate the impact of dielectric property on the flexoelectric effect, dielectric spectra from the PZT ceramic were measured and shown in Fig. 3, where a strong but rounded dielectric maximum suggests a diffuse phase transition around 220 °C. The plot of μ_{12} versus χ is shown in Fig. 4. Comparison of experimental data obtained in BST, PZT, and PMN reveals that, at similar level of relative dielectric permittivity, μ_{12} in BST is roughly one order of magnitude higher than that in PMN or PZT. It remains unclear as to why the Pb-based ferroelectrics should have lower values of flexoelectric coefficients.

As shown in Figs. 2 and 4, the initial drop of μ_{12} with χ is unexpected but may correspond to the increase of loss tangent (Fig. 3) in the temperature range (24–50 °C). A linear relation between μ_{12} and χ with $\gamma=1$ is seen to exist in the χ range of 2100–2800 (or temperature range of 40–74 °C). The μ_{12} versus χ curve deviates from the $\gamma=1$ line at the $\chi \sim 2800$ and the rise of μ_{12} with χ becomes essentially nonlinear, with μ_{12} reaching 9.5 at $\chi \sim 11\,000$.

Nonlinearity in flexoelectric coefficient was found in temperature-dependent experimental investigations of BST,⁷ where μ_{12} was raised to 100 $\mu\text{C}/\text{m}$ when approaching the dielectric peak from the paraelectric state. Such nonlinear

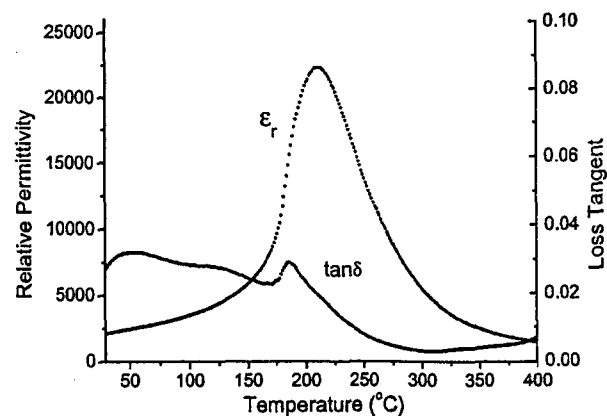


FIG. 3. Dielectric permittivity and loss tangent for the unpoled PZT ceramic measured as function of temperature at a frequency of 1 kHz.

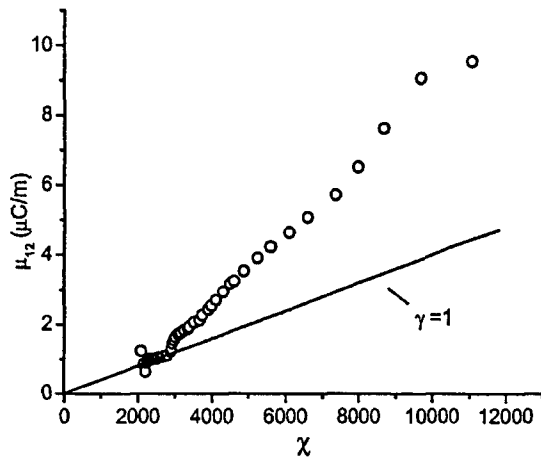


FIG. 4. Flexoelectric coefficient μ_{12} vs dielectric susceptibility χ for the unpoled PZT ceramic. The dotted line shows a linear relation between μ_{12} and χ at lower level of dielectric permittivity with a $\gamma=1$.

enhancement was suggested to be due to the survival of some ferroelectric domains in the BST ceramic above the Curie transition temperature T_C . In the previous studies of ceramic PMN,⁶ nonlinear enhancement of μ_{12} with χ was also observed and found to be closely associated with the pre-existing polar microdomains in this prototypic relaxor ferroelectric material.¹⁷ Apart from the nonlinear behavior of flexoelectric coefficient with dielectric permittivity, previous static investigations⁸ in PZT ceramic revealed nonlinear relation between flexoelectric coefficient and mechanical strain gradient, where the jump of μ_{12} from $0.5 \mu\text{C}/\text{m}$ at lower strain gradients to $2 \mu\text{C}/\text{m}$ at much higher strain gradients was shown to be associated with the onset of domain wall motion induced by the very high level of inhomogeneous strain achievable with the four-point bend fixture. As discussed earlier, nonlinearity in the flexoelectric effect can be tentatively attributed to the domain-related processes in ferroelectrics and the scaling factor γ in Eq. (3) depends on the materials investigated, the level of dielectric permittivity, and the magnitude of strain gradient. The experimental findings of nonlinear phenomena are in good agreement with the theoretical studies by Catalan *et al.*,¹⁴ where it was shown that flexoelectric coefficient is only a linear function of the strain gradient or permittivity when the induced flexoelectric polarization is small. In addition to the extrinsic influence of domain-related processes discussed earlier, it is possible that a part of the nonlinearity in the flexoelectric effect may also

be of intrinsic origin as shown in the theoretical work of Catalan *et al.*¹⁴

In epitaxial ferroelectric thin films and mesoscopic structures, Curie phase transition temperature T_C or dielectric peak can be adjusted to around room temperature where ultrahigh dielectric permittivity becomes available, by appropriate selection of lattice misfit and film thickness as shown in recent theoretical¹⁸ and experimental¹⁹ studies. Likewise, strain gradient in these ferroelectric structures can also be adjusted by tailoring the structure dimensions or controlling the relaxation of the misfit strain. The nonlinear enhancement of flexoelectric coefficients with the dielectric permittivity and strain gradient can lead to a significant impact of flexoelectric effect in these properly engineered thin film ferroelectric heterostructures.

In summary, flexoelectric effect was investigated in the ferroelectric state of unpoled lead zirconate titanate (PZT) ceramics. Temperature-dependent flexoelectric investigations showed that μ_{12} essentially increases with relative dielectric permittivity and the nonlinear phenomenon was found at higher level of dielectric permittivity, which is suggested to be associated with domain-related processes.

¹Sh. M. Kogan, *Sov. Phys. Solid State* **5**, 2069 (1964).

²V. L. Indenbom, E. B. Loginov, and M. A. Osipov, *Sov. Phys. Crystallogr.* **26**, 656 (1981).

³A. K. Tagantsev, *Sov. Phys. JETP* **61**, 1246 (1985).

⁴M. Marvan and A. Havránek, *Prog. Colloid Polym. Sci.* **78**, 33 (1988).

⁵W. Ma and L. E. Cross, *Appl. Phys. Lett.* **78**, 2920 (2001).

⁶W. Ma and L. E. Cross, *Appl. Phys. Lett.* **79**, 4420 (2001).

⁷W. Ma and L. E. Cross, *Appl. Phys. Lett.* **81**, 3440 (2002).

⁸W. Ma and L. E. Cross, *Appl. Phys. Lett.* **82**, 3293 (2003).

⁹J. Fousek, L. E. Cross, and D. B. Litvin, *Mater. Lett.* **39**, 287 (1999).

¹⁰N. Setter and R. Waser, *Acta Mater.* **48**, 151 (2000).

¹¹P. Imperatori, F. J. Lamelas, and P. H. Fuoss, *J. Appl. Phys.* **80**, 5723 (1996).

¹²A. Gruverman, B. J. Rodriguez, A. I. Kingon, R. J. Nemanich, A. K. Tagantsev, J. S. Cross, and M. Tsukada, *Appl. Phys. Lett.* **83**, 728 (2003).

¹³V. Lyahovitskaya, I. Zon, Y. Feldman, S. R. Cohen, A. K. Tagantsev, and I. Lubomirsky, *Adv. Mater. (Weinheim, Ger.)* **15**, 1826 (2003).

¹⁴G. Catalan, L. J. Sinnamon, and J. M. Gregg, *J. Phys.: Condens. Matter* **16**, 2253 (2004).

¹⁵B. Jaffe, W. Cook, and H. Jaffe, *Piezoelectric Ceramics* (Academic, New York, 1971).

¹⁶A. M. Bratkovsky and A. P. Levanyuk, arXiv: cond-mat/0402100.

¹⁷L. E. Cross, *Ferroelectrics* **76**, 241 (1987).

¹⁸N. A. Pertsev, A. G. Zembilgotov, and A. K. Tagantsev, *Phys. Rev. Lett.* **80**, 1988 (1998).

¹⁹J. H. Haeni, P. Irvin, W. Chang, R. Uecker, P. Reiche, Y. L. Li, S. Choudhury, W. Tian, M. E. Hawley, B. Craigo, A. K. Tagantsev, X. Q. Pan, S. K. Streiffer, L. Q. Chen, S. W. Kirchoefer, J. Levy, and D. G. Schlom, *Nature (London)* **430**, 758 (2004).

APPENDIX 6

Intermediate states in $\text{Pb}(\text{B}_{1/3}^{\text{I}}\text{B}_{2/3}^{\text{II}})\text{O}_3\text{-PbTiO}_3$ ferroelectric single crystals

A. Amin and L. E. Cross

Optical and dielectric studies of oriented and poled single crystal compositions on both sides of the morphotropic phase boundary in $(1-x)\text{Pb}(\text{Zn}_{1/3}\text{Nb}_{2/3})\text{O}_3\text{-}x\text{PbTiO}_3$ have revealed an intermediate, metastable, ferroelectric orthorhombic state (F_{O}) in a narrow composition range between the ferroelectric rhombohedral (F_{R}) and tetragonal (F_{T}) phases, which has also been identified from pyroelectric and dielectric data. Recently published structural data confirm this orthorhombic state for $0.08 < x < 0.11$. Similarly, dielectric studies and electromechanical measurements on rhombohedral $\text{Pb}(\text{Mg}_{1/3}\text{Nb}_{2/3})\text{O}_3\text{-PbTiO}_3$ single crystals have revealed an intermediate, metastable F_{O} state at high temperature. Structural evidence of the orthorhombic phase in this system has also recently been reported. In the present paper it is shown that a metastable orthorhombic state is always close to but unstable with respect to the $F_{\text{R}}\text{-}F_{\text{T}}$ degenerate states (morphotropy), as predicted by a phenomenological model for $A(\text{B}_{1-x}^{\text{I}}\text{B}_x^{\text{II}})\text{O}_3$ ferroelectrics. Conditions for stabilising the nearly degenerate F_{R} , F_{T} and F_{O} states in the $\text{Pb}(\text{B}_{1/3}^{\text{I}}\text{B}_{2/3}^{\text{II}})\text{O}_3\text{-PbTiO}_3$ single crystal system are discussed in terms of the energy function tensor coefficients. BCT/656

Keywords: Electromechanical properties, Ferroelectric single crystals, Intermediate states, Morphotropic phase boundary, Piezoelectric coefficient.

Dr Amin (aminah@npt.nuwc.navy.mil) is with the US Naval Sea Systems Command, Newport, RI 02841, USA and Professor Cross is at the Materials Research Laboratory, Pennsylvania State University, University Park, PA 16802, USA. Paper presented at the symposium '55 years of ferroelectrics' held in Leeds, UK on 21–23 September 2003. Manuscript accepted 24 February 2004.

© 2004 IoM Communications Ltd. Published by Maney for the Institute of Materials, Minerals and Mining.

INTRODUCTION

The large longitudinal piezoelectric coefficient d_{33} (≈ 1500 pC N $^{-1}$) and electromechanical coupling factor k_{33} (≈ 0.92) of $\langle 001 \rangle$ oriented and poled multidomain single crystals of $0.91\text{Pb}(\text{Zn}_{1/3}\text{Nb}_{2/3})\text{O}_3\text{-}0.09\text{PbTiO}_3$ were first reported by Kuwata *et al.*^{1,2} who examined relaxor ferroelectric single crystals by a standard resonance–antiresonance method under a low drive field level, significantly below that required to induce saturation in electrically induced strain. In the relaxor–ferroelectric system $(1-x)\text{Pb}(\text{B}_{1/3}^{\text{I}}\text{B}_{2/3}^{\text{II}})\text{O}_3\text{-}x\text{PbTiO}_3$, where $\text{B}^{\text{I}} = \text{Mg, Zn or Sc}$ and $\text{B}^{\text{II}} = \text{Nb}$, lead zinc niobate–lead titanate (PZN–PT) and lead magnesium niobate–lead titanate (PMN–PT) have attracted much attention in recent years.^{3,4} Research has focused on com-

positions close to the morphotropic phase boundary (MPB) between rhombohedral and tetragonal ferroelectric states. Unprecedented strain levels in excess of 1.5% have been induced in rhombohedral morphotropic PZN–PT 92/8 and PMN–PT 70/30 single crystals with an electric field $E \approx 3$ MV m $^{-1}$ applied along the $[001]$ axis.^{3,4} These strain levels are about an order of magnitude larger than in conventional lead zirconate titanate (PZT) piezoceramics.

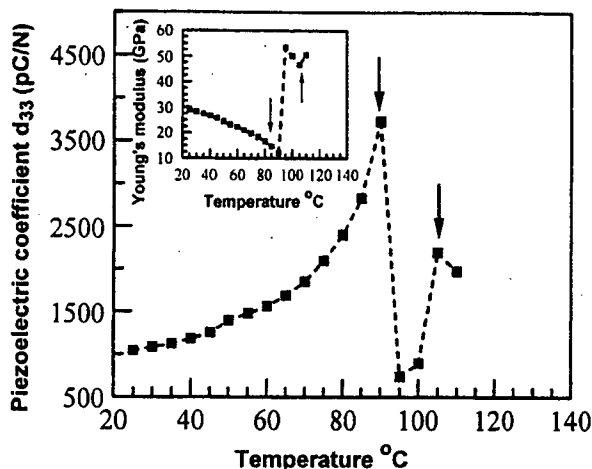
Because of their high electromechanical coupling, single crystal compositions offer the potential for both broadband and high acoustic energy density when compared with standard PZT8. They show great promise in medical ultrasound imaging systems, underwater sonar projectors and receiving arrays. There is the potential for a vast improvement in the axial resolution and contrast of medical ultrasound and sonar systems as a result of the broadband capabilities of single crystals. The origin of this enhanced electromechanical behaviour has been attributed to an electrically induced rhombohedral ferroelectric F_{R} (space group R3m) to tetragonal ferroelectric F_{T} (space group P4mm) phase transformation.^{3–7} The F_{R} phase has a much smaller c/a ratio than F_{T} , and accordingly under field the large c/a ratio change results in enhanced electrically induced strain.

INTERMEDIATE STATES

Optical studies augmented by high temperature dielectric measurements on $[001]$, $[110]$ and $[111]$ oriented and poled compositions, on both sides of the MPB in $(1-x)\text{Pb}(\text{Zn}_{1/3}\text{Nb}_{2/3})\text{O}_3\text{-}x\text{PbTiO}_3$ system, have revealed the existence of an intermediate, metastable, orthorhombic state for the poled multidomain $[110]$ and poled monodomain $[111]$ orientations, but not for poled multidomain $[001]$.⁸ Synchrotron X-ray powder diffraction measurements confirm that an intermediate ferroelectric orthorhombic state F_{O} (space group Bmm2) exists for a narrow composition range ($0.08 < x < 0.11$) with near vertical phase boundaries on both sides of the MPB.⁹ For $x = 0.08$ and 0.09 an electrically induced orthorhombic state has been reported.^{10–12}

Dielectric and optical studies of $[110]$ oriented and poled ferroelectric rhombohedral (F_{R}) multidomain $0.67\text{Pb}(\text{Mg}_{1/3}\text{Nb}_{2/3})\text{O}_3\text{-}0.33\text{PbTiO}_3$ crystals revealed a transformation sequence on heating to an intermediate ferroelectric orthorhombic state (F_{O}) near 80°C, followed by $F_{\text{O}}\text{-}F_{\text{T}}$ transition at 100°C. Transition to the cubic state occurred at 145°C.¹³ On the other hand at a higher poling field (> 5 kV cm $^{-1}$) an orthorhombic monodomain F_{O} state was induced at room temperature. The $F_{\text{O}}\text{-}F_{\text{T}}$ transition of the monodomain state occurred at 80°C, much lower than for the multidomain state. The varied temperature range of existence of the intermediate F_{O} state suggested metastability.¹³ No evidence of an intermediate F_{O} state was found for the poled multidomain $[100]$ crystal.

Further evidence of an intermediate high temperature F_{O} state between the F_{R} and F_{T} phases has recently been reported for $0.70\text{Pb}(\text{Mg}_{1/3}\text{Nb}_{2/3})\text{O}_3\text{-}0.30\text{PbTiO}_3$ single



1 Variation of piezoelectric coefficient d_{33} with temperature for poled multidomain [110] oriented $0.70\text{Pb}(\text{Mg}_{1/3}\text{Nb}_{2/3})\text{O}_3$ - 0.30PbTiO_3 single crystal: arrows indicate ferroelectric rhombohedral F_R -ferroelectric orthorhombic F_O transition ($\approx 85^\circ\text{C}$) and ferroelectric orthorhombic F_O -ferroelectric tetragonal F_T transition ($\approx 100^\circ\text{C}$); Curie temperature of this composition is $\approx 125^\circ\text{C}$. Inset shows variation of Young's modulus with temperature near two ferroelectric transitions (data from Ref. 14)

crystals.¹⁴ Figure 1 plots longitudinal piezoelectric response versus temperature for the [110] oriented and poled multidomain crystal. The inset illustrates the temperature dependence of Young's modulus. The data in Fig. 1 are taken from Ref. 14, excluding the responses from the other two orientations for clarity. Note the excellent piezoelectric properties of the [110] oriented crystal. Arrows indicate the F_R - F_O transition near 85°C and the F_O - F_T transition near 100°C , with the Curie transition occurring at 125°C .¹⁴ The dielectric data are qualitatively similar to previously published results.¹³ The data suggest that the boundary between the F_R and F_M phases near 85°C has a thin orthorhombic sliver extending over 15°C . This supports the recent suggestion of mixed states in this system.¹⁵ No evidence of an intermediate F_O state was found for the poled multidomain [100] crystal. Simulations from first principles indicate that the transformation under electric field between F_R and F_T proceeds by rotation of the polarisation between $\langle 111 \rangle$ and $\langle 001 \rangle$ via an intermediate monoclinic or orthorhombic ferroelectric state.⁷ These results open up the interesting possibility that intermediate states may be responsible for the enhanced electromechanical performance.

Recent synchrotron X-ray powder diffraction experiments have revealed a new phase diagram for the $(1-x)\text{Pb}(\text{Mg}_{1/3}\text{Nb}_{2/3})\text{O}_3$ - $x\text{PbTiO}_3$ system.¹⁵ The proposed phase diagram is a complex landscape of phase mixtures. Morphotropic compositions $0.31 \leq x \leq 0.33$ have a monoclinic symmetry M_C (space group Pm) with the unique axis oriented along the pseudocubic [010] direction. For $x=0.31$ the symmetry is very close to orthorhombic, and it is possible for compositions with x between 0.30 and 0.31 to be entirely orthorhombic. In this case the transition between rhombohedral and monoclinic M_C phases will occur via the orthorhombic phase. For $x \leq 0.31$ the symmetry is rhombohedral, and for $x \geq 0.37$ it is tetragonal.

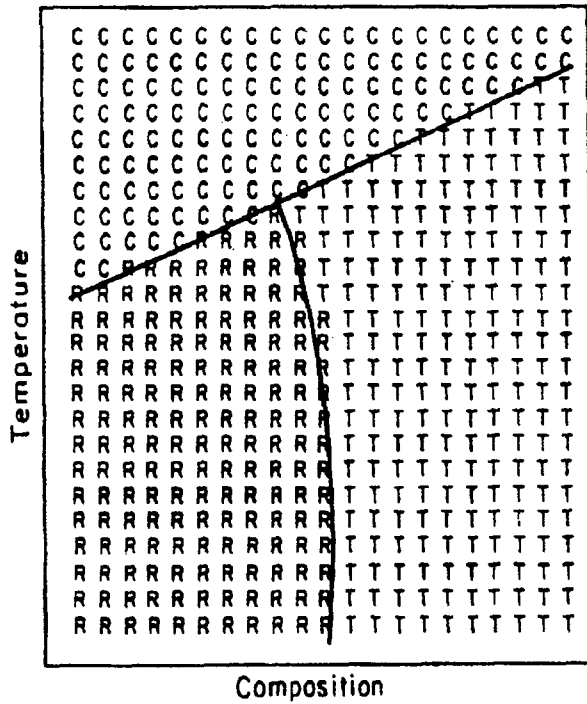
Powder diffraction patterns for the relaxor-ferroelectric system $(1-x)\text{Pb}(\text{B}_{1/3}\text{B}_{2/3}^{\text{II}})\text{O}_3$ - $x\text{PbTiO}_3$ are extremely difficult to analyse.^{9,15} Two major factors contribute to this complexity, and to the difficulty of unequivocal symmetry determination, especially for compositions close to the MPB. The first is inhomogeneity due to the concentration

gradient, which is typical of crystal growth from the melt of incongruently melting compositions, and the second is the broad diffraction maxima characteristic of (disordered) relaxor-ferroelectric systems. This complicates peak deconvolution of the overlapping or partially overlapping reflections common in pseudosymmetric structures, for example the F_R , F_T and F_O phases. To obtain sharp diffraction maxima, an electric field is applied to the crystal to induce an ordered state, and the powder pattern is then recorded for the ordered state.⁹ Conversely, the possibility of a field induced phase transition and of assigning a lower symmetry for mixed phase patterns also exists.

ENERGY FUNCTION

To account for the recently observed monoclinic phase in PZT, an extension of the Devonshire theory of perovskite ferroelectrics has been developed.¹⁶ In this model, the ground state energy is represented by an analytic function defined on the surface of a sphere and truncated at the eighth power of the order parameter. The order parameter in this case is the polarisation vector normalised to unity. The parameter space is thus a unit sphere spanned by the polar and azimuth angles α and β respectively, where $0 < \alpha < \pi$ and $0 < \beta < 2\pi$. The ferroelectric phases are obtained by numerically searching for constrained minima of energy as a function of orientation. The constraints are taken such that the order parameter must lie along a symmetry axis [001], [111] or [011] for ferroelectric tetragonal, rhombohedral and orthorhombic phases respectively, or in a symmetry plane (mirror) for the monoclinic ferroelectric phases. Three monoclinic solutions are admissible. These are denoted by M_A (Cm), M_B (Bm) and M_C (Pm), the space group symbol being given between parentheses. The polarisation vector is constrained in a mirror plane along [uuv] with $u < v$, [uuv] with $u > v$, or [0uv] for each of the monoclinic species respectively. A two dimensional representation of the ferroelectric phase diagram in terms of the linearly independent parameters α and β is obtained by mapping the unit sphere onto a plane. All six ferroelectric phases enumerated above are accessible by the eighth power model. This model can only describe transitions among the ferroelectric phases, and not transitions to the high temperature, higher symmetry phases. It cannot access the rhombohedral (R3m)-rhombohedral (R3c) transition, associated with condensation of the triply degenerate Brillouin zone corner R_{25} lattice mode observed in the PZT system. Besides, temperature, compositional, elastic, and electric variables are not explicit. To access a triclinic ferroelectric phase, a twelfth order model is required.

The observed metastable orthorhombic state in the single crystal $\text{Pb}(\text{Zn}_{1/3}\text{Nb}_{2/3})\text{O}_3$ - PbTiO_3 system and the high temperature orthorhombic state in single crystal $\text{Pb}(\text{Mg}_{1/3}\text{Nb}_{2/3})\text{O}_3$ - PbTiO_3 can be readily visualised, and further insights can be gained into these complex systems within the limitations of a sixth order theory. The energy landscape in terms of composition and temperature has been previously developed by the present authors and coworkers¹⁷⁻²⁰ for a generalised $\text{A}(\text{B}_{1-x}^{\text{I}}\text{B}_x^{\text{II}})\text{O}_3$ MPB phase diagram between ferroelectric-ferroelectric and ferroelectric-antiferroelectric end members. For the PZT system the theory predicts the position of the MPB as a function of composition and temperature and the rhombohedral (R3m)-rhombohedral (R3c) phase boundary associated with the triply degenerate Brillouin zone corner R_{25} lattice mode. Semiquantitatively, the single crystal-single domain dielectric, piezoelectric and elastic properties are accessible in terms of temperature, composition, stress¹⁹ and electric field.²⁰ The derived single crystal polarisation versus temperature results for the end member PbTiO_3 are for example within a few per cent of the published experimental results.¹⁷



2 Generalised $A(B_{1-x}^{I}B_x^{II})O_3$ phase diagram as computed from free energy minima of equation (1), showing equilibrium states and near vertical MPB between F_R and F_T states¹⁷

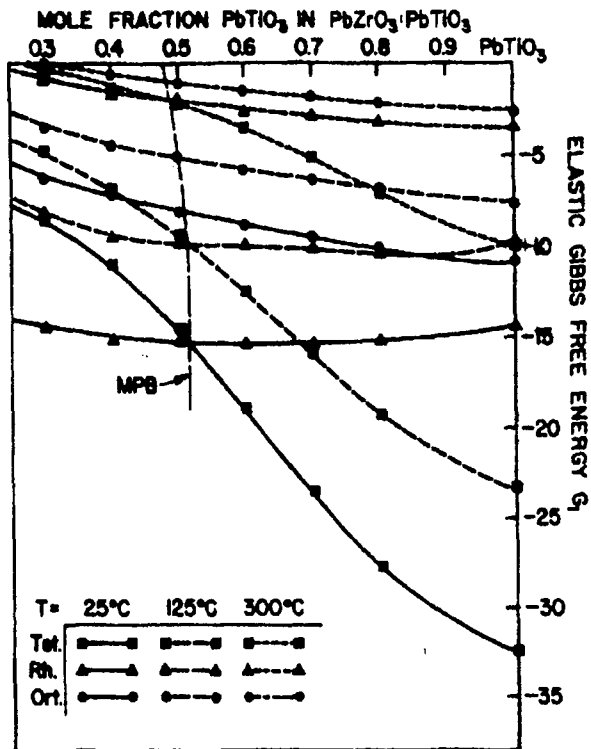
It must again be emphasised that the monoclinic and triclinic ferroelectric solutions are outside the region of validity of this sixth power function.

The free energy function G_1 for a simple proper ferroelectric derived from a prototypic phase with symmetry $Pm3m$, considering only Brillouin zone centre lattice modes, takes the following form for electric and elastic free boundaries:

$$G_1 = \alpha_1(P_1^2 + P_2^2 + P_3^2) + \alpha_{11}(P_1^4 + P_2^4 + P_3^4) + \alpha_{12}(P_1^2P_2^2 + P_2^2P_3^2 + P_3^2P_1^2) + \alpha_{111}(P_1^6 + P_2^6 + P_3^6) + \alpha_{112}(P_1^4(P_2^2 + P_3^2) + P_2^4(P_3^2 + P_1^2) + P_3^4(P_1^2 + P_2^2)) + \alpha_{123}P_1^2P_2^2P_3^2 \dots \dots \dots (1)$$

In this equation the function is truncated at the sixth order invariant of the order parameter, i.e. the dielectric polarisation vector P . The surviving α_{ijk} coefficients are determined by the generating elements of the point group $m3m$. The coefficient α_1 is a linearly increasing function of temperature passing through 0 at the Curie-Weiss temperature θ . The higher order α_{ijk} coefficients are related to the dielectric stiffness and higher order stiffness coefficients that are required to account for dielectric nonlinearity of the ferroelectric states.

Careful numerical analysis suggests that even if the α_{ijk} coefficients in equation (1) are given a linear temperature dependence, a rhombohedral ($R3m$)-tetragonal ($P4mm$) degeneracy (morphotropy) cannot be developed from a simple Devonshire function ($\alpha_{112} = \alpha_{123} = 0$). By adding a positive α_{112} term to destabilise the orthorhombic phase and a negative α_{123} to restabilise the rhombohedral phase, a morphotropic phase boundary (Fig. 2) between the rhombohedral and tetragonal states can be generated over a wide temperature range without any interleaving orthorhombic region. Numerical values of the energy density function G_1 are illustrated in Fig. 3 for PZT. It is important to reemphasise that the orthorhombic ferroelectric phase (filled circles in Fig. 3) is always close to but metastable with respect to the rhombohedral and tetragonal phases.



3 Numerical values of energy density function G_1 versus composition and temperature for F_R , F_T , and F_O states of $Pb(Zr_{1-x}Ti_x)O_3$ (PZT) system: note near vertical MPB (dashed line) near Zr:Ti ratio of unity and nearly degenerate F_R , F_T and F_O states over narrow composition range ($x \approx 0.3$) at around $300^\circ C$ (Ref. 17)

In summary, recent dielectric, piezoelectric, elastic, optical and structural investigations have demonstrated a complex transformation sequence in $A(B_{1-x}^{I}B_x^{II})O_3$ ferroelectric piezocrystals that is dependent upon orientation, domain states and electrical history. An intermediate F_O state was shown to exist between F_R and F_T , the temperature range of existence of which varied, suggesting metastability. Furthermore, the results indicate that the margin of stability in the F_R , F_O and F_T states is sufficiently small that changes in orientation, electrical history or mechanical constraints may affect the free energy balance. The data suggest that the boundary between the F_R and F_T phases near $85^\circ C$ has a thin orthorhombic sliver extending over $15^\circ C$. This result supports the recent suggestion of mixed states in this system.¹⁵

Phenomenological models that explicitly include temperature, compositional, elastic and electrical boundaries are valuable for computing phase stability and physical properties as a function of these boundaries. Deeper insights can be gained from model extension to account for the monoclinic and triclinic solutions where needed, and to compute the single crystal, single domain macroscopic observables and the influence of elastic and electrical boundaries.

ACKNOWLEDGEMENT

This work was sponsored by the US Office of Naval Research under contract N0001404WX20406.

REFERENCES

1. J. KUWATA, K. UCHINO and S. NOMURA: *Ferroelectrics*, 1981, 37, 579-582.
2. J. KUWATA, K. UCHINO and S. NOMURA: *Jpn. J. Appl. Phys.*, 1982, 21, 1298-1302.
3. S.-E. PARK and T. R. SHROUT: *J. Appl. Phys.*, 1997, 82, 1804-1811.

4. S.-E. PARK and T. R. SHROUT: *IEEE Trans. Ultrason., Ferroelectr., Freq. Control*, 1997, **44**, 1140–1147.
5. S.-F. LIU, S.-E. PARK, T. R. SHROUT and L. E. CROSS: *J. Appl. Phys.*, 1999, **85**, 2810–2814.
6. M. K. DURBIN, E. W. JACOBS, J. C. HICKS and S.-E. PARK: *Appl. Phys. Lett.*, 1999, **74**, 2848–2850.
7. H. FU and R. E. COHEN: *Nature*, 2000, **403**, 281–283.
8. Y. LU, D.-Y. JEONG, Z.-Y. CHENG, T. R. SHROUT and Q. M. ZHANG: *Appl. Phys. Lett.*, 2002, **80**, 1918–1920.
9. D. LA-ORAUPTAPONG, B. NOHEDA, Z.-G. YE, P. M. GERING, J. TOULOUSE, D. E. COX and G. SHIRANE: *Phys. Rev. B*, 2002, **65**, 144101–144107.
10. B. NOHEDA, D. E. COX, G. SHIRANE, S.-E. PARK, L. E. CROSS and Z. ZHONG: *Phys. Rev. Lett.*, 2001, **86**, 3891–3894.
11. D. VIEHLAND: *J. Appl. Phys.*, 2000, **88**, 4794–4806.
12. D. E. COX, B. NOHEDA, G. SHIRANE, Y. UESU, K. FUJISHIRO and Y. YAMADA: *Appl. Phys. Lett.*, 2001, **79**, 400–402.
13. Y. LU, D.-Y. JEONG, Z.-Y. CHENG, T. R. SHROUT, Q. M. ZHANG and D. VIEHLAND: *Appl. Phys. Lett.*, 2001, **78**, 3109–3111.
14. D. VIEHLAND, J. F. LI and A. AMIN: *J. Appl. Phys.*, 2002, **92**, 3985–3989.
15. B. NOHEDA, D. E. COX, G. SHIRANE, J. GAO and Z.-G. YE: *Phys. Rev. B*, 2002, **66**, 541041–5410410.
16. D. VANDERBILT and M. H. COHEN: *Phys. Rev. B*, 2001, **63**, 941081–941089.
17. A. AMIN, M. J. HAUN, B. BADGER, H. MCKINSTRY and L. E. CROSS: *Ferroelectrics*, 1985, **65**, 107–130.
18. M. J. HUAN, E. FURMAN, S. J. JANG and L. E. CROSS: *Ferroelectrics*, 1989, **99**, 13–25.
19. A. AMIN, R. E. NEWNHAM and L. E. CROSS: *Phys. Rev. B*, 1986, **34**, 1595–1598.
20. A. AMIN and L. E. CROSS: *Jpn. J. Appl. Phys.*, 1985, **24**, 229–231.

APPENDIX 7

Dielectric relaxation and strain behavior of 95.5% $\text{Pb}(\text{Zn}_{1/3}\text{Nb}_{2/3})\text{O}_3$ –4.5% PbTiO_3 single crystals at cryogenic temperatures

Zhi Yu^{a)}*Materials Research Laboratory, The Pennsylvania State University, University Park, Pennsylvania 16802*Chen Ang^{b)}*Department of Physics, The University of Akron, Akron, Ohio 44325*

E. Furman and L. E. Cross

Materials Research Laboratory, The Pennsylvania State University, University Park, Pennsylvania 16802

(Received 19 August 2002; accepted 7 December 2002)

The dielectric behavior of 95.5% $\text{Pb}(\text{Zn}_{1/3}\text{Nb}_{2/3})\text{O}_3$ –4.5% PbTiO_3 single crystals oriented along $\langle 001 \rangle$ direction with and without dc electric field has been studied at cryogenic temperatures. A pronounced low-temperature dielectric relaxation process was observed below 200 K; the relaxation rate follows the Arrhenius law ($\tau_0 \sim 1.0 \times 10^{-15}$ s and $U = 0.24$ eV). An additional dielectric anomaly showed up around 250 K at 10 kHz under a dc electric field. These results indicate rather complicated polarization mechanisms at cryogenic temperatures which clearly need more detailed study. The strain levels at cryogenic temperatures suggest that this material is very promising for space applications, in which the performance at cryogenic temperatures is critical. © 2003 American Institute of Physics. [DOI: 10.1063/1.1541936]

Since the discovery of the electric-field-induced ultra-high strain ($>1\%$) in lead-based single crystals $\text{Pb}(\text{Zn}_{1/3}\text{Nb}_{2/3})\text{O}_3$ and $\text{Pb}(\text{Zn}_{1/3}\text{Nb}_{2/3})\text{O}_3$ – PbTiO_3 (PZN–PT),^{1,2} much work has been focused on the growth and characterization of related lead-based single crystals as well as on the understanding of the mechanisms governing their ferroelectric and strain behavior. Moreover, many efforts have been devoted to establishing complete phase diagrams over a wide temperature range in order to better understand the relationships between the phase transformations and the strain characteristics under electric fields,^{3–6} in which x-ray measurements with or without fields were performed. It is well known that the study of dielectric spectra is a powerful tool in determining various dielectric peaks as well as dielectric relaxation behavior, which is critical in understanding the dielectric polarization mechanisms in relation to piezoelectric strains. In addition, the studies of dielectric properties with or without an electric field will also provide basic thermodynamic parameters for phenomenological calculations. Most work on dielectric properties was carried out above room temperature or a little below. Dielectric spectra at even lower temperatures, especially below liquid nitrogen temperature, are rarely studied, in particular under a dc electric field.^{7–10}

The discovery of very high strain in PZN–PT, single crystals also motivates possible application of the material in space technology, in which it is demanded that actuators have a reasonably good performance at cryogenic temperatures, for example, around 100 K and even lower. A question is raised, “How much of the excellent strain at room temperature remains at such low temperatures?”

In this work, we study the dielectric properties from 300

K down to 12 K, with and without a bias electric field. The results show various dielectric anomalies with frequency dispersion in the PZN–PT system with or without dc electric fields below room temperature. The strain levels are also measured down to 110 K; preliminary results show that the PZN–PT single crystals have great potential for applications in space.

Two $\langle 001 \rangle$ -oriented single-crystal samples with the composition of 95.5% $\text{Pb}(\text{Zn}_{1/3}\text{Nb}_{2/3})\text{O}_3$ –4.5% PbTiO_3 (hereafter denoted as PZN–4.5 PT) were used for this study. The crystal orientation was determined by the Laue back-reflection technique using a Northstar real-time orientation system. The dielectric constant and loss of the samples were measured using an HP4284A LCR meter in the temperature range 12 to 300 K with a cooling/heating rate of 1 K/min. A dc voltage was applied to the sample and a blocking circuit was adopted to isolate the high dc voltage from the LCR meter.

The temperature dependence of the dielectric constant (ϵ) and loss ($\tan \delta$) as a function of frequency of PZN–4.5 PT single crystals measured in a cooling cycle is shown in Fig. 1. From 300 to 12 K, an interesting characteristic is that there are two dielectric relaxation processes, as seen clearly in $\tan \delta$. One is a set of broad $\tan \delta$ peaks (denoted as peak A) around ~ 100 K, which are strongly frequency dependent. The other is around 250 K (denoted as peak B).

For peak A, the relaxation rate for the polarization derived from the temperature dependence of the imaginary part of the permittivity for the sample is plotted in the inset of Fig. 1. The data were fitted to the Arrhenius relation

$$\tau = \tau_0 \exp[U/k_B T], \quad (1)$$

where τ is the relaxation time, τ_0 is the pre-exponential term, U the activation energy for relaxation, k_B the Boltzmann's constant, and T the temperature. The fit parameters are U

^{a)}Electronic mail: yuzhi@psu.edu^{b)}Electronic mail: angchen@physics.uakron.edu

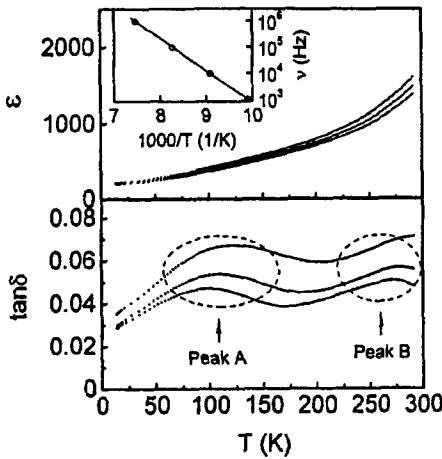


FIG. 1. Temperature dependence of ϵ and $\tan \delta$ of PZN-4.5 PT single crystals measured in a cooling cycle at 10, 100, and 1000 kHz (ϵ : from top to bottom; $\tan \delta$ from bottom to top). Inset shows the relaxation rate (ν) as a function of inverse temperature (circles: experimental data; solid line: fitting to the Arrhenius relation).

$=0.24$ eV, and $\tau_0 \sim 1.0 \times 10^{-15}$ s. The fitting curve is shown by the solid line in the inset of Fig. 1. A similar dielectric relaxation behavior was also observed in other samples with the activation energy of 0.22 ± 0.2 eV.

It is known that the thermal/electric field history has great influence on the dielectric and piezoelectric/ferroelectric behavior of PZN-4.5 PT single crystals above room temperature. It is interesting to study the electric-field effect on the dielectric and ferroelectric properties of the system at cryogenic temperatures. In this work, we measured the temperature dependence of the dielectric constant and loss with and without dc fields (i.e., 0–10 kV/cm). The temperature dependence of ϵ and $\tan \delta$ at 10 kHz under bias fields of 0, 5, and 10 kV/cm measured in a cooling cycle is shown in Fig. 2. An obvious dielectric peak, peak B, in $\tan \delta$ shows up under a dc electric field of 10 kV/cm around 250 K. Although no obvious dielectric peak in ϵ is present, a change in the slope of ϵ occurs at this particular temperature.

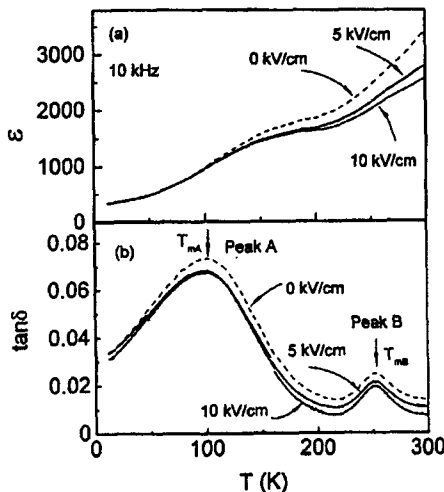


FIG. 2. Temperature dependence of ϵ and $\tan \delta$ of PZN-4.5 PT single crystals measured at 10 kHz under dc bias field 0, 5, and 10 kV/cm in a cooling cycle.

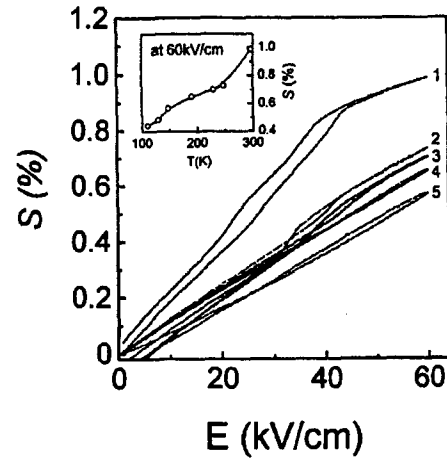


FIG. 3. Unipolar strain (S) vs electric field (E) of PZN-4.5 PT single crystals measured at 0.2 Hz at cryogenic temperatures: 296, 248, 229, 190, and 148 K, labeled as 1 to 5, respectively. Inset shows the temperature dependence of the strain level at 60 kV/cm.

In fact, even without dc bias, a slim trace of peak B can be also seen, as shown in Fig. 1. It should be pointed out that peak B is clearly seen from the data obtained at zero electric field after application of a dc electric field, as shown in Fig. 2, which is different from that of the virgin sample in Fig. 1. This implies the effect of the electrical history on the sample. In addition, peak A around 100 K is also more clearly seen under dc bias.

Both peaks A and B are also observed in other PZN-PT samples with different PT contents, such as 8% PT and 12% PT, indicating a reproducible behavior for the PZN-PT system.

The unipolar strain (S) versus electric field (E) behavior for PZN-4.5 PT single crystals measured at cryogenic temperatures and 0.2 Hz is shown in Fig. 3. The inset shows the temperature dependence of the strain level at 60 kV/cm. At room temperature, the strain level of $\sim 1\%$ is obtained at 60 kV/cm, and a field-induced phase transition is observed. All these are consistent with the results reported in the literature.^{2,3} With decreasing temperature, the strain is decreased, and the field-induced phase transition gradually narrowed, disappearing at ~ 190 K. At a temperature as low as 110 K, the strain is $\sim 0.45\%$ at 60 kV/cm, which is still relatively high, indicating excellent potential of this material for practical applications at cryogenic temperatures.

From the dielectric spectra obtained, the major dielectric characteristics for the PZN-4.5 PT samples can be summarized as follows,

- (1) Peak A around 100 K with obvious frequency dispersion is observed. The relaxation time as a function of temperature follows the Arrhenius law with the activation energy $U=0.24$ eV and $\tau_0 \sim 1.0 \times 10^{-15}$ s.
- (2) There is a peak B around 250 K, which can be seen more clearly under dc bias, whose peak temperature is independent of dc bias, although its intensity is suppressed by the dc bias.

Peak B seems to be a more “intrinsic” behavior. It is reasonable to assume it exists even without dc bias. It shows up clearly under dc bias, because the dc bias greatly sup-

presses the contribution from other polarization mechanisms in the sample. In addition, it is also found that the temperature of this peak is independent of dc bias levels. This is very similar to the Bi-induced dielectric anomalies in SrTiO₃: the so called "dielectric relaxor" behavior, in which the ϵ maximum temperature does not shift with dc field, but the amplitude is suppressed.¹¹ All these characteristics support that this anomaly may relate to an "intrinsic" behavior. It is reminiscent of the results reported by Kamzina and Krainik¹⁰ for pure PZN single crystals, that there is a dielectric anomaly around 250 K induced by application of a dc bias, which was attributed to a real ferroelectric–paraelectric phase transition. A clear understanding of this anomaly needs further study.

For peak A, in fact, a low-temperature dielectric relaxation with the activation energy in the range 0.2–0.5 eV below 200 K has been observed in many solid solutions, such as PZT,¹² Ba(Ti,Ce)O₃,¹³ and (Sr,Ba)Nb₂O₆,¹⁴ etc. Usually, it is attributed to domain-wall motions/relaxation at low temperature.

From the temperature dependence of the dielectric constant and loss at very low temperatures (Fig. 1), it can be seen that around 100 K and even below, the dielectric constant is still high and keeps decreasing, indicating that the polarization mechanism that contributes to high strain is not completely frozen out as yet. This is different from the piezoelectric copolymers, in which the strain lost its major, and the material only retains less than 1% of the value at room temperature. Correspondingly, the dielectric constant and loss of the copolymer are already frozen out below 150 K; that is, the temperature dependence of ϵ and $\tan \delta$ just is flattened below that temperature.¹⁵

A study of the dielectric behavior for 95.5% Pb(Zn_{1/3}Nb_{2/3})O₃–4.5% PbTiO₃ single crystals with and without a dc electric field shows two sets of dielectric anomalies at cryogenic temperatures. Peak A is observed

around 100 K. The relaxation time follows the Arrhenius law with $\tau_0 \sim 1.0 \times 10^{-15}$ s and $U = 0.24$ eV, as observed in many solid solution systems. It may be attributed to domain-wall motions. Peak B, occurring around 250 K at 10 kHz under a dc electric field, is related to a more intrinsic behavior. The strain level is above $\sim 0.45\%$, at 60 kV/cm, down to 110 K, indicating this material is very promising for applications in space.

This work was supported by a grant from Office of Naval Research under Contract No. N00014-98-1-0530.

- ¹J. Kuwata, K. Uchino, and S. Nomura, *Jpn. J. Appl. Phys., Part 1* **21**, 1298 (1982).
- ²S.-E. Park and T. R. Shrout, *J. Appl. Phys.* **82**, 1804 (1997).
- ³S. F. Liu, S. E. Park, T. R. Shrout, and L. E. Cross, *J. Appl. Phys.* **85**, 2810 (1998).
- ⁴M. K. Durbin, E. W. Jacobs, J. C. Hicks, and S. E. Park, *Appl. Phys. Lett.* **74**, 2848 (1999).
- ⁵D. E. Cox, B. Noheda, G. Shirane, Y. Uesu, K. Fujishiro, and Y. Yamada, *Appl. Phys. Lett.* **79**, 400 (2001).
- ⁶Y. Lu, Z. Y. Cheng, Q. M. Zhang, and T. R. Shrout, *Appl. Phys. Lett.* **80**, 1918 (2002).
- ⁷S. E. Park, M. L. Mulvihill, G. Risch, and T. R. Shrout, *Jpn. J. Appl. Phys.* **36**, 1154 (1997).
- ⁸S. F. Liu, S. E. Park, L. E. Cross, and T. R. Shrout, *J. Appl. Phys.* **92**, 461 (2002).
- ⁹Z. P. Chang, A. S. Bhalla, and L. E. Cross, in *Proceedings of Sixth IEEE International Symposium on Applications of Ferroelectrics, Lehigh University, Bethlehem, PA* (IEEE, New York, 1986), p. 482.
- ¹⁰L. S. Kamzina and N. N. Krainik, *Phys. Solid State* **40**, 485 (1998) [*Fiz. Tverd. Tela (Leningrad)* **40**, 527 (1998)].
- ¹¹A. Chen and Y. Zhi, *J. Appl. Phys.* **91**, 1487 (2002).
- ¹²X. L. Zhang, Z. X. Chen, L. E. Cross, and W. A. Schulze, *J. Mater. Sci.* **18**, 968 (1983).
- ¹³Y. Zhi, A. Chen, P. M. Vilarinho, and J. L. Baptista, *J. Phys.: Condens. Matter* **9**, 3081 (1997).
- ¹⁴R. Guo, A. S. Bhalla, C. A. Randall, and L. E. Cross, *J. Appl. Phys.* **67**, 6405 (1990).
- ¹⁵A. Chen, Y. Zhi, and L. E. Cross (unpublished).

APPENDIX 8

Polarization relaxation anisotropy in $\text{Pb}(\text{Zn}_{1/3}\text{Nb}_{2/3})\text{O}_3\text{-PbTiO}_3$ single-crystal ferroelectrics as a function of fatigue history

Metin Ozgul,^{a)} Eugene Furman, Susan Trolier-McKinstry, and Clive A. Randall^{b)}
*Materials Research Institute, Pennsylvania State University, University Park,
 Pennsylvania 16802-4800, U.S.A.*

(Received 4 September 2003; accepted 21 November 2003)

Polarization relaxation was studied in $\text{Pb}(\text{Zn}_{1/3}\text{Nb}_{2/3})\text{O}_3\text{-PbTiO}_3$ (PZN-PT) single crystals that show fatigue anisotropy. To excite prepoled crystals, a modest dc voltage ($<1/2$ of the coercive field) was applied along the poling direction. Upon removal of the voltage, the polarization decay in the time domain was measured. Experimental data were modeled with a stretched exponential function. Stretching exponent ($\beta_{(hkl)}$) and characteristic time ($\tau_{(hkl)}$) constants for polarization relaxation were determined from data over four decades in the time domain at different stages of bipolar cycling. $\beta_{(hkl)}$ values after 10^1 cycles were 0.146 ± 0.002 and 0.247 ± 0.0004 in the $\langle 001 \rangle$ and $\langle 111 \rangle$ orientations, respectively. The $\beta_{\langle 111 \rangle}$ constant increased up to 0.453 ± 0.104 after 10^5 cycles in $\langle 111 \rangle$ oriented crystals that show fatigue. However, much less change is observed in $\beta_{\langle 001 \rangle}$ as a function of cycling for $\langle 001 \rangle$ crystals. Characteristic time constants for relaxation ($\tau_{(hkl)}$) were calculated for $\langle 001 \rangle$ and $\langle 111 \rangle$ orientations as 0.401 ± 0.048 s and 57.46 ± 0.10 s, respectively. These results suggest a faster polarization relaxation in $\langle 001 \rangle$ than in the $\langle 111 \rangle$ orientation of rhombohedral PZN-PT ferroelectric crystals. © 2004 American Institute of Physics. [DOI: 10.1063/1.1641183]

I. INTRODUCTION

The $\text{Pb}(\text{Zn}_{1/3}\text{Nb}_{2/3})\text{O}_3\text{-PbTiO}_3$ (PZN-PT) system is a complete solid solution, based on the perovskite crystal structure, of relaxor (PZN) and normal (PT) ferroelectric compounds. Since the discovery of their extraordinary piezoelectric properties ($d_{33} \sim 2500$ pC/N) with large, electric-field-induced strain ($\sim 1.7\%$) in rhombohedral crystals oriented along $[001]_C$ (where the subscript denotes measurements with respect to the cubic axes), numerous investigations have been made in this system.¹⁻⁸ It has been widely noticed that the measured properties of PZN-PT single crystals are strongly anisotropic. Park *et al.* explored the dependence of electric-field-induced strains on crystallographic orientation in PZN-PT crystals. Large piezoelectric strains with extremely low hysteresis were observed in $[001]_C$ poled crystals, compared to lower strain with large hysteresis in the $[111]_C$ orientation. The very high strains, coupled with the low hysteresis of $[001]_C$ oriented crystals, were attributed to the engineered domain configuration in which the domain walls are not driven by applied fields in the poled state.³ Electric-field-induced domain configurations and domain switching under pulsed electric field conditions have been investigated by Yu *et al.*⁸ in PZN-PT crystals oriented at various crystallographic directions. Both domain wall mobility and activation energies were reported to be higher in the $[001]_C$ direction than for $[111]_C$. The observed anisotropy in the switching under pulse conditions was believed to indicate that the engineered domain state along the $[001]_C$ direction is more stable than that in the $[111]_C$ direction. Consequently, a higher activation field is needed in

$[001]_C$ oriented crystals. However, once the energy barrier is overcome during the switching process, domain walls move faster in $[001]_C$ oriented crystals.^{6,8}

Many ferroelectric materials show a progressive loss in switchable polarization on cycling through the hysteresis loop repeatedly. This process is known as polarization fatigue. Fatigue studies in PZN-PT crystals also revealed anisotropy.⁹⁻¹¹ It was found that $[001]_C$ oriented rhombohedral PZN-PT demonstrates excellent fatigue resistance, while $[111]_C$ oriented rhombohedral PZN-PT fatigues as shown in Fig. 1. Fatigue is also observed in $[001]_C$ crystals when tetragonal material is generated by changes in temperature or driving field strength.¹¹ The superior fatigue resistance along the $[001]_C$ direction is consistent with the observation of higher domain wall mobility (at least in the rhombohedral phase field).⁸ It is important to note that in some studies, fatigue has been correlated with a slowing down of domain walls.¹²

There is likely to be a complex interaction between existing sources of depolarizing fields under switching conditions, and the evolution of domains and polarization after external field is removed (polarization relaxation from an excited state). One way in which this could be manifested is in time variation in the remanent polarization due to spontaneous polarization reversal. This is sometimes referred to as retention loss, and is widely studied in thin films.¹³⁻¹⁶ Some of the recent studies on polarization relaxation focused on the physical origins of the relaxation kinetics during polarization reversal. Different retention studies covered different time frames, from very short times ($t < 1$ s) to long times ($t > 1$ s). The main concern in practical ferroelectric memory applications is the long-time retention. However, the short-time retention is also important in probing the polarization dynamics that govern the fast decay of polarization upon removal of the electric field. Kang *et al.* investigated the

^{a)}Present address: Afyon Kocatepe University, Faculty of Engineering, Department of Ceramic Engineering, Afyon, Turkey

^{b)}Author to whom correspondence should be addressed; electronic mail: car4@psu.edu

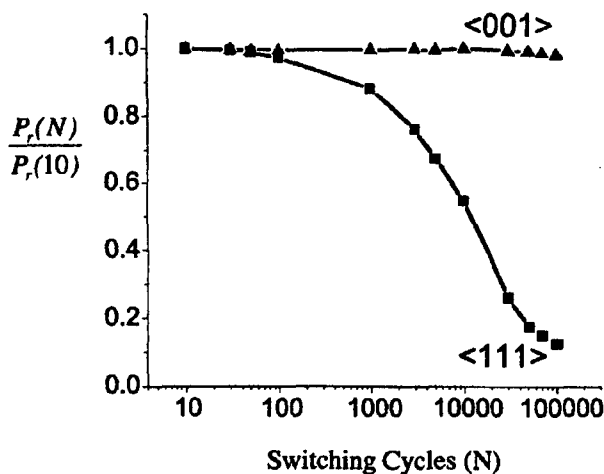


FIG. 1. Fatigue anisotropy in PZN-4.5PT single crystal for $\langle 001 \rangle$ and $\langle 111 \rangle$ directions, comparing remanent polarization behavior for N th cycle versus 10 switched case.

short-time retention loss properties and reported that fatigued capacitors showed a significant loss in retained polarization in the short-time regime. This was interpreted in terms of increasing depolarization fields with fatigue.¹⁷ Thus, it appears that collective information on the polarization dynamics both in the presence and absence of external fields may be helpful to characterize and understand the polarization switching and fatigue anisotropy.

The purpose of this study is to gain insight into the anisotropy in PZN-PT and related materials by probing the relaxation of dc field-excited domains upon removal of the electric field. We utilize the classical time decay approach to understand the effect of local perturbations on polarization as a function of orientation and cycling history.^{18–22} Here, the focus is the relaxation kinetics of polarization in prepoled crystals after exposure to a subcoercive field level dc field perturbation applied along the poling direction. The polarization decay in the time domain was measured for two different crystallographic orientations in PZN-4.5PT single crystals that demonstrate different fatigue behavior, and in crystals that have experienced different switching histories. The aim of the work was to determine if there are differences in polarization relaxation in $[001]_C$ and $[111]_C$, as well as to determine how the relaxations change as a function of bipolar cycling.

The dynamic processes occurring in complex systems such as the PZN-4.5%PT relaxor crystals encompass different length and time scales for the polarization. Both fast and slow rearrangements take place within the microscopic, mesoscopic, and macroscopic organization of the systems. A common aspect of relaxor or glassy ferroelectric systems is a certain amount of order at an intermediate, so-called mesoscopic, scale, while they are disordered at the microscopic scale and are homogeneous at the macroscopic scale.²³ A simple exponential relaxation law cannot describe the relaxation phenomena and kinetics in such materials. There are two mechanisms driving nonexponential relaxation in quenched, disordered media with stretched exponential relaxation. One is related to random pinning sites.²⁴ Secondly,

in disordered systems such as spin glasses, complex relaxation is caused by the existence of frustrated antiferromagnetic/ferromagnetic-type interactions,^{25–27} which are a direct consequence of the quenched disorder.²⁸ A polarization analogy to spin glasses has been made in dipole glasses. In such materials, the nature of the polarization dynamics is influenced by a variety of perturbation sources (e.g., micro- and mesoscopic chemical heterogeneities, random site occupancy, and dipolar interactions). During relaxation from higher energy levels, domains will relax to lower energy configurations by multiple pathways influenced by perturbation sources. This study is intended to determine how polarization relaxation correlates with the orientation-dependent fatigue behavior in PZN-PT crystals.

II. EXPERIMENTAL PROCEDURE

Single crystals of $0.955\text{Pb}(\text{Zn}_{1/3}\text{Nb}_{2/3})\text{O}_3-0.045\text{PbTiO}_3$ (PZN-4.5PT) solid solutions were grown by a high-temperature flux technique.²⁹ The crystals of this composition have a perovskite structure and are rhombohedral (pseudocubic) at room temperature. The crystals were oriented either along the $[111]_C$ or along the $[001]_C$ axes to within $\pm 2^\circ$ by using a Laue Camera (Multiwire Laboratories Ltd., real-time Laue machine).

For electrical characterization, plate-shaped samples were cut from the oriented crystals and prepared by polishing with silicon carbide and alumina polishing powders (down to $\sim 1 \mu\text{m}$) to achieve flat and parallel surfaces onto which silver paste electrodes were applied. Silver paste electrodes were preferred because they can be removed easily by washing with acetone without changing the nature of the crystal/electrode interface after the electrode removal. The thickness of samples used in this study ranged from 450 to 600 μm . Coercive fields (measured at 20 kV/cm and 0.1 Hz) for the crystals are about 3 and 5 kV/cm in $\langle 001 \rangle$ and $\langle 111 \rangle$ directions, respectively.

High-field measurements utilized a modified Sawyer-Tower circuit. A high-voltage amplifier (Trek Model 609C-6) was used in both poling and polarization fatigue measurements. The experimental procedure for the relaxation studies is shown in Fig. 2. Crystals were exposed to electric fields (E) as high as $5E_C$ for poling to achieve saturated polarization prior to time domain experiments. For fatigue measurements, electric fields were applied with a triangular bipolar wave form. The magnitude and the frequency of the applied field were 20 kV/cm and 10 Hz, respectively, for $[001]_C$ crystals. The applied field was higher (40 kV/cm) for $[111]_C$ samples to ensure full switching due to the increasing coercive field with fatigue. During measurements, the samples were submerged in Fluorinert,TM an insulating liquid, to prevent arcing.

To investigate the influence of continuous bipolar cycling on domain dynamics, the relaxation in the time domain was probed for both orientations at different stages in the cycling history: 1, 10, 10^2 , 10^3 , 10^4 , and 10^5 cycles. That is, fatigue experiments were interrupted at these numbers of cycles to track the influence of cycling-induced changes on domain dynamics. To maintain as constant as possible a do-

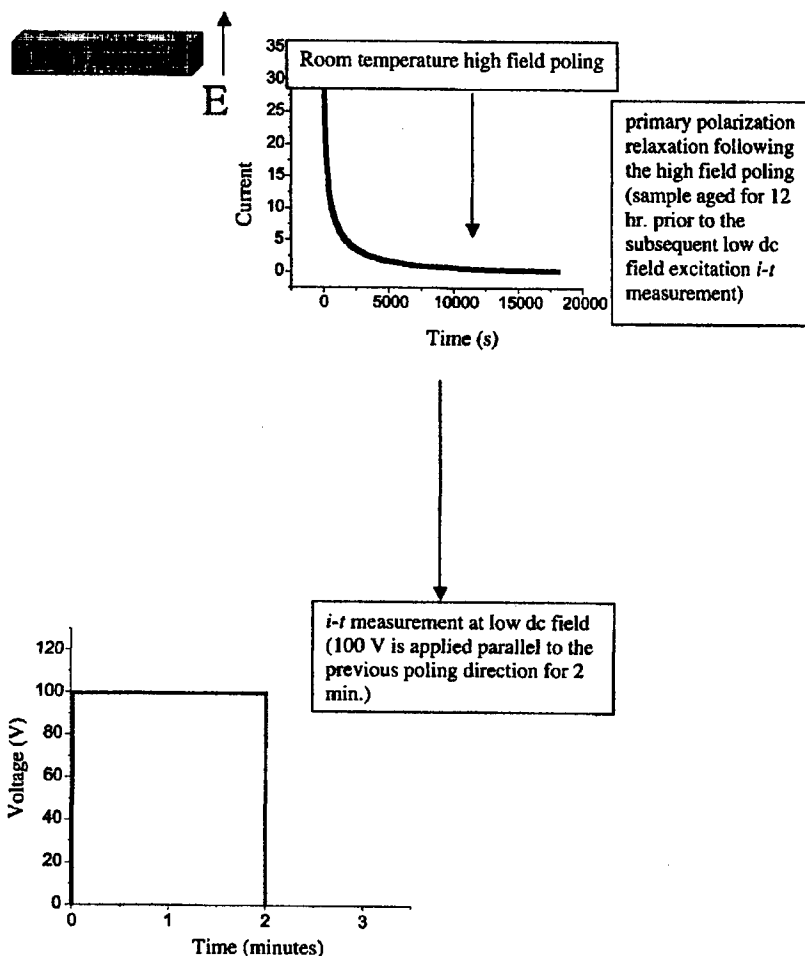


FIG. 2. Experimental procedure for polarization relaxation measurements in prepoled PZN-4.5PT single crystals.

main state for comparison, crystals were always repoled following bipolar cycling. Crystals exposed to a few number of electrical cycles (i.e., up to 10 cycles) are called "virgin." In the case of no electric field cycling, unipolar electric-field-poled crystals are called "uncycled."

It should be mentioned here that the main concern in this study is to probe domain relaxation due to perturbation of the domain structure with a comparatively weak excitation field. Thus, it was important to separate this type of response from the primary relaxation that occurs in crystals following the

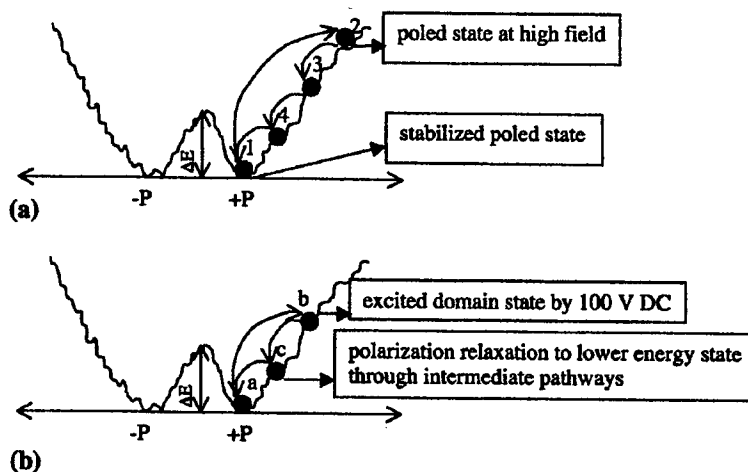


FIG. 3. A schematic of polarization states during (a) high-field poling and partial depoling and (b) low-field excitation and relaxation in ferroelectric crystals.

high-field poling process schematically depicted in Fig. 3(a). When a field much higher than a coercive field is applied to the crystal, domains are driven to a high-energy level (2) from the lower energy level (1). Following high-field poling, crystals will experience a primary relaxation (partial depoling) back to a lower energy state. In order to minimize the complication associated with these two different processes, prepoled crystals were given at least 12 h to stabilize after the primary relaxation process. After reaching a more stable polarization configuration, a weak, constant (~ 1.6 kV/cm depending on the sample thicknesses) dc field was applied for about 2 min in the poling direction to excite the polarization to a higher energy state, as shown in Fig. 3(b). After 2 min, the voltage source was turned off and the current decay due to the domain relaxation was measured by a HP4140B pA-meter/dc-voltage source. This setup was able to measure the current after about 0.5 s. In this study, current was monitored over four decades in the time domain. In this case, the polarization is excited from a lower energy state (a) to a higher energy level (b) by a low dc field. Upon removal of the field, domains relax back to lower the crystal's total free energy through intermediate pathways via domain wall motion as well as mesoscopic and atomic scale rearrangements. These experiments were performed in both orientations to relate the fatigue anisotropy to domain dynamics. The measured currents in the time domain during relaxation reflect the nature of the domains in two distinct orientations.

The measured current versus time ($I-t$) data were converted to polarization versus time ($P-t$). The time dependence of the polarization $P(t)$ was fitted to a stretched exponential function to extract the constants which give information about the relative polarization relaxation in both directions as a function of the cycling history (fatigue).

Polarization relaxation experiments are very dependent on the measurement conditions and techniques utilized to probe them. Time-dependent processes can be influenced by temperature, the total time over which the properties probed, and the magnitude of the perturbation used to make the measurements. Consequently, the results reported here correspond to the specific measurement conditions described.

III. RESULTS AND DISCUSSION

A typical time dependence for the measured current ($I-t$), along with the converted polarization data $P(t)$, measured at room temperature, are presented in Fig. 4. In this case, a 1.6 kV/cm ($< 1/2$ of E_C) constant dc field acts as the driving force for the polarization excitation. The polarization relaxation (from an excited state) occurs when the external field is removed, as depicted in Fig. 3(b). The measured polarization decay in the time domain ($P-t$) data was fitted to a well-known phenomenological relaxation function; namely, the Kohlrausch-Williams-Watts^{30,31} (KWW) function

$$P(t) = P_1 - P_2 \exp[-(t/\tau)^\beta], \quad (1)$$

where τ is a characteristic relaxation time, and β is the stretched-exponent coefficient ranging from 0 to 1. Recently, this function has been used to analyze different types of relaxation data in the time domain.^{14,15,32} It has also been sug-

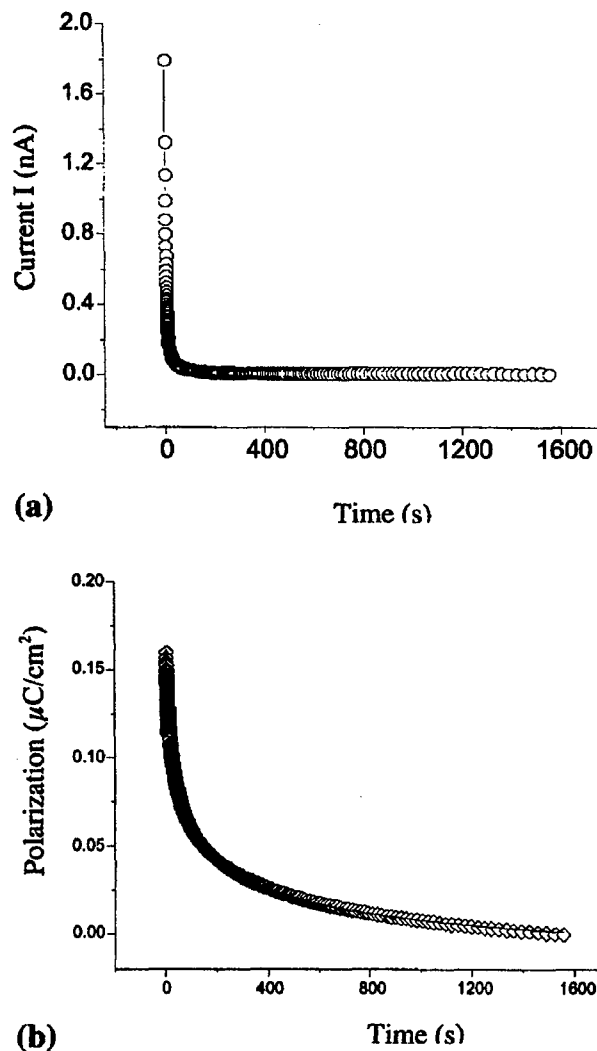
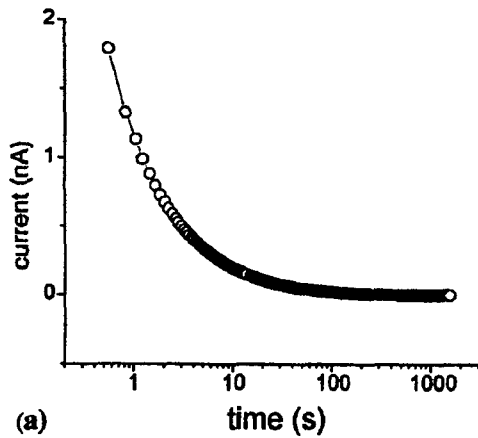


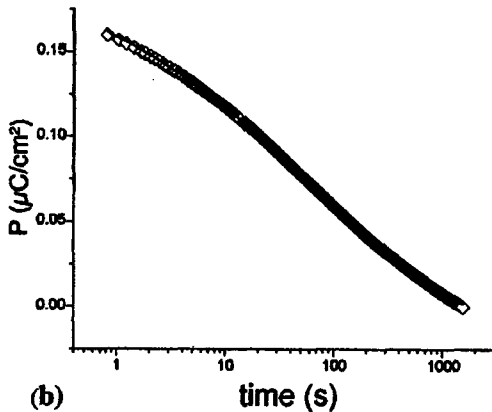
FIG. 4. Polarization relaxation probed by (a) dc measurements in the time domain and (b) calculated decrease in polarization. (time scale is linear).

gested that there is a direct connection between the stretched exponential behavior and the fractal nature of the disordered material.³³ In recent years, dynamical heterogeneity was established as a possible source of stretched exponential relaxation.²¹ The components of the relaxation response in most materials are related to the size distribution of relaxing entities (domains).²¹ A droplet model was proposed to describe the existence of polarization irregularities (i.e., polar droplets) within the poled state.³⁴⁻³⁶ Priya *et al.* have studied the mechanical aging behavior in relaxor-PT crystals close to the morphotropic phase boundary, and concluded that poled single crystals may not have simple domain states, but rather may have many irregular small polar regions within domains.³⁷ These domain structures are common in relaxor materials and solid solutions, as previously reported.^{38,39}

A typical KWW fit of experimental $P(t)$ data for $\langle 001 \rangle$ and $\langle 111 \rangle$ orientation is shown (the solid line is the fitting, the symbols are the experimental data) in Fig. 5. For both orientations, the magnitude of the polarization relaxation detected is modest, at most a few tenths of a $\mu\text{C}/\text{cm}^2$ when the



(a)

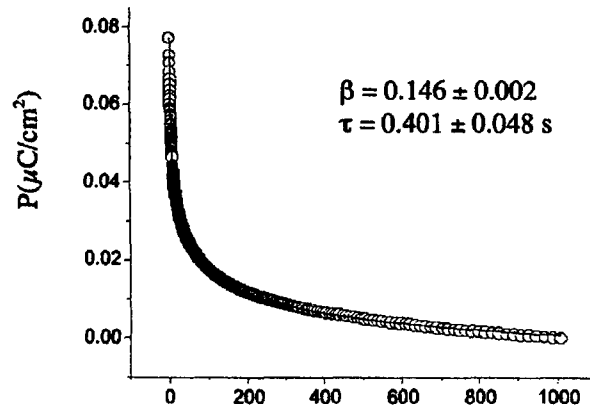


(b)

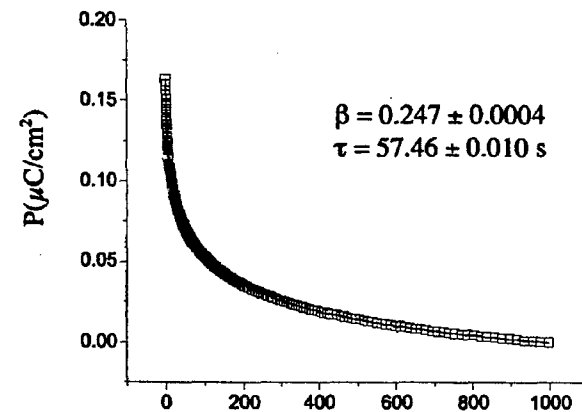
FIG. 5. Probed current decay in time (a) and calculated polarization relaxation (b). (time scale is logarithmic).

fit is extrapolated back to $t=0$ s. Thus, the polarization changes that are being probed in this measurement do, in fact, correspond to small perturbations, rather than to significant rewriting of the domain state. Furthermore, a relatively small difference in the magnitude of the polarization relaxation current was detected in $\langle 111 \rangle$ oriented crystals before and after the fatigue process (the amount of relaxing polarization decreases by about a factor of two after 10^5 cycles).

The fitting parameters β and τ were determined from the KWW fits as a function of the number of bipolar switching cycles and plotted in Fig. 6 for both orientations. As shown in Fig. 6(a), the stretching exponent (β) values are close for both orientations in virgin crystals: 0.146 ± 0.002 for $\langle 001 \rangle$ and 0.247 ± 0.0004 for $\langle 111 \rangle$ after 10 cycles. However, a remarkable increase was recorded in $\beta_{\langle 111 \rangle}$ to 0.453 ± 0.104 after 10^5 switching cycles. An average, low $\beta_{\langle 001 \rangle}$ value (0.1545 ± 0.0085) was maintained throughout the cycling experiments. Greatly different characteristic time constants (τ) were determined for the $\langle 001 \rangle$ and $\langle 111 \rangle$ orientations as 0.401 ± 0.048 and 57.46 ± 0.10 s, respectively. There is not much change in the relaxation time constant values during cycling, regardless of fatigue. This may be because only mobile domains contribute to the measured relaxation data in these conditions. These results are consistent with both the fatigue anisotropy observation shown in Fig. 1 and the literature



(a)



(b)

FIG. 6. Polarization relaxation data fit to the stretched exponential function (KWW) for (a) $\langle 001 \rangle$; (b) $\langle 111 \rangle$ orientations. (linear time scale).

relating fatigue to the frozen islands of nonswitching regions.^{12,40,41} As fatigue evolves in the $\langle 111 \rangle$ oriented crystal, it seems that the slow-moving domain walls are gradually frozen out and that their contribution to the total switching processes diminishes, reducing the total effective volume of switchable ferroelectric crystal. $\langle 111 \rangle$ oriented crystals may be more susceptible to fatigue because of the higher τ values. An increase in $\beta_{\langle 111 \rangle}$ corresponds to a less stretched relaxation, and this is observed in the fatiguing orientation. On the other hand, the low, stable $\beta_{\langle 001 \rangle}$ values for $\langle 001 \rangle$ crystals are a reflection of a very broad time distribution for switching. These analyses are summarized schematically in Fig. 7, where $g(\tau)$ is the distribution function for time constants τ .

Comparable fitting constants were reported in other ferroelectric systems for long-time relaxation experiments.^{15,17} Gruverman *et al.*¹⁵ reported a stretching exponent in tetragonal $\text{Pb}(\text{Zr}_{0.2}\text{Ti}_{0.8})\text{O}_3$ (PZT) films of 0.24. Kang *et al.*¹⁷ investigated short-time retention loss in PZT films before and after fatigue. The decay of retained polarization $\Delta P(t)$ was analyzed in terms of polarization relaxation with a distribution of relaxation time, and was found to follow a power law $\Delta P(t) = \Delta P_{\infty} + \Delta P_0 [1 + (t/t_0)]^{-n}$,

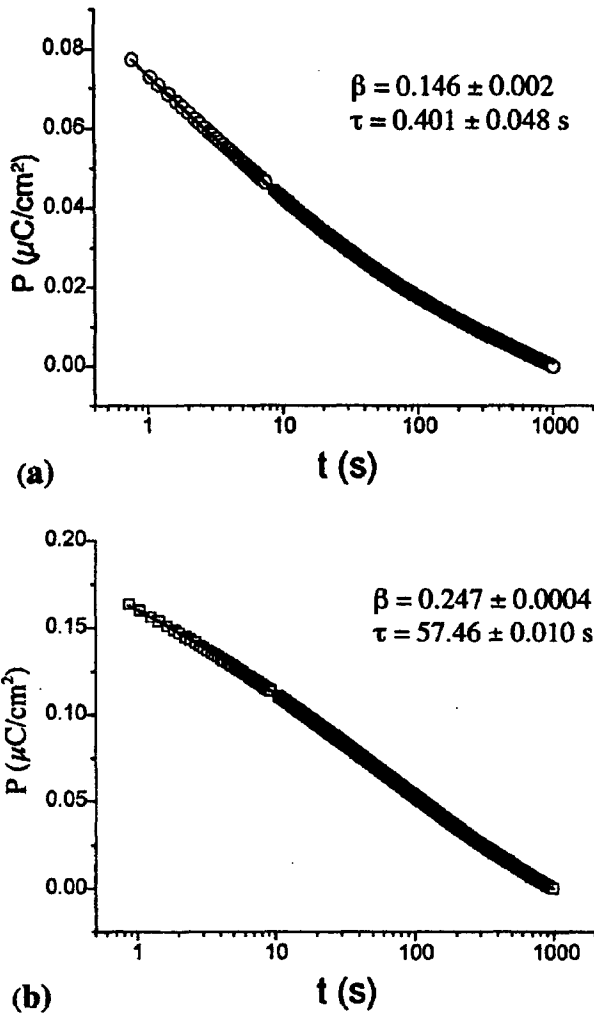


FIG. 7. Polarization relaxation data fit to the stretched exponential function (KWW) for (a) <001>; (b) <111> orientations. (logarithmic time scale).

where ΔP_∞ and $(\Delta P_\infty + \Delta P_0)$ are the asymptotic values of ΔP at $t = \infty$ and 0, respectively, and t_0 is a characteristic relaxation time. The power law exponent n values were 0.07 and 0.23 ± 0.02 before and after fatigue, respectively. The relaxation parameters obtained in this study seem to be in a reasonable range, and an increase with fatigue in stretching exponent is consistent with the study by Kang *et al.*

It is difficult to make a sensible comparison of τ values with data from the literature, since relaxation processes in ferroelectrics take place over such wide time scales (τ values ranging over more than 10 orders of magnitude in time have been reported) and the field excitation is applied under different conditions. Any set of measurements samples only a portion of the distribution. Furthermore, it is not clear that the relaxation times associated with spontaneous polarization reversal (which are presumably governed by net internal fields) will be identical to those associated with polarization decay after weak excitation, or those associated with characteristic time constants for polarization reversal under applied fields. Consequently, comparisons should only be made for τ values of samples exposed to the same type of excitation.

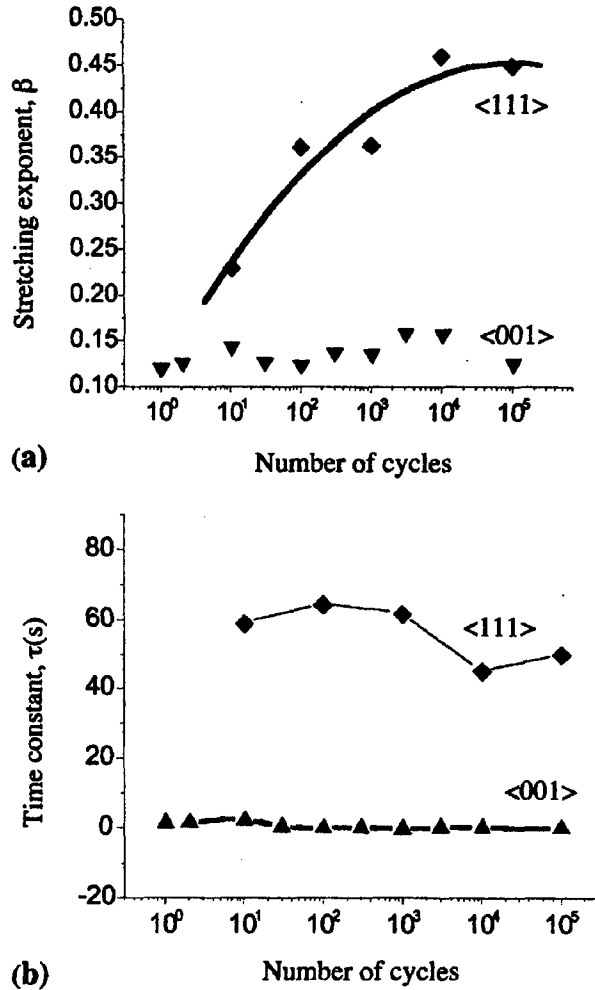


FIG. 8. Stretched exponential constants with the number of cycles for (001) and (111) orientations: (a) stretching exponent β and (b) characteristic time for relaxation τ .

Although it is difficult to make any comparison of the τ values measured here to those measured elsewhere, an internal comparison of $\tau_{(001)}$ and $\tau_{(111)}$ measured under the same conditions is revealing (see Fig. 8). It is clear that $\tau_{(001)}$ is

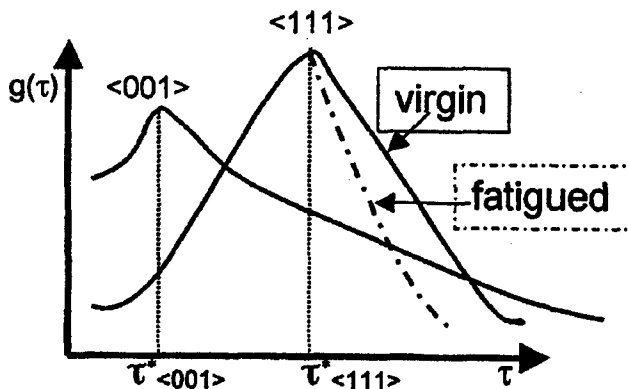


FIG. 9. A schematic depiction of time constant distribution function for relaxation in (001) and (111) orientations based on fitting data.

appreciably smaller than $\tau_{\langle 111 \rangle}$, which is consistent with prior reports of higher domain wall mobilities in PZN-PT crystals.^{6,8}

The major difference in relaxation response of crystals with different orientations could be related to the different domain configurations adopted. In poled rhombohedral crystals, the spontaneous polarization is along the $\langle 111 \rangle$ direction. Thus, at least one of the polarization vectors is parallel to the poling direction in $\langle 111 \rangle$ oriented crystals. This state is sampled during the (initial) switching and poling experiments, as evidenced by the large polarizations observed for $\langle 111 \rangle$ crystals (see Fig. 9). The instability of this domain state is, however, widely discussed, and at lower fields, the sample drops back to a multidomain configuration. Thus, it is likely that in the polarization relaxation experiments, excitation of the polarization is from the three canted polarization directions with one component parallel to $[111]$. Note that the magnitudes of the polarization currents in this case are small (comparable to those of the $\langle 001 \rangle$ crystals), suggesting that the polarization relaxation measurement is not probing a switching/depoling process. It is also interesting that there is now experimental evidence that $\langle 111 \rangle$ crystals switch through the inclined axes, rather than by 180° switching.⁴² This would suggest that as the fatigue process proceeds, the sample has been cycled through states in which domains continually appear and disappear, presumably by nucleation and growth processes.

Pinning of domain walls in this case would be consistent with the observed fatigue and the increase in $\beta_{\langle 111 \rangle}$, since the exponent β is characteristic of the domain size and shape distribution in the material.¹⁷

In contrast, all of the polarization vectors are inclined to the poling direction in $\langle 001 \rangle$ crystals. For this orientation, large concentrations of domain walls (many of them charged) are built in during the poling process, and the resulting domain states are known to be stable. The domain structures in $\langle 001 \rangle$ and $\langle 111 \rangle$ orientations are known to differ. The mechanics of the polarization reversal process are not known for $\langle 001 \rangle$ crystals, but in any event, the large existing concentrations of domain walls (as well as the presence of a mechanism for absorbing and desorbing charges at the charged domain walls) may be related to the increase in fatigue resistance.

IV. CONCLUSIONS

Single-crystal PZN-PT exhibits a stretched exponential-type relaxation in the time domain at room temperature. Relaxation data fit to a stretched exponential function (KWW) with small β values (<0.25), implying a relatively broad distribution of relaxation times. The crystallographic orientation dependence of the slow relaxation process has been studied as a function of bipolar switching cycles (fatigue). Stretched exponential analysis of the experimental results for $\langle 001 \rangle$ and $\langle 111 \rangle$ orientations at different levels of cycling demonstrated an orientation dependence of the stretching exponent β and characteristic relaxation time τ . Small values for β and τ were determined for the $\langle 001 \rangle$ orientation, and these remained relatively stable throughout the cycling.

However, β increased with fatigue for the $\langle 111 \rangle$ orientation. The characteristic time constant τ is much higher for $\langle 111 \rangle$ crystals. Both $\tau_{\langle 111 \rangle}$ and $\tau_{\langle 001 \rangle}$ are independent of fatigue. These observations would be consistent with a picture in which the slow domains freeze out with fatigue, so that their contribution to the relaxation diminishes, for $\langle 111 \rangle$ oriented crystals. The polarization relaxation is much faster in $\langle 001 \rangle$ oriented PZN-PT. Constant and relatively small $\beta_{\langle 001 \rangle}$ and $\tau_{\langle 001 \rangle}$ values imply a broader distribution of relaxation processes in $\langle 001 \rangle$ crystals, peaked at a shorter time than for the $\langle 111 \rangle$ orientation. Additional work to clarify the relation between the polarization relaxation kinetics and differences in the domain structures is needed to clarify the impact of kinetics on the fatigue process.

ACKNOWLEDGMENTS

This work was partially supported by The Center for Dielectric Studies at Pennsylvania State University. Crystals used for this study were provided by Dr. T. R. Shrout and Dr. S. Zhang. One of the authors (M. O.) would like to acknowledge Ministry of National Education of Turkey for the financial support.

- ¹ J. Kuwata, K. Uchino, and S. Nomura, *Ferroelectrics* **37**, 579 (1981).
- ² J. Kuwata, K. Uchino, and S. Nomura, *Jpn. J. Appl. Phys.* **21**, 1298 (1982).
- ³ S.-E. Park and T. R. Shrout, *J. Appl. Phys.* **82**, 1804 (1997).
- ⁴ S.-E. Park and T. R. Shrout, *Mater. Res. Innovations* **1**, 20 (1997).
- ⁵ S.-F. Liu, S.-E. Park, T. R. Shrout, and L. E. Cross, *J. Appl. Phys.* **85**, 2810 (1999).
- ⁶ H. Yu and C. A. Randall, *J. Appl. Phys.* **86**, 5733 (1999).
- ⁷ M. Shen and W. Cao, *Appl. Phys. Lett.* **75**, 3713 (1999).
- ⁸ H. Yu, V. Gopalan, J. Sindel, and C. A. Randall, *J. Appl. Phys.* **89**, 561 (2001).
- ⁹ V. Bornand, S. Trolier-McKinstry, K. Takemura, and C. A. Randall, *J. Appl. Phys.* **87**, 3965 (2000).
- ¹⁰ K. Takemura, M. Ozgul, V. Bornand, S. Trolier-McKinstry, and C. A. Randall, *J. Appl. Phys.* **88**, 7272 (2000).
- ¹¹ M. Ozgul, K. Takemura, S. Trolier-McKinstry, and C. A. Randall, *J. Appl. Phys.* **89**, 5100 (2001).
- ¹² V. Ya. Shur, E. L. Rumyantsev, E. V. Nikolaeva, E. I. Shishkin, and I. S. Baturin, *J. Appl. Phys.* **90**, 6312 (2001).
- ¹³ J. F. Scott, C. A. Araujo, H. B. Meadows, L. D. McMillan, and A. Shababkeh, *J. Appl. Phys.* **66**, 1444 (1989).
- ¹⁴ T. Mihara, H. Yoshimori, H. Watanabe, and C. A. Araujo, *Jpn. J. Appl. Phys., Part 1* **34**, 2380 (1995).
- ¹⁵ A. Gruverman, H. Tokumoto, A. S. Prakash, S. Aggarwal, B. Yang, M. Wuttig, R. Ramesh, O. Auciello, and T. Venkatesan, *Appl. Phys. Lett.* **71**, 3492 (1997).
- ¹⁶ I. G. Jenkins, T. K. Song, S. Madhukar, A. S. Prakash, S. Aggarwal, and R. Ramesh, *Appl. Phys. Lett.* **72**, 3300 (1998).
- ¹⁷ B. S. Kang, J. Yoon, T. W. Noh, T. K. Song, S. Seo, Y. K. Lee, and J. K. Lee, *Appl. Phys. Lett.* **82**, 248 (2003).
- ¹⁸ A. T. Fiory, *Phys. Rev. B* **4**, 614 (1971).
- ¹⁹ Y. Imry and S. Ma, *Phys. Rev. Lett.* **35**, 1399 (1975).
- ²⁰ V. Westphal, W. Kleemann, and M. Glinchuk, *Phys. Rev. Lett.* **68**, 847 (1992).
- ²¹ R. V. Chamberlin, *Phase Transitions* **65**, 169 (1998).
- ²² T. Granzow, U. Dorfler, Th. Wolke, M. Wohlecke, R. Pankrath, M. Imlau, and W. Kleemann, *Phys. Rev. B* **63**, 174101 (2001).
- ²³ Y. Feldman, A. Puzenko, and Y. Ryabov, *Chem. Phys.* **284**, 139 (2002).
- ²⁴ A. Diaz-Sanchez, A. Perez-Garrido, A. Urbina, and J. D. Catala, *Phys. Rev. E* **66**, 031403 (2002).
- ²⁵ M. Randeria, J. P. Sethna, and R. G. Palmer, *Phys. Rev. Lett.* **54**, 1321 (1985).
- ²⁶ F. Cesì, C. Maes, and F. Martinelli, *Commun. Math. Phys.* **188**, 135 (1997).
- ²⁷ G. Franzese and A. Coniglio, *Phys. Rev. E* **58**, 2753 (1998).

- ²⁸A. Fierro, A. de Candia, and A. Coniglio, *Phys. Rev. E* **56**, 4990 (1997).
- ²⁹M. L. Mulvihill, S.-E. Park, G. Risch, Z. Li, K. Uchino, and T. Shrout, *Jpn. J. Appl. Phys., Part 1* **35**, 3984 (1996).
- ³⁰R. Kohlrausch, *Ann. Phys. Chem.* **91**, 179 (1854).
- ³¹G. Williams and D. C. Watts, *Trans. Faraday Soc.* **66**, 80 (1970).
- ³²A. A. Bokov, M. M. Kumar, Z. Xu, and Z.-G. Ye, *Phys. Rev. B* **64**, 224101 (2001).
- ³³P. Jund, R. Jullien, and I. Campbell, *Phys. Rev. E* **63**, 036131 (2001).
- ³⁴W. McMillian, *Phys. Rev. B* **30**, 476 (1980).
- ³⁵A. Bray and M. Morre, *J. Phys. C* **17**, L463 (1984).
- ³⁶D. Fisher and D. Huse, *Phys. Rev. Lett.* **56**, 1601 (1986).
- ³⁷S. Priya, J. Ryu, K. Uchino, and D. Viehland, *Appl. Phys. Lett.* **79**, 2624 (2001).
- ³⁸C. A. Randall, D. J. Barber, and R. W. Whatmore, *J. Microsc.* **145**, 275 (1987).
- ³⁹A. D. Hilton, C. A. Randall, D. J. Barber, and T. R. Shrout, *Ferroelectrics* **93**, 379 (1989).
- ⁴⁰E. L. Colla, S. Hong, D. V. Taylor, A. K. Tagantsev, N. Setter, and K. No, *Appl. Phys. Lett.* **72**, 2763 (1998).
- ⁴¹E. L. Colla, I. Stolichnov, P. E. Bradely, and N. Setter, *Appl. Phys. Lett.* **82**, 1604 (2003).
- ⁴²J. Yin and W. W. Cao, *Appl. Phys. Lett.* **79**, 4556 (2001).

APPENDIX 9

Direct evidence of ferroelastic participation in 180° polarization switching and fatigue for 111 oriented rhombohedral ferroelectric 0.955 Pb(Zn_{1/3}Nb_{2/3})O₃:0.045 PbTiO₃ single crystals

Wenyi Zhu and L. Eric Cross^{a)}

187 Materials Research Institute, The Pennsylvania State University, University Park, Pennsylvania 16802

(Received 10 November 2003; accepted 3 February 2004)

Direct elastic deformation measurements taken during polarization reversal in 111 oriented 0.955 Pb(Zn_{1/3}Nb_{2/3})O₃-0.045 PbTiO₃ single crystals confirm the observation by W. Cao [Ferroelectrics **290**, 107 (2003)] that a ferroelastic reorientation of the domain polarization vectors is involved, and the observed strain changes are consistent with the model he proposed. First cycle nonrecoverable fatigue occurring in our crystals and the associated changes of shape in polarization and strain hysteresis are suggested to be due to microcracking associated with the large very rapid strain changes associate with the ferroelastic switching mode. © 2004 American Institute of Physics. [DOI: 10.1063/1.1690869]

Single crystals in the ferroelectric rhombohedral structure phase of the lead zinc niobate: lead titanate (PZN:PT) solid solution family show outstanding but highly anisotropic piezoelectric properties. Samples poled along the prototypic 001 direction can have piezo-coupling k_{33} up to 95% and $d_{33} \sim 2500$ pC/N.^{1,2} Surprisingly for carefully poled samples at composition not too close to the rhombohedral:tetragonal phase boundary, the behavior is fully intrinsic and associated with easy field induced tilting of the macroscopic P_S vector in the poled domain away from the equilibrium $\langle 111 \rangle$ orientation. A model now confirmed by phenomenological calculation from prototypic Q_{ij} ³ optical observation⁴ and first principles *ab initio* calculation.⁵ As would be expected on this model, 111 field poled crystals at the same composition have much more modest piezo properties.

Ferroelectric switching for both 001 and 111 oriented fields shows excellent "square" dielectric hysteresis with similar low coercive fields. For the 001 oriented fields both single crystals⁶ and epitaxial oriented thin films⁷ show remarkable fatigue free switching which is unexpected as the remanent state is necessarily polydomain. Further, for 111 oriented fields where the crystal can be driven to a single macrodomain state there is evidence of strong fatigue. For this 111 oriented switching, however, recently Cao *et al.*⁸ have shown from acoustic measurements that switching is not by a simple 180° domain wall process, but most likely involves a Ferroelastic wall motion.

In this study carried out on (0.955) Pb(Zn_{1/3}Nb_{2/3})O₃ (0.045) PbTiO₃ crystals we have measured both longitudinal and transverse strain and dielectric hysteresis for 180° polarization switching in the 111 oriented crystal. The results are consistent with the model suggested by Cao and indicate that reorientation from 111 to $\bar{1}\bar{1}\bar{1}$ is via a ferroelastic mechanism. Fatigue studies on repeated switching also suggest that in our crystals there is a rapid initial damage which is not recoverable by annealing above the Curie temperature fol-

lowed by a slower more substantial fatigue which is recoverable by annealing. Both elastic and dielectric response are consistent with the probability that the unrecoverable fatigue involves a microcracking under the stress concentrations associated with the ferroelectric component of switching. The precise mechanism for the preferred ferroelectric trajectory is not clear; however the massive transverse permittivity and the adaptive state models of Jin *et al.*⁹ underscore the propensity for rotational instability of the domain polarization vectors.

Crystal of PZN:PT at the 0.955 Pb(Zn_{1/3}Nb_{2/3})O₃ 0.045 PbTiO₃ composition were supplied by TRS State College. The ferroelectric Curie temperature of 162 °C agreed well with that expected for the 4.5% PT composition. Samples with 111, $0\bar{1}\bar{1}$ and $11\bar{2}$ orthogonal faces had dimensions in the range $5 \times 5 \times 1$ mm (larger 111 face) to $2 \times 2 \times 2$ mm. Gold electrodes were applied to the 111 faces by sputter coating. Dielectric hysteresis was measured on a modified Sawyer-Tower circuit and associated strain measured using a linear variable displacement transducer (LVDT) driven by a lock-in amplifier (Stanford Research system model SR 830). Cyclic triangular bipolar waves at 0.2 Hz with field levels up to 10 kV/cm were supplied from a Trek 609 C-6 high voltage amplifier. For longitudinal (33) strain measurement the LVDT's insulating probes contacted directly onto the 111 face electrodes. In transverse (11,22) strain measurements the sample was now mounted with $1\bar{1}0$ or $11\bar{2}$ faces contacted by LVDT probes and electric field supplied by fine silver wires attached by air drying silver paint to the electrode faces. All measurements were carried through in an air conditioned room at 20 °C.

Initial hysteresis on first cycling of any of the 111 oriented crystal tested showed excellent near square hysteresis as in Fig. 1(a) with an abrupt transition into the poled condition for both positive and negative switches. Associated longitudinal ferroelastic hysteresis is evidenced in Fig. 1(b) carried out at the same time and on the same sample. It is interesting to note that the peaks in the longitudinal strain occur on the steeply falling part of the polarization curve,

^{a)}Author to whom correspondence should be addressed; electronic mail: lec3@psu.edu

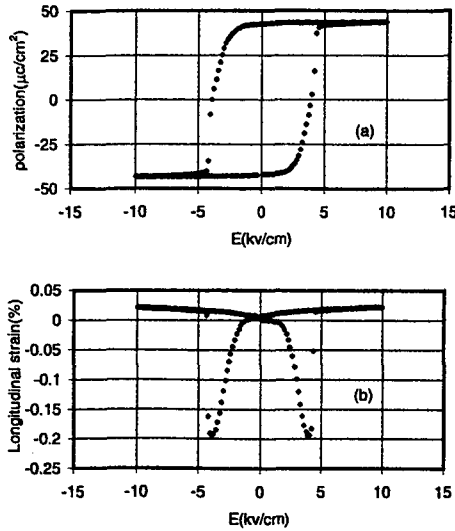


FIG. 1. (Color) (a) First cycle of hysteresis in polarization vs field for a 111 oriented $0.955 \text{Pb}(\text{Zn}_{1/3}\text{Nb}_{2/3})\text{O}_3:0.045 \text{PbTiO}_3$ single crystal subjected to a triangular bipolar wave of 10 kV/cm at 0.2 Hz. (b) Longitudinal strain S_{33} during first cycle switchover from 111 oriented P_r to $\bar{1}\bar{1}\bar{1}$ oriented P_r .

longitudinal strain being all negative. Unfortunately, with our simple setup it is not possible to measure both longitudinal and transverse strain on the same sample at the same time. For the crystal for which data are presented in Fig. 2, transverse then longitudinal strain were measured in sequence [Fig. 2(b)] with the polarization loop [Fig. 2(a)] corresponding to the second cycle. Again the strain changes are nicely abrupt but there is a minor rounding associated with the initial fatigue mechanism. As in all 111 samples measured the transverse strain occurring during switching is all positive but the maximum transverse strain is less than half the magnitude of the maximum longitudinal change.

In a number of crystals tested the initial shape change both in dielectric and elastic hysteresis was more severe as in

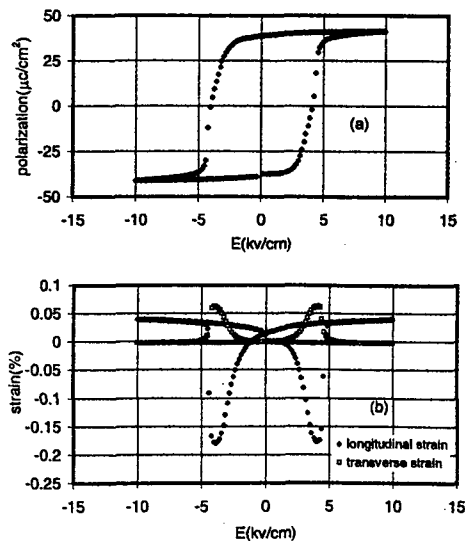


FIG. 2. (Color) (a) Second cycle hysteresis in polarization vs field for a 111 oriented $0.955 \text{Pb}(\text{Zn}_{1/3}\text{Nb}_{2/3})\text{O}_3:0.045 \text{PbTiO}_3$ single crystal subjected to a triangular bipolar wave of 10 kV/cm amplitude at 0.2 Hz. (b) Second cycle longitudinal strain (blue) and first cycle transverse strain (red) in a 111 oriented $0.955 \text{Pb}(\text{Zn}_{1/3}\text{Nb}_{2/3})\text{O}_3:0.045 \text{PbTiO}_3$ crystal subjected to cycling under a triangular bipolar wave of 10 kV/cm of amplitude at 0.2 Hz.

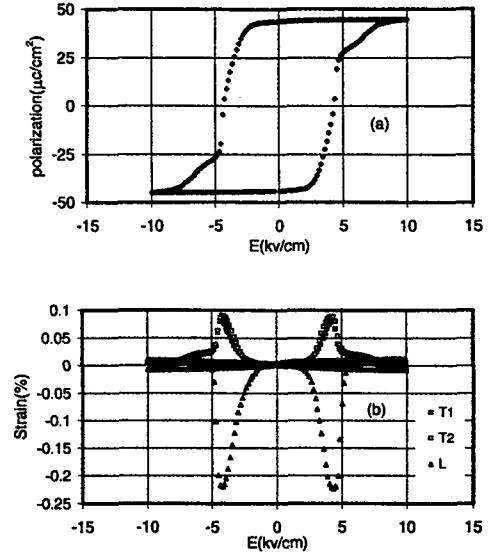


FIG. 3. (Color) (a) Early cycle of hysteresis in 111 oriented $0.955 \text{Pb}(\text{Zn}_{1/3}\text{Nb}_{2/3})\text{O}_3:0.045 \text{PbTiO}_3$ single crystal under 10 kV/cm triangular bipolar wave at 0.2 Hz. (b) Early cycle transverse and longitudinal strain under 0.2 Hz cyclic triangular wave field L is longitudinal strain T_1 $0\bar{1}\bar{1}$ transverse strain T_2 $1\bar{1}\bar{2}$ transverse strain.

Fig. 3 where the field required for complete switchover is almost doubled and dominantly the transverse dilatation persists to these higher field levels. As has been reported earlier⁷ repeated cycling leads to more severe fatigue and loss of remanent polarization. For our crystals only 200 cycles at 0.2 Hz with peak triangular bipolar wave of 10 kV/cm lowers remanent polarization from 42.2 to $\sim 30 \mu\text{C}/\text{cm}^2$ and raises coercivity from 3.95 to 5.5 kV/cm. In agreement with the earlier studies, the more severe fatigue is recoverable by annealing at 200 °C which is above T_c , but the polarization does not “square up” and the curvature of both longitudinal and transverse strain persists. It has been suggested by Cao⁸

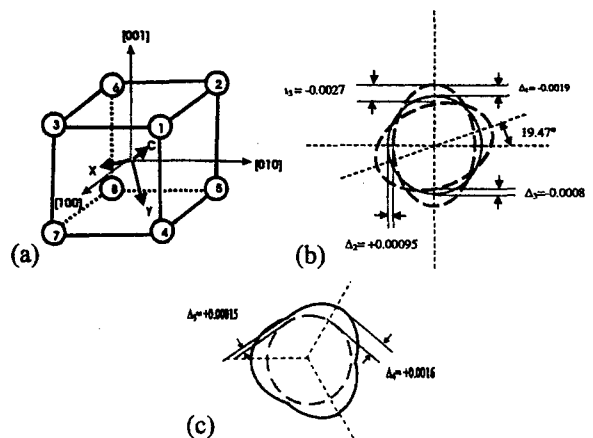


FIG. 4. (Color) (a) Relationship between rhombohedral and prototypic cubic coordinates and labeling of the eight possible polar directions in rhombohedral domain state (taken from Cao in Ref. 18) Proposed switching path in 111 oriented $0.955 \text{Pb}(\text{Zn}_{1/3}\text{Nb}_{2/3})\text{O}_3:0.045 \text{PbTiO}_3$. State 1 domains may switch to any one of states 2, 3, 4 before switching over to state 8 to complete the reversal process. (b) Orientation of the spontaneous strain ellipsoids during the switching process indicating the origin of $\Delta_1 \Delta_3$ which contribute the large contraction along 111 during switching. (c) Plan view normal to 111 indicating the origin of the expansions $\Delta_4 \Delta_5$ which contribute to the transverse elongation. Note: Eccentricities have been grossly exaggerated for illustrative purposes.

that for PZN:4.5 PT 180° switching for 111 oriented crystals is a two stage process, as indicated in Fig. 4 taken from his article. The suggestion is that the polarization vector in single domain (1) in the 111 poled state "folds out" into domains with orientations (2), (3), (4) before folding over into the reverse state⁷ with $\bar{1}\bar{1}\bar{1}$ orientation. X-ray measurements of the ferroelectric spontaneous shear in the 4.5 PT composites give a value at the shear angle $\alpha = 89.89^\circ$ ¹⁰ corresponding to an equivalent elongation along 111 in the Ref. 8 direction

$$\frac{\Delta L}{L} = \Delta_1 = 0.0019.$$

Since under pure shear deformation volume is conserved, the transverse strain

$$\Delta_2 = \frac{\Delta T}{T} \text{ is given by}$$

$$\Delta_1 + 2\Delta_2 = 0 \quad \Delta_2 = -\frac{1}{2}\Delta_1 = -0.00095.$$

An estimate of the maximum possible longitudinal strain at switchover may be taken as the loss of the state 1 elongation Δ_1 , together with the contraction from the zero strain state associated with the domain deformation ellipsoids for 2, 3, and 4 states [Fig. 4(a)] now being tilted 19.47° above the plane perpendicular to 111 through the center of these strain ellipsoids [Fig. 4(b)]. This yields an additional contraction of

$$\Delta_3 = -0.0008$$

so that the total contraction as evidenced in Fig. 4(b) is

$$-\Delta_1 + \Delta_3 = -0.0019 - 0.0008 = -0.0027.$$

For the transverse strain, the tilted strain ellipsoid for the single domain gives a maximum dilation [Fig. 4(c)]

$$\Delta_4 = 0.0016.$$

However, there are now three equivalent (2), (3), (4) domains making angles of 120° with each other. The smallest dilation will take place at the intersection of the three ellipsoids. Taking note of the fact that the circular section in Fig. 4(c) is not that in Fig. 4(b), but corresponds to the smaller diameter circular section of the full spontaneously deformed single domain yield

$$\Delta_5 = 0.00015.$$

Since Δ_4 and Δ_5 are not collinear we make a crude approximation to the transverse strain

$$\left(\frac{\Delta_4 + \Delta_5}{2}\right) = \frac{(0.0016 + 0.00015)}{2} = 0.00087.$$

For the virgin crystals measured, the average maximum longitudinal strain was

$$\frac{\Delta L}{L} = -0.0020 \pm 0.0001$$

and the average maximum transverse strain was

$$\frac{\Delta T}{T} = +0.0008 \pm 0.0001$$

suggesting that switchover is close to a two stage process, and lending strong support for the switching model of Cao.

Perhaps the most interesting feature of the fatigue behavior in our crystals is the changeover in the character of the loops after just the first cycle. The most severe we have seen is the change exhibited in Fig. 3 where the normally very steeply changing completion of switchover is now strongly delayed and particularly the transverse strain persists to much higher field levels Fig. 3(b). Since the longitudinal contraction appears to complete while the transverse expansion persists, there must be an increase of volume and we suspect microcracking. If some of these cracks make an angle with the E field direction which appears probable, the field seen by the crystal in that region will be reduced and switchover of polarization to the final $\bar{1}\bar{1}\bar{1}$ orientation delayed.

It is not unlikely that the propensity for cracking may depend in a complex manner on finishing, electroding, mounting of the crystals and on internal impedance and other details of the electric field supply. Differences in the severity of the behavior have been observed as indicated, but so far we have not observed any sample in our experimental setup which does not show some initial degradation of the form described.

¹S. E. Park and T. R. Shrout, *Science* **275**, 1878 (1997).

²S. E. Park and T. R. Shrout, *Mater. Res. Innovations* **1**, 20 (1997).

³L. E. Cross, *Fundamental Physics of Ferroelectrics*, 2000 Aspen CO, edited by R. E. Cohen, AIP Conf. Proc. No. 535, pp. 1–15.

⁴Z. G. Ye, *Piezo-Crystal Workshop*, Herndon, VA, July, 2001.

⁵H. Fu and R. E. Cohen, *Nature (London)* **403**, 281 (2000).

⁶K. Takemura, M. Ozgul, V. Bernard, S. Trolier-McKinstry, and C. A. Randall, *J. Appl. Phys.* **88**, 7272 (2000).

⁷V. Barnard, S. Trolier-McKinstry, K. Takemura, and C. A. Randall, *J. Appl. Phys.* **87**, 3965 (2000).

⁸W. Cao, *Ferroelectrics* **290**, 107 (2003).

⁹J. M. Jin, Y. U. Wang, A. K. Katchaturyan, J. F. Li, and D. Viehland, *J. Appl. Phys.* **94**, 3629 (2003).

¹⁰B. Noheda, A. Zhang, D. E. Cos, G. Shirane, S.-E. Park, and P. Rehring, *Phys. Rev. B* **65**, 224101 (2002).

APPENDIX 10



Hydrostatic Piezoelectric Coefficient d_h of PZT Ceramics and PZN-PT and PYN-PT Single Crystals

L. BURIANOVA,^{1*} P. HANA,¹ S. PANOS,¹ E. FURMAN,² S. ZHANG² & T.R. SHROUT²

¹Technical University of Liberec, Department of Physics and International Center for Piezoelectric Research,
Halkova 6, CZ-461 17 Liberec 1, Czech Republic

²Materials Research Institute, The Pennsylvania State University, University Park, PA 16802, USA

Submitted March 5, 2003; Revised March 11, 2004; Accepted March 11, 2004

Abstract. The hydrostatic piezoelectric coefficient d_h of $\text{Pb}(\text{Zr}_x\text{Ti}_{1-x})\text{O}_3$ ceramics (PZT), and of $\text{Pb}(\text{Zn}_{1/3}\text{Nb}_{2/3})\text{O}_3\text{-PbTiO}_3$ and $\text{Pb}(\text{Yb}_{1/2}\text{Nb}_{1/2})\text{O}_3\text{-PbTiO}_3$ (PZN-PT, PYN-PT, respectively) single crystals with compositions near to the morphotropic phase boundary (MPB) have been measured using a dynamic hydrostatic method. The effects of DC electric field and static component of hydrostatic stress on d_h of PZT ceramics, PZN-PT and PYN-PT single crystals were studied. Changes of the piezoelectric hydrostatic coefficients d_h caused by an electric field (DC bias) were observed along with pressure and temperature dependencies. The measurement of the hydrostatic piezoelectric coefficient d_h seems to be promising for investigation of intrinsic (single domain) and extrinsic (domain-walls) contributions to piezoelectric behavior of single crystals and ceramic materials.

Keywords: PZT ceramics, PZN-PT and PYN-PT relaxors, morphotropic phase boundary, hydrostatic piezoelectric coefficients

1. Introduction

It is well known that perovskite solid solutions have been intensively investigated because of their excellent piezoelectric and dielectric properties. They consist of simple cubic structure at high temperatures and variety of phases with polar states at lower temperatures. Among these materials are the ferroelectric $\text{Pb}(\text{Zr}_x\text{Ti}_{1-x})\text{O}_3$ (PZT) solid solutions that present such properties in the morphotropic phase boundary (MPB) where rhombohedral and tetragonal phases coexist practically independently of temperature. Excellent piezoelectric properties were found for relaxor-based single crystals such as $\text{Pb}(\text{Zn}_{1/3}\text{Nb}_{2/3})\text{O}_3\text{-PbTiO}_3$ and $\text{Pb}(\text{Yb}_{1/2}\text{Nb}_{1/2})\text{O}_3\text{-PbTiO}_3$ (PZN-PT, and PYN-PT, respectively) near MPB [1–4]. This is the basis for practically all transducers and other piezoelectric devices.

Recently, considerable research has been focused on the piezoelectric d_{33} and d_{31} parameters and dielectric properties of PZT bulk ceramics and thin-films. The temperature dependence of piezoelectric coefficients of PZT ceramics using resonance method was reported in [5]. The effect of hydrostatic stress on piezoelectric coefficients of PZT was published in [9]. Besides d_{33} and d_{31} , no much attention was given to study the hydrostatic piezoelectric coefficient d_h variation under different influences (as DC electric field, temperature, pressure). Thus, in our previous papers [6–8], the methods for determining PZT material parameters as piezoelectric coefficients d_{33} , d_{31} , and hydrostatic piezoelectric coefficients d_h , g_h were described. In this article our work deals with d_h measurements by a dynamic hydrostatic method combining a static and variable superimposed pressure. The effect of a DC electric field and temperatures on the hydrostatic piezoelectric coefficients d_h of PZT ceramics as well as relaxor-based single crystals as PZN-PT and PYN-PT were investigated and described.

*To whom all correspondence should be addressed. E-mail: lidmila.burianova@vslib.cz

2. Hydrostatic Piezoelectric Coefficients

The determination of the dynamic hydrostatic coefficients utilizes a poled sample along z-axis under hydrostatic pressure $pT_{ii} = -p$, all other components of stress tensor equal to zero). Simultaneously, the applied electric field $E_3 = 0$, i.e. a short-circuit condition.

The polarisation P_3 on the sample induced by hydrostatic pressure p [7], is

$$\begin{aligned} P_3 &= (d_{31} + d_{32} + d_{33}) \cdot (-p) \\ &= (d_{33} + 2d_{31}) \cdot (-p) = d_h \cdot (-p), \end{aligned} \quad (1)$$

where $d_{i\lambda}$ are piezoelectric coefficients, $d_{31} = d_{32}$, and d_h is hydrostatic coefficient.

Measurement of the induced charge Q on the area A of the electrodes and pressure p permits calculation of the hydrostatic piezoelectric coefficient d_h .

The dynamic method was described in [7] by equation

$$\frac{dQ}{dt} \frac{1}{A} = d_h \cdot \frac{dp}{dt}, \quad \text{where } Q = Q_0 \sin \omega t. \quad (2)$$

For the combined static and dynamic (with the sinusoidal shape) pressure excitation

$$p = p_0 \sin \omega t + p_{static}, \quad (3)$$

we can express the dynamic hydrostatic piezoelectric coefficient d_h as:

$$d_h = \frac{I_0}{p_0 \omega A}, \quad (4)$$

where I_0 is the amplitude of the current, p_0 is the amplitude of the dynamic pressure excitation, and ω is the angular frequency.

The hydrostatic piezoelectric coefficient d_h can be also calculated from the Eq. (1),

$$d_h = d_{33} + 2d_{31}. \quad (5)$$

Equation (5) was used for calculation of d_h values in our previous paper [6].

3. Experiment

The dynamic method of d_h measurement is based on dynamic oscillations of pressure around an appointed

static pressure mastered by an auxiliary hydraulic piston at a frequency of about 0.5–1 Hz. The temperature control is realized by the PID temperature controller with a resistive heater and by the compressor cooler. The advantage of the described method is the elimination of pyroelectric effect and higher accuracy of the measurement. The possibility of an applied electric field influence on the device under test was realized. The block diagram of the experimental set up is shown in Fig. 1.

We studied PZT ceramics and PZN-PT, PYN-PT crystals. The PZT samples EPC856 and APC856 soft PZT ceramics with composition of $\text{Pb}(\text{Zr}_{58}\text{Ti}_{42})\text{O}_3$ were provided by American Piezoceramics International, Mackeyville, PA, USA. These samples were machined in disk-shaped (1 mm thick and diameter of 10 mm) and square plates $4 \times 4 \times 2 \text{ mm}^3$.

The $\text{Pb}(\text{Zn}_{1/3}\text{Nb}_{2/3})\text{O}_3\text{-PbTiO}_3$ and $\text{Pb}(\text{Yb}_{1/2}\text{-Nb}_{1/2})\text{O}_3\text{-PbTiO}_3$ (PZN-PT, PYN-PT, respectively) single crystals were grown at the Pennsylvania State University, Material Research Institute, University Park, PA, USA. The used PZN-4.5% PT (001) and (111) cuts, and PYN-40% PT (111) cut were machined in rectangular plate-shaped samples with side length from 1.3 mm to 6.8 mm and thickness from 0.4 mm up to 0.6 mm. The measurements of the dynamic hydrostatic piezoelectric coefficient d_h were performed in the temperature range from 283 K to 433 K at a static pressure of 10 MPa and a dynamical pressure of 100 kPa.

All samples were electroded on both major surfaces and poled by the manufacturers.

4. Results and Discussion

The dependencies of the hydrostatic coefficient d_h of the soft PZT ceramics (EPC856) on DC electric field measured at various temperatures are displayed in Fig. 2. The typical relative decrease of d_h , caused by DC electric field change from zero to 700 kV m^{-1} was smaller than 20% at temperatures between 283 K and 423 K. The $d_h(E)$ increases to vicinity of Curie temperature ($T_C = 423 \text{ K}$).

Figure 3 shows the similar dependencies of d_h vs. DC electric field and temperature for the soft PZT ceramics (APC 856). The comparison of the d_h values obtained from resonance method and dynamic hydrostatic method shows, that the second method gives slightly smaller values by up to 10%. The details are shown in the Table 1.

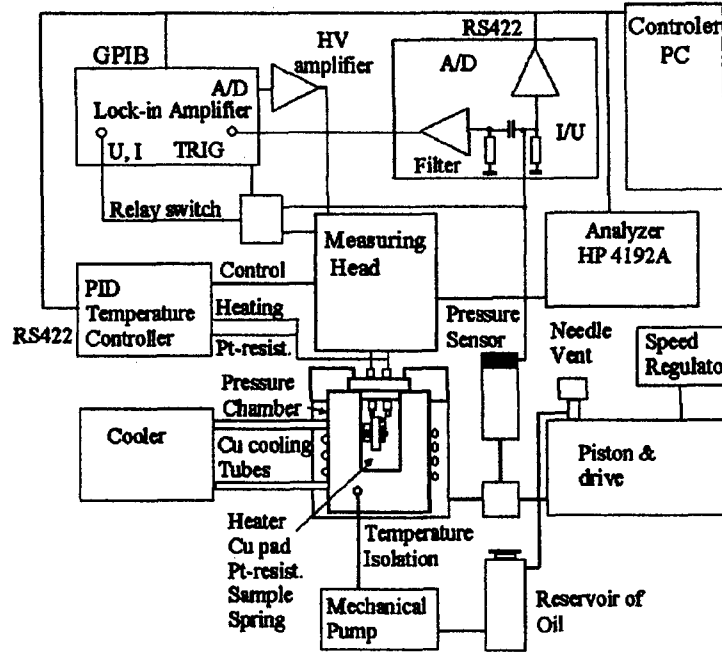


Fig. 1. A measuring set of high pressure dynamic method with the possibility of application of electric field onto sample.

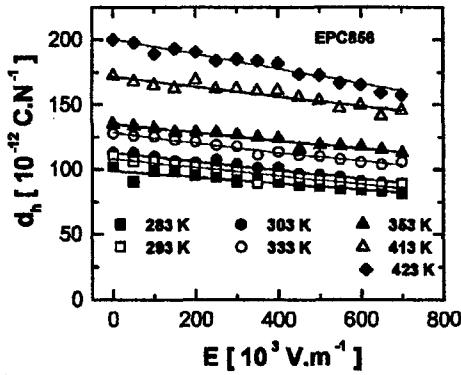


Fig. 2. Hydrostatic coefficient d_h of PZT ceramics (EPC 856) vs. DC electric field and various temperatures. Disk-shaped, 10 mm in diameter, 1 mm in thickness.

The temperature dependencies of the d_h coefficients at different DC electric field values applied to APC856 ceramics are shown in Fig. 4. A noticeable influence of the electric field on Curie temperature T_C position was exhibited.

Apparently, the phase transition is shifted to higher temperature by increasing the electric field. This is due

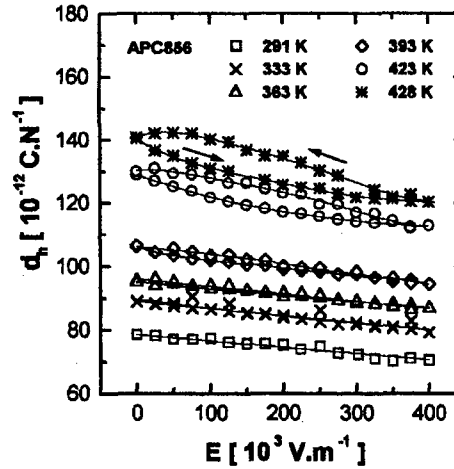


Fig. 3. Hydrostatic coefficient d_h of PZT ceramics (APC 856) vs. DC electric field and various temperatures. Plate-shaped, $4 \times 4 \times 2 \text{ mm}^3$.

to the upkeep of polar state by the applied electric field which delays the phase transition ferroelectric-paraelectric to high temperature.

The samples of PZN-PT single crystals exhibit small variation of d_h with hydrostatic pressure in the pressure

Table 1. Hydrostatic piezoelectric coefficients d_h of PZT ceramics at room temperature (APC International, Mackeyville, PA, USA.)

		PZT (APC856)	PZT (EPC856)
Resonance method	d_{33} [10^{-12} C.N $^{-1}$]	558	591
	$-d_{31}$ [10^{-12} C.N $^{-1}$]	236	237
	d_h [10^{-12} C.N $^{-1}$]	86	117
Dynamic hydrostatic method	d_h [10^{-12} C.N $^{-1}$]	79	111

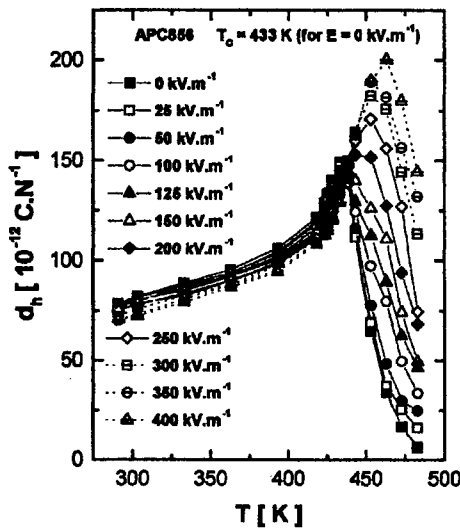


Fig. 4. Temperature dependencies of hydrostatic coefficient d_h of PZT ceramics (APC 856) at various DC electric field. Plate-shaped, $4 \times 4 \times 2$ mm 3 .

range of zero to 70 MPa. Decrease of d_h value does not exceed 5% of initial values as shown in Fig. 5.

In Fig. 6 is plotted the hydrostatic coefficient d_h of PZN-4.5%PT (001) cut vs. DC electric field at various temperatures. We can observe a change of the shapes of curves at temperatures above 373 K and low DC electric fields. We suppose that it is connected with the phase transition from ferroelectric phase to paraelectric phase. In vicinity of Curie temperature $T_C = 423$ K the value of d_h is very low at zero DC bias. For low electric field values we can observe a sharp peak of the coefficient d_h and its consequent exponential decay with increasing bias. The peak position shifts toward higher applied electric field values with increasing tempera-

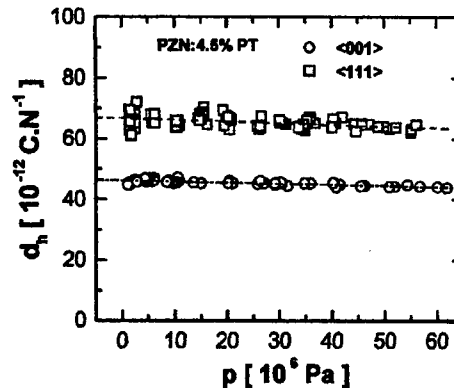


Fig. 5. Hydrostatic coefficient d_h of PZN-4.5%PT (001) cut and PZN-4.5%PT (111) cut vs. hydrostatic pressure. Plate-shaped, $6.8 \times 6.8 \times 0.48$ mm 3 , $3.2 \times 3.2 \times 0.6$ mm 3 , respectively.

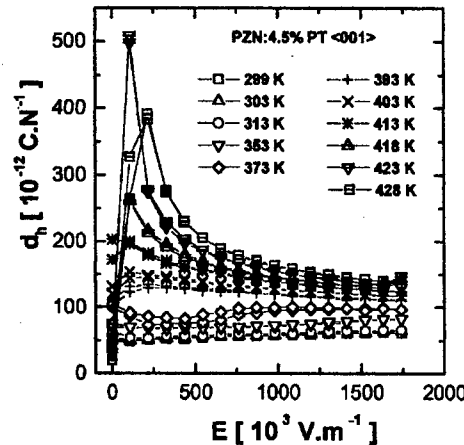


Fig. 6. Hydrostatic coefficient d_h of PZN-4.5%PT (001) cut vs. DC electric field at various temperatures. Plate-shaped, $2.0 \times 4.2 \times 0.46$ mm 3 .

tures. Furthermore, the peak magnitude undergoes a decrease with increasing electric field. The piezoelectric hydrostatic coefficient peak could be due to the domain subdivision which takes place when the temperatures approach T_C . Thus, an increase of temperature engages an increase in the domain density. The influence of electric field on domains (domain reorientation) will depend on their density, and consequently, an increase in domain density will need a high electric field for domain alignment. This could explain the peak shift to high electric fields when the temperature increases [10, 11]. The exponential decay of right

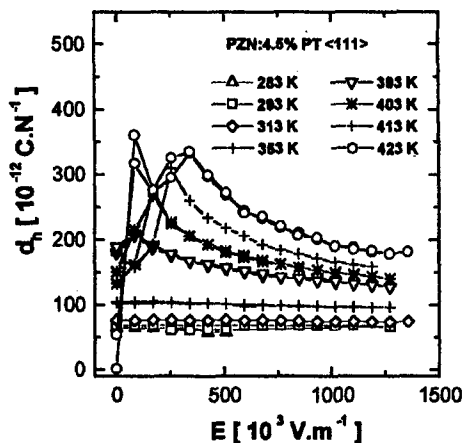


Fig. 7. Hydrostatic coefficient d_h of PZN-4.5%PT (111) cut vs. DC electric field at various temperatures. Plate-shaped, $3.2 \times 3.2 \times 0.59 \text{ mm}^3$.

side of the peak could be associated to a relaxation phenomenon stimulated by charge carrier screening in the material bulk due to the increase conductivity with temperatures. It was shown, in our experimental measurement, the value of d_h equaled to $47 \cdot 10^{-12} \text{ CN}^{-1}$ for $T = 298 \text{ K}$ and $E = 0 \text{ Vm}^{-1}$. This value is smaller than $d_h \approx 250 \cdot 10^{-12} \text{ CN}^{-1}$, which was calculated from Eq. (5) using measured d_{33} and d_{31} [1]. To put in evidence this difference further investigation of the effect of a DC electric field on domain engineering states and domain wall configuration is required.

The hydrostatic coefficient d_h of PZN-4.5%PT (111) cut vs. DC electric field at various temperatures is plotted on Fig. 7. In this case we can observe significantly different behavior for temperatures in vicinity of Curie temperature $T_C = 423 \text{ K}$. The coefficient d_h reaches two maxima for low bias fields. Possibly it could be caused by presence of intermediate orthorhombic phase. The values of d_h at low temperatures up to 353 K show slight change. Experimental value of $d_h = 68 \cdot 10^{-12} \text{ CN}^{-1}$ for $T = 298 \text{ K}$ and $E = 0 \text{ Vm}^{-1}$ is in good agreement with [1].

The hydrostatic coefficient d_h of PYN-40%PT (111) cut vs. DC electric field at various temperatures is plotted in Fig. 8. The relative change of d_h , caused by DC electric field of 1600 kVm^{-1} was smaller than 6% at temperatures between 303 K and 393 K. The d_h increases with increasing temperature up to $T_C = 523 \text{ K}$.

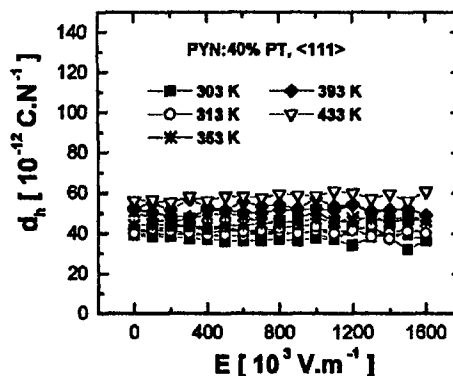


Fig. 8. Hydrostatic coefficient d_h of PYN-PT (111) cut vs. DC electric field at various temperatures. Plate-shaped, $2.2 \times 1.3 \times 0.5 \text{ mm}^3$.

5. Conclusion

The non-linear effects of DC bias electric field on the hydrostatic piezoelectric coefficient d_h for variable temperature in soft PZT ceramics, and PZN-PT and PYN-PT relaxor based single crystals were studied. The hydrostatic coefficient d_h was determined by the dynamic hydrostatic method. We believe that the discrepancy between the values of the d_h , determined by Eq. (5), and those measured directly (using dynamic hydrostatic method) is mainly caused by extrinsic contributions of domain walls. This hypothesis supports the significant contribution of domain walls motion observed and described in the paper [1] on domain engineered samples of PZN-4.5%PT single crystals, (001) cut.

Acknowledgments

This work was supported by the Grant Agency of the Czech Republic (GACR 202/03/0569) and by the Ministry of Education of Czech Republic (Project Code MSM 242200002). We are grateful to Dr. S. Zhang and Prof. T.R. Shrout for providing crystals used in this study.

References

1. S.F. Liu, S.E. Park, T.R. Shrout, and L.E. Cross, *J. Appl. Phys.*, **85**, 2810 (1999).
2. S. Zhang, S. Rhee, C.A. Randall, and T.R. Shrout, *Jpn. J. Appl. Phys.*, **41**, 772 (2002).

3. S.E. Park and T.R. Shrout, *J. Appl. Phys.*, **82**, 1804 (1997).
4. S. Zhang, S. Priya, E. Furman, T.R. Shrout, and C.A. Randall, *J. Appl. Phys.*, **91**, 6002 (2002).
5. Q.M. Zhang, H. Wang, N. Kim, and L.E. Cross, *J. Appl. Phys.*, **75**, 445 (1994).
6. L. Burianova, M. Sulc, M. Prokopova, and J. Nosek, *Ferroelectrics*, **292**, 111 (2003).
7. P. Hana, L. Burianova, and S. Panos, *Sensors and Actuators*, (2003, in print).
8. L. Burianova, M. Sulc, and M. Prokopova, *J. European Cer. Soc.*, **21**, 1387 (2001).
9. T. Yamamoto and Y. Makino, *Jpn. J. Appl. Phys.*, **35**, 3214 (1996).
10. Y. Wang, W. Sun, X. Chen, H. Shen, and B. Lu, *Phys. Status Solidi A*, **102**, 279 (1987).
11. Y. N. Huang, Y. N. Wang, and H. M. Shen, *Phys. Rev. B*, **46**, 3290 (1992).

APPENDIX 11

Epitaxially induced high temperature (>900 K) cubic-tetragonal structural phase transition in BaTiO₃ thin films

Feiming Bai

Department of Materials Science and Engineering, Virginia Tech, Blacksburg, Virginia 24061

Haimei Zheng

Department of Materials and Nuclear Engineering, University of Maryland, College Park, Maryland 20742

Hu Cao

Department of Materials Science and Engineering, Virginia Tech, Blacksburg, Virginia 24061

L. E. Cross

Materials Research Institute, Pennsylvania State University, State College, Pennsylvania 16802

R. Ramesh

Department of Materials and Nuclear Engineering, University of California, Berkeley, California 94720

Jiefang Li and D. Viehland^{a)}

Department of Materials Science and Engineering, Virginia Tech, Blacksburg, Virginia 24061

(Received 25 May 2004; accepted 1 September 2004)

For (001)_c oriented BaTiO₃ thin films, it has been found that epitaxial constraint can result in a dramatic increase in the temperature of a tetragonal (*T*) structural phase transition. For 2000-Å-thick films grown directly on SrTiO₃ substrates, a *T*→cubic (*C*) phase transition was found on heating at >950 K, where the lattice constant changed smoothly with temperature. It was also found for films of the same thickness that the *T*→*C* transition is nearly restored to that of bulk crystals by the use of a buffer layer, which relaxes the epitaxial constraint. These results provide evidence of an epitaxially induced high temperature structural phase transition in BaTiO₃ thin films, where the ferroelectric (internal) and structural (external) aspects of the phase transition are decoupled. © 2004 American Institute of Physics. [DOI: 10.1063/1.1812579]

The classic first order ferroelectric phase transformation is the cubic (*C*) to tetragonal (*T*) one in BaTiO₃ bulk crystals,^{1,2} which occurs near a Curie temperature of $T_C \cong 405$ K. Subsequent ferroelectric transitions occur to lower symmetry orthorhombic and rhombohedral phases with decreasing temperature. Thin films of BaTiO₃ have also been intensively investigated for applications in ferroelectric memories, integrated capacitors, and electro-optic modulators.³⁻⁷ Both epitaxial⁸⁻¹³ and polycrystalline¹⁴ films have been studied.

Investigations of epitaxial BaTiO₃ films from on SrTiO₃⁸ and MgO⁹⁻¹¹ have reported the lack of structural phase transformations. This was evidenced by the lack of anomalies in the temperature dependence of the lattice parameters. In particular, studies by Yoneda *et al.*⁹ have found the lack of a *T*→*C* transition on heating for films of 100, 1000, and 4000 Å thickness grown on MgO—the tetragonal structure remained present at all temperatures measured upto 850 K. However, corresponding electrical property measurements revealed a maximum in the temperature dependent dielectric constant (*K*) at $T \cong 410$ K, in near agreement with that of bulk BaTiO₃ single crystals and ceramics. These results have recently been interpreted as the effect of epitaxial constraint that prevents external dimension changes of the film due to clamping, while permitting a ferroelectric phase transition with internal displacive rearrangements.¹⁵

Recently, a Landau–Ginzburg–Devonshire (LGD) thermodynamic theory has been developed by Pertsev *et al.*¹⁶ to describe the effect of epitaxial constraint on the structural phase transitions of SrTiO₃ thin films grown with differing misfits on various substrates. SrTiO₃ bulk crystals undergo a *C*→*T* transition on cooling at $T = 105$ K which is ferroelastic in nature, but not ferroelectric. Rather, it is an incipient ferroelectric. Using the LGD theory,¹⁶ the epitaxial phase diagram of (001)_c oriented SrTiO₃ as calculated for films grown on various cubic substrates. It was shown that decoupled ferroelectric and ferroelastic instabilities could be driven by epitaxial constraint, where various ferroelectric phase transitions could occur as internal atomic rearrangements within ferroelastically distorted *T* phases.

The thermodynamic investigations of constrained thin layers of SrTiO₃¹⁶ suggest that epitaxy might result in decoupled ferroelectric and ferroelastic phase transitions from prototypic cubic (*m3m*) to tetragonal symmetries in many perovskite films. However, it has yet to be shown whether there is an independent ferroelastic *T*→*C* structural phase transition in epitaxially constrained ferroelectric films at higher temperatures, or not. In this letter, we will report a high-temperature *T*→*C* phase transition (>900 K) in epitaxially constrained (001)_c oriented BaTiO₃ films grown directly on SrTiO₃ substrates. It will also be shown for films of the same thickness that the *T*→*C* phase transition temperature can be restored to that of bulk single crystals by the use of a buffer layer, which relaxes the epitaxial constraint.

^{a)}Electronic mail: dviehlan@vt.edu

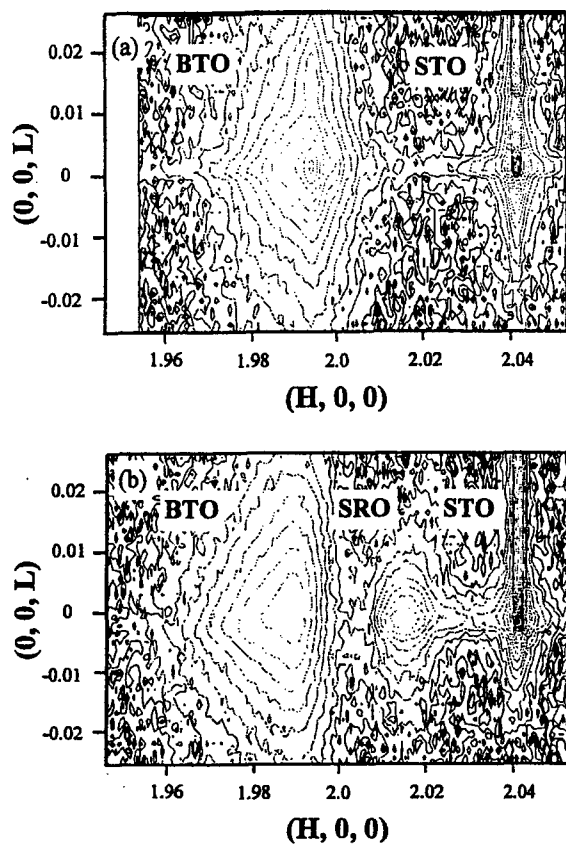


FIG. 1. Reciprocal space scans for $(001)_c$ oriented BaTiO_3 thin layers taken along the (HOL) zone for (a) a 2000-Å-thick BaTiO_3 films grown directly on $(001)_c$ SrTiO_3 substrate; and (b) a 2000-Å-thick BaTiO_3 films grown on a 600-Å-thick SrRuO_3 electrode (or buffer layer), which was grown on top of a $(001)_c$ SrTiO_3 substrate. The values of (HKL) are normalized to those of BaTiO_3 single crystals, i.e., $(H, K, L)_{\text{crystal}} = (1, 1, 1)$. Intensity is given on a log scale.

We have grown phase-pure BaTiO_3 (BTO) thin films of 2000 Å thickness by pulsed laser deposition onto $(001)_c$ single crystal substrates of SrTiO_3 . Some of the films were grown directly on SrTiO_3 : deposited at 670 °C in an oxygen ambient of 20 mTorr at a growth rate of 0.7 Å/s. Others films were grown on top of a conducting perovskite oxide electrode. SrRuO_3 (SRO)¹⁷ was chosen as the bottom electrode due to the closest lattice mismatch with the BTO structure: films of SRO of 500 Å were deposited at 600 °C in an oxygen ambient of 100 mTorr, and followed by the BTO film deposition as described earlier. X-ray diffraction studies were performed using a Phillips MPD system. Careful investigations were performed using a high resolution x-ray diffractometer equipped with a two bounce hybrid monochromator, an open three-circle Eulerian cradle, and a doomed hot stage. A $\text{Ge}(220)$ cut crystal was used as an analyzer, which had a theta-resolution of $\sim 0.0068^\circ$ (or 0.43 arc sec). The x-ray wavelength was that of $\text{Cu}_{K\alpha}$ ($\lambda = 1.5406$ Å) and the x-ray generator was operated at 45 kV and 40 mA. The penetration depth in BaTiO_3 at this x-ray wavelength is much greater than that of the film thickness. The lattice constants of $(001)_c$ oriented BaTiO_3 films measured as a function of temperature on heating over the range of 300–1000 K. The a -lattice parameter of BaTiO_3 bulk single crystals at $T = 300$ K is $a = 3.99$ Å, and thus we use one reciprocal lattice unit as corresponding to $a^* (= b^*) = 2\pi/a$

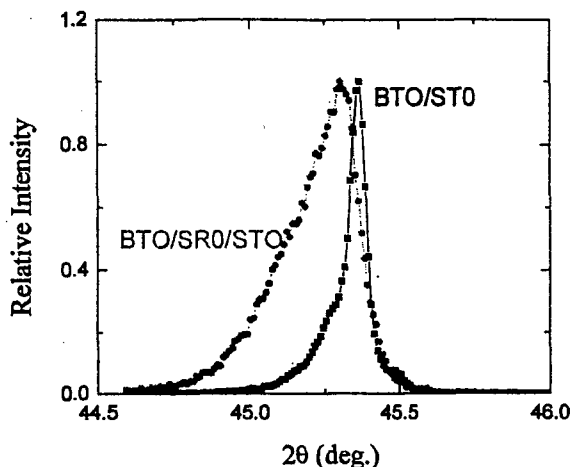


FIG. 2. Longitudinal (200) profile for a 2000-Å-thick BaTiO_3 films grown directly on $(001)_c$ SrTiO_3 substrate; and a 2000-Å-thick BaTiO_3 films grown on a 600-Å-thick SrRuO_3 electrode (or buffer layer), which was grown on top of a $(001)_c$ SrTiO_3 substrate.

$= 1.547 \text{ \AA}^{-1}$. The mesh scans presented in this letter are plotted in this reciprocal unit.

Figure 1 shows reciprocal lattice scans taken along the (HOL) zone for $(001)_c$ BaTiO_3 films (a) grown directly on SrTiO_3 ; and (b) grown on a SrRuO_3 buffer layer. The mesh scans reveal two peaks for the film grown directly on SrTiO_3 , whereas three peaks can be seen for that grown on the SrRuO_3 buffer layer. The phases corresponding to the peaks are identified in the figures. These results confirm that the SrRuO_3 buffer layer has a lattice parameter close to its bulk value ($a = 3.98$ Å), and that the BaTiO_3 layer is much better lattice matched to it than to the SrTiO_3 substrate. Accordingly, for a given thickness, films grown on a SrRuO_3 buffer layer will be significantly more elastically relaxed. It is also relevant to note that both films had a relatively small mosaic spread of $\sim 0.2^\circ$, revealing satisfactory film quality. Figure 2 shows longitudinal (200) profiles of $(001)_c$ BaTiO_3 films grown directly on SrTiO_3 , and on a SrRuO_3 buffer layer. The data reveal the coexistence of c and a domains for films grown on the buffer layer, whereas those grown directly on SrTiO_3 consisted mostly of only a domains.

A complete structural analysis was then done using longitudinal (200) and (202) profiles for both types of films. Figure 3 shows the lattice parameters as a function of temperature for films grown (a) directly on the substrate; and (b) on the buffer layer. Comparisons of data in the figure will reveal a dramatic difference in the $T \rightarrow C$ phase transition temperature on heating between these two types of films. For 2000-Å-thick films grown on SrTiO_3 substrates, the $T \rightarrow C$ phase transition occurred on heating near 950 K (maybe slightly deviated due to fitness error). However, for an identical 2000-Å-thick film grown on SrRuO_3 buffer layers, the $T \rightarrow C$ phase transition occurred near 470 K—which is close to $T_C = 405$ K of bulk BaTiO_3 single crystals.^{1,2} These results provide evidence of an epitaxially induced high temperature structural phase transition in BaTiO_3 thin films, which is relaxed by growth of an identical film on a SrRuO_3 buffer layer.

It is also important to note several other features in Fig. 3. First, the a -lattice parameter for both films exhibited no indications of a phase transition. Rather, the lattice parameters changed gradually with temperature, similar to a simple

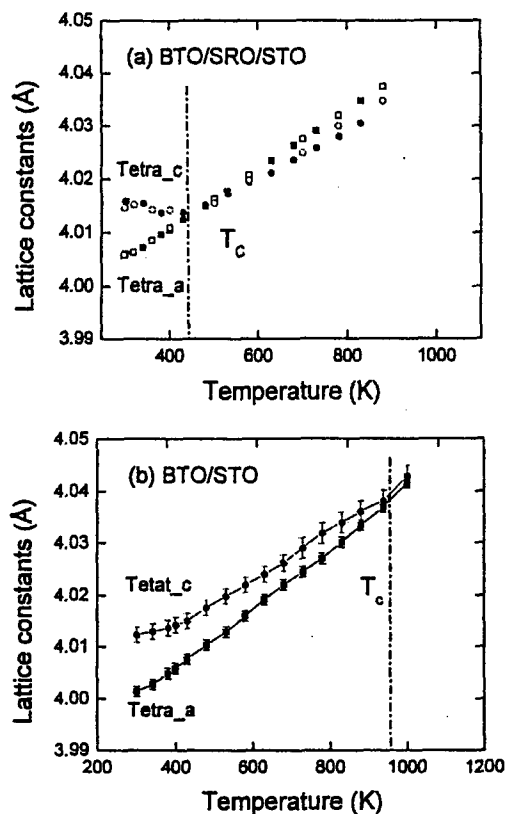


FIG. 3. Temperature dependent lattice parameters for (a) a 2000-Å-thick BaTiO₃ films grown directly on (001)_c SrTiO₃ substrate; and (b) a 2000-Å-thick BaTiO₃ films grown on a 600-Å-thick SrRuO₃ electrode (or buffer layer), which was grown on top of a (001)_c SrTiO₃ substrate. Solid circles and squares represent increasing temperature and open circles and squares represent decreasing temperature.

thermal expansion. This is because any changes in the *a*-lattice parameter with temperature must be invariant with respect to corresponding ones in the substrate or buffer layer. Second, the *c/a* ratio is nearly equal for both films at 300 K: in fact, for both types of films, the relative changes in *c/a* with temperature below 470 K were gradual and of similar magnitude. These results suggest that the ferroelectric phase transformation temperature is nearly the same for both films, as *T_C* is generally expected to be proportional to *c/a*.¹ This is also supported by previous dielectric and structural studies of (001)_c BaTiO₃ thin films grown on Pt/MgO that demonstrated the lack of a *T*→*C* phase transition, in spite of a maximum in the dielectric constant at 470 K.⁹ Our structural

data for the films grown directly on the SrTiO₃ substrate are qualitatively similar—except we clearly show that a *T*→*C* phase transition occurs near 950 K. In our case, for films grown directly on the substrate, the ferroelectric (internal) and structural (external) aspects of the phase transition must clearly be decoupled.

In summary, 2000-Å-thick BaTiO₃ films grown directly on (001)_c SrTiO₃ substrates have a tetragonal structure until a temperature greater than 900 K. However, an identical film of the same thickness grown on a 500-Å-thick SrRuO₃ buffer layer on top of the substrate undergoes a *T*→*C* transition at 470 K, in close proximity to *T_C*=405 K of bulk BaTiO₃ crystals. These results provide evidence of an epitaxially induced high temperature structural phase transition in BaTiO₃ thin films, where the ferroelectric (internal) and structural (external) aspects of the phase transition are decoupled.

The authors are pleased to acknowledge support from the office of Naval Research (ONR) under Contract Nos. MURI N000140110761, N000140210340, and N000140210126; and the NSF-MRSEC DMR-00-80008.

¹M. E. Lines and A. M. Glass, *Principles and Applications of Ferroelectrics and Related Materials* (Clarendon, Oxford, 1977).

²F. Jona and G. Shirane, *Ferroelectric Crystals* (Pergamon, New York, 1962).

³D. Roy and S. Krupanidhi, *Appl. Phys. Lett.* **61**, 2057 (1992).

⁴K. Nashimoto, D. Fork, F. Ponce, and J. Tramotoana, *Jpn. J. Appl. Phys., Part 1* **32**, 4099 (1990).

⁵K. Iijima, T. Terashima, K. Yamamoto, K. Hirata, and Y. Bando, *Appl. Phys. Lett.* **56**, 527 (1990).

⁶H. Lu, L. Wills, and B. Wessels, *Appl. Phys. Lett.* **64**, 2973 (1994).

⁷R. McKee, F. Walker, E. Specht, G. Jellison, and L. Boatner, *Phys. Rev. Lett.* **72**, 2741 (1994).

⁸H. Terauchi, Y. Wantanabe, H. Kasatani, K. Kamigaki, Y. Yano, T. Terashima, and Y. Bando, *J. Phys. Soc. Jpn.* **61**, 2194 (1992).

⁹Y. Yoneda, H. Kasatani, H. Terauchi, Y. Yano, T. Terashima, and Y. Bando, *J. Phys. Soc. Jpn.* **62**, 1840 (1993).

¹⁰Y. Yoneda, K. Sakaue, and H. Terauchi, *J. Phys.: Condens. Matter* **13**, 9575 (2001).

¹¹S. Kim and J. Je, *J. Mater. Res.* **14**, 3734 (1999).

¹²C. Li, Z. Chen, D. Cui, Y. Zhou, H. Lu, C. Dong, F. Wu, and H. Chen, *J. Appl. Phys.* **86**, 4555 (1999).

¹³Y. Yoneda, T. Okabe, K. Sakaue, H. Terauchi, H. Kasatani, and K. Deguchi, *J. Appl. Phys.* **83**, 2458 (1998).

¹⁴M. Frey, Ph.D dissertation, University of Illinois, Urbana, IL, 1997.

¹⁵F. He, B. Wells, S. Shapiro, M. Zimmermann, A. Clark, and X. Xi, e-print arXiv: cond-mat/0303317 (2004).

¹⁶N. Pertsev, A. Tagantsev, and N. Setter, *Phys. Rev. B* **61**, R825 (2000).

¹⁷C. Eom, R. J. Cava, R. Fleming, and J. Phillips, *Science* **258**, 1766 (1992).

APPENDIX 12

A phenomenological thermodynamic potential for BaTiO₃ single crystals

Y. L. Li^{a)}

Department of Materials Science and Engineering, The Pennsylvania State University, University Park, Pennsylvania 16802

L. E. Cross

Department of Electrical Engineering and Materials Research Institute, The Pennsylvania State University, University Park, Pennsylvania 16802

L. Q. Chen

Department of Materials Science and Engineering, The Pennsylvania State University, University Park, Pennsylvania 16802

(Received 4 April 2005; accepted 4 August 2005; published online 16 September 2005)

A phenomenological thermodynamic potential was constructed based on the properties of bulk BaTiO₃ single crystals. An eighth-order polynomial of Landau-Devonshire expansion was employed. It reproduces bulk properties including the three possible ferroelectric transition temperatures and their dependence on electric fields, as well as the dielectric and piezoelectric constants. Different from the existing thermodynamic potential, it is applicable to predicting the ferroelectric phase transitions and properties of BaTiO₃ thin films under large compressive biaxial strains. © 2005 American Institute of Physics. [DOI: 10.1063/1.2042528]

I. INTRODUCTION

Ferroelectric BaTiO₃ ceramics and single crystals have been extensively studied for many decades, and their bulk ferroelectric phase transitions, crystal structures, and ferroelectric properties are well established. Based on the structures and properties of bulk ceramics and single crystals, a thermodynamic description of the Landau-Devonshire theory was developed by Bell and Cross.¹ It reproduces quite well most of the single-crystal structural and ferroelectric properties including the various ferroelectric phase-transition temperatures. It has been used to predict the effect of strain on the phase transitions and ferroelectric properties of BaTiO₃ thin films.²⁻⁴ However, it is only applicable to BaTiO₃ films under relatively small compressive strains ($\leq 0.4\%$).²⁻⁴ For a certain temperature range, there is no solution for equilibrium polarization under larger compressive strains, i.e., no ferroelectric phase transition. On the other hand, it has been shown that BaTiO₃ thin films may be subjected to much higher compressive strains, $>1\%$, due to substrate constraints. For example, it is recently discovered that BaTiO₃ films can be compressively strained as much as 1.6%, and the cubic to tetragonal ferroelectric transition temperature of BaTiO₃ thin films can be increased to over 600 °C,^{5,6} a huge shift compared with bulk BaTiO₃ single crystals (~ 125 °C).⁷⁻¹⁰

In order to predict the phase transitions, domain structures, and ferroelectric properties of BaTiO₃ thin films under such large compressive constraints, a thermodynamic potential is required. The main objective of the paper is to construct such a thermodynamic potential.

II. PHENOMENOLOGICAL THERMODYNAMIC POTENTIAL

In a phenomenological description of the ferroelectric phase transitions in BaTiO₃, the spontaneous polarization $\mathbf{P} = (P_1, P_2, P_3)$ is chosen as the order parameter. The Landau-Devonshire potential is expanded as a polynomial of the polarization components $P_i (i=1, 2, 3)$.^{11,12} In this work, we employed an eighth-order polynomial for the Landau-Devonshire potential. Under mechanical stress-free boundary condition, it is

$$\begin{aligned} f_0 = & \alpha_1(P_1^2 + P_2^2 + P_3^2) + \alpha_{11}(P_1^4 + P_2^4 + P_3^4) \\ & + \alpha_{12}(P_1^2 P_2^2 + P_2^2 P_3^2 + P_1^2 P_3^2) + \alpha_{111}(P_1^6 + P_2^6 + P_3^6) \\ & + \alpha_{112}[P_1^2(P_2^4 + P_3^4) + P_2^2(P_1^4 + P_3^4) + P_3^2(P_1^4 + P_2^4)] \\ & + \alpha_{123}P_1^2 P_2^2 P_3^2 + \alpha_{1111}(P_1^8 + P_2^8 + P_3^8) \\ & + \alpha_{1112}[P_1^6(P_2^2 + P_3^2) + P_2^6(P_1^2 + P_3^2) + P_3^6(P_1^2 + P_2^2)] \\ & + \alpha_{1122}(P_1^4 P_2^4 + P_2^4 P_3^4 + P_1^4 P_3^4) \\ & + \alpha_{1123}(P_1^4 P_2^2 P_3^2 + P_2^4 P_3^2 P_1^2 + P_3^4 P_1^2 P_2^2), \end{aligned} \quad (1)$$

where all of the coefficients are assumed to be temperature independent except α_1 . α_1 is linearly dependent on temperature and obeys the Curie-Weiss law. The coefficients obtained in this work are listed in Table I. α_{11} , α_{111} , and α_{1111} were fitted to the ferroelectric transition temperature from paraelectric cubic phase to ferroelectric tetragonal phase and to the spontaneous polarization and dielectric constant of the tetragonal phase. α_{12} , α_{112} , α_{1112} , and α_{1122} were fitted to the properties of ferroelectric orthorhombic phase while the remaining two coefficients α_{123} and α_{1123} were determined from the ferroelectric rhombohedral phase. It should be noted that the existing thermodynamic potential¹ employed a sixth-order polynomial. In order to fit the three ferroelectric phase transitions as well as the ferroelectric properties as a

^{a)} Author to whom correspondence should be addressed; electronic mail: Yil1@psu.edu

TABLE I. Coefficients of Landau-Devonshire potential in Eq. (1) where T is temperature in $^{\circ}\text{C}$.

Coefficients	This work	Bell and Cross ^a	Units
α_1	$4.124 \times 10^5(T-115)$	$3.34 \times 10^5(T-108)$	$\text{C}^{-2} \text{m}^2 \text{N}$
α_{11}	-2.097×10^8	$4.69 \times 10^6(T-120) - 2.02 \times 10^8$	$\text{C}^{-4} \text{m}^6 \text{N}$
α_{12}	7.974×10^8	3.23×10^8	$\text{C}^{-4} \text{m}^6 \text{N}$
α_{111}	1.294×10^9	$-5.52 \times 10^7(T-120) + 2.76 \times 10^9$	$\text{C}^{-6} \text{m}^{10} \text{N}$
α_{112}	-1.950×10^9	4.47×10^9	$\text{C}^{-6} \text{m}^{10} \text{N}$
α_{123}	-2.500×10^9	4.91×10^9	$\text{C}^{-6} \text{m}^{10} \text{N}$
α_{1111}	3.863×10^{10}	0.0	$\text{C}^{-8} \text{m}^{14} \text{N}$
α_{1112}	2.529×10^{10}	0.0	$\text{C}^{-8} \text{m}^{14} \text{N}$
α_{1122}	1.637×10^{10}	0.0	$\text{C}^{-8} \text{m}^{14} \text{N}$
α_{1123}	1.367×10^{10}	0.0	$\text{C}^{-8} \text{m}^{14} \text{N}$

^aReference 1.

function of temperature, the coefficients α_1 , α_{11} , and α_{111} were assumed to be dependent on temperature. It is the dependence of α_{11} and α_{111} on temperature that limits the application of the existing potential to small compressive strains. For comparison, the coefficients from Bell and Cross¹ are listed in the table as well.

With the new coefficients listed in Table I, the potential in Eq. (1) yields the transition temperatures: $T_{c(\text{Cubic} \rightarrow \text{Tetragonal})} = 125^{\circ}\text{C}$, $T_{c(\text{Tetragonal} \rightarrow \text{Orthorhombic})} = 8^{\circ}\text{C}$, and $T_{c(\text{Orthorhombic} \rightarrow \text{Rhombohedral})} = -71^{\circ}\text{C}$ for BaTiO_3 single crystals under the stress-free condition. The ferroelectric properties calculated at room temperature are compared in Table II with available experimentally measured values^{10,13-20} and those from the coefficients of Bell and Cross.^{1,21} The polarizations and dielectric constants as a function of temperature obtained from the potential are shown in Figs. 1 and 2, respectively.

Since only the second-order coefficient is dependent on temperature linearly, the entropy change for a phase transition at the transition temperature T_c can be related to polarization as $\Delta S = [P_{\text{product}}^2(T_c) - P_{\text{parent}}^2(T_c)] / 2\epsilon_0 C$,¹¹ where ϵ_0 is the permittivity of vacuum and C is the Curie-Weiss constant. The entropy changes ΔS at the three transition points calculated from the thermodynamic potential are listed in Table III. The experimental data from Jona and Shirane¹¹ are included in the table for comparison. Although they were not used in the fitting of the potential, the calculated and experimentally measured values agree with each other very well.

III. PHASE TRANSITIONS UNDER ELECTRICAL FIELD

Under the presence of an external electric field $E = (E_1, E_2, E_3)$, the Landau-Devonshire potential is rewritten as follows in order to take into account its effect:^{1,21}

$$f = f_0 - E_1 P_1 - E_2 P_2 - E_3 P_3. \quad (2)$$

Based on Eq. (2), phase diagrams as a function of temperature and external applied electric field were constructed. Figures 3(a)–3(c) show the results for the cases where electric fields $E = (0, 0, E_0)$, $E = (E_0, 0, E_0)$, and $E = (E_0, E_0, E_0)$ are applied, respectively. The stable ferroelectric phase corresponds to the minimum of f in Eq. (2) for a given temperature and electric field. For the applied electric field $E = (0, 0, E_0)$ our results are in good agreement with the experimental results from Fesenko and Popov.²²

There is a renewed interest in the piezoelectric properties of BaTiO_3 single crystals since it is believed that a significant enhancement could be achieved through domain engineering by applied electric fields.^{19,20,23} We calculated the piezoelectric coefficient d_{3i} ($i=1, 2, 3$) through the derivatives of strains with respect to the electric field for a BaTiO_3 single crystal polarized along the [001], [101], and [111] crystallographic axes, respectively. Under a stress-free condition, the strains in the single crystal are the spontaneous strains. For example, the spontaneous strain $e_{[l,m,n]}$ along any arbitrary direction $[l, m, n]$ with respect to the pseudocubic cell is calculated through

TABLE II. Properties of BaTiO_3 at room temperature $T=25^{\circ}\text{C}$.

Properties	This work	Others	Units
P_s	0.26	0.25, ^b 0.26, ^{c,d} 0.265 ^a	C m^{-2}
ϵ_{33}	188	168, ^e 150, ^b 130 ± 5 , ^{f,g,h} 193 ^a	
ϵ_{11}	3600	2920, ^e 3600, ^b 4400 ± 400 , ^{f,g,h} 3300 ^a	
d_{33}	86.3	85.6, ^e 68.5, ^f 90 ± 5 , ^g 125, ⁱ 128, ^j 99.8 ^k	10^{-12}C N^{-1}
d_{31}	-29.4	-34.5, ^e -33.4, ^f -32.5 ± 2 , ^g -40.8 ^k	10^{-12}C N^{-1}

^aReference 1.^bReference 10.^cReference 13.^dReference 14.^eReference 15.^fReference 16.^gReference 17.^hReference 18.ⁱReference 19.^jReference 20.^kReference 21.

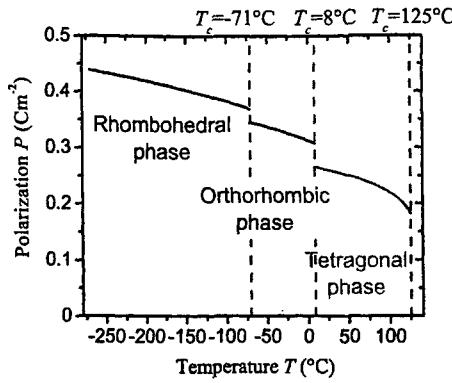


FIG. 1. (Color online) Polarizations vs temperature in BaTiO₃ single crystal under stress-free condition, where $P=|P|$, $P=(0,0,P_r)$ in tetragonal phase, $P=(P_o,0,P_o)$ in orthorhombic phase, and $P=(P_r,P_r,P_r)$ in rhombohedral phase.

$$e_{[l,m,n]} = e_{11}^0 l^2 + e_{22}^0 m^2 + e_{33}^0 n^2 + 2e_{12}^0 lm + 2e_{13}^0 ln + 2e_{23}^0 mn, \quad (3)$$

where e_{ij}^0 is the spontaneous strain or transformation strain along pseudocubic axes,

$$\begin{aligned} e_{11}^0 &= Q_{11}P_1^2 + Q_{12}P_2^2 + Q_{12}P_3^2, \\ e_{22}^0 &= Q_{12}P_1^2 + Q_{11}P_2^2 + Q_{12}P_3^2, \\ e_{33}^0 &= Q_{12}P_1^2 + Q_{12}P_2^2 + Q_{11}P_3^2, \\ e_{12}^0 &= Q_{44}P_1P_2, \quad e_{13}^0 = Q_{44}P_1P_3, \quad e_{23}^0 = Q_{44}P_2P_3. \end{aligned} \quad (4)$$

The electrostrictive coefficients $Q_{11}=0.10$, $Q_{12}=-0.034$, and $Q_{44}=0.029(\text{C}^{-1}\text{m}^2)$ from Yamada²⁴ were used for calculating the piezoelectric coefficients $d_{3i}(i=1,2,3)$ at room temperature as a function of applied electric field. Wada *et al.* investigated the enhancement of piezoelectric properties by applying an electric field along the [111] direction and found that $d_{33} \sim 203 \text{ pC N}^{-1}$ when $E_{[111]} < 0.6 \text{ MV m}^{-1}$, $d_{33} \sim 145 \text{ pC N}^{-1}$ when $4.0 \text{ MV m}^{-1} < E_{[111]} < 5.0 \text{ MV m}^{-1}$, and d_{33} had its maximum of 295 pC N^{-1} when $1.6 \text{ MV m}^{-1} < E_{[111]} < 2.6 \text{ MV m}^{-1}$.¹⁹ The experimental data agreed well

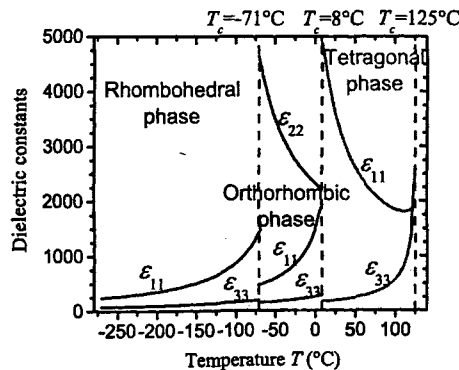


FIG. 2. (Color online) Dielectric constants in the corresponding ferroelectric phases where ϵ_{33} is along the polarization direction and ϵ_{11} and ϵ_{22} are along the two directions which are orthogonal to each other and to the polarization. For tetragonal and rhombohedral phases, $\epsilon_{11}=\epsilon_{22}$. For orthorhombic phase of $P=(P_o,0,P_o)$, ϵ_{22} is along the [010] direction.

TABLE III. Entropy changes ΔS of BaTiO₃ for the three ferroelectric transitions.

Transition	This work		Others ^a
	[J m ⁻³ K ⁻¹]	[cal/(mole K)]	
Cubic to tetragonal	13535.1	0.124	0.12~0.125
Tetragonal to orthorhombic	9939.8	0.091	0.054~0.091
Orthorhombic to rhombohedral	6970.9	0.064	0.04~0.07

^aReference 11.

with our prediction (see Fig. 4). It may be noted that the piezoelectric coefficient d_{33} is the highest at phase-transition temperatures. A similar feature is found in Fig. 5 when the applied electric field is along the [101] direction. There is no significant variation in the piezoelectric coefficients d_{33} and

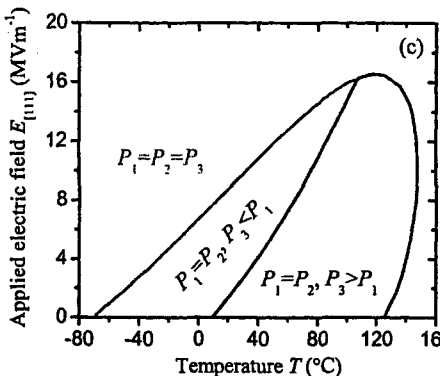
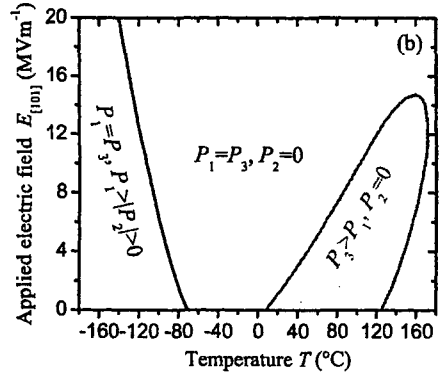
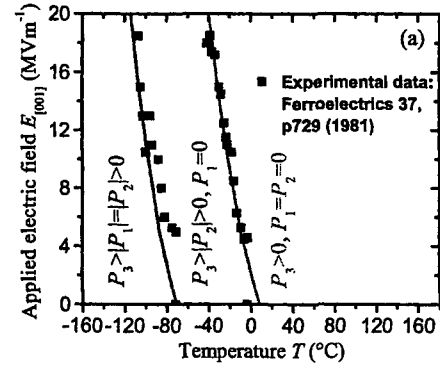


FIG. 3. (Color online) Phase diagram as a function of temperature and applied electric field (a) $E=(0,0,E_0)$ so that $E_{[001]}=E_0$; (b) $E=(E_0,0,E_0)$ so that $E_{[101]}=\sqrt{2}E_0$; (c) $E=(E_0,E_0,E_0)$ so that $E_{[111]}=\sqrt{3}E_0$.

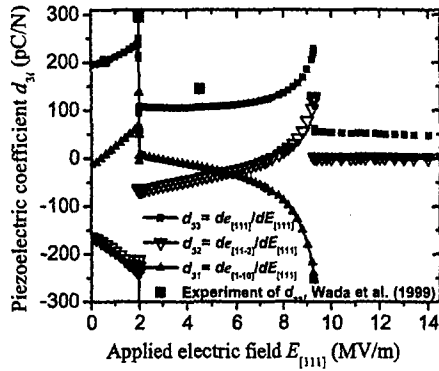


FIG. 4. (Color online) Piezoelectric coefficient d_{3i} vs applied electric field $E_{[111]}$ at room temperature.

d_{31} , however, with applied electric field $E_{[001]}$ (Fig. 6). This is consistent with the fact that there is no additional ferroelectric transition induced by the applied electric field $E_{[001]}$.

IV. SUMMARY

An eighth-order polynomial Landau-Devonshire potential was proposed for bulk BaTiO₃ single crystals. It reproduces the ferroelectric properties of BaTiO₃ single crystals as a function of temperature. The dependence of the ferroelectric transition temperatures and piezoelectric properties on applied electric field calculated from the potential agrees well with reported experimental data. It is found that the highest piezoelectric coefficient d_{33} always coincides with a ferroelectric transition.

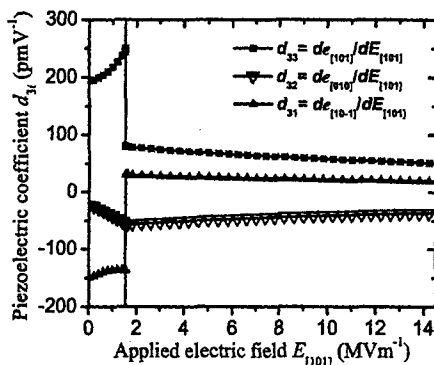


FIG. 5. (Color online) Piezoelectric coefficient d_{3i} vs applied electric field $E_{[101]}$ at room temperature.

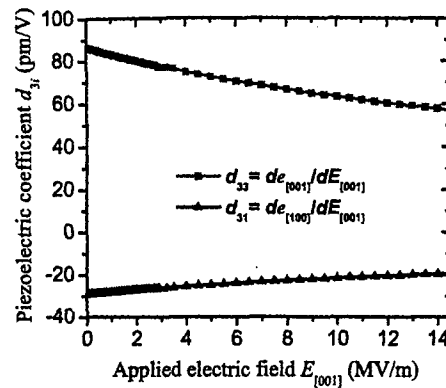


FIG. 6. (Color online) Piezoelectric coefficients d_{33} and d_{31} vs applied electric field $E_{[001]}$ direction at room temperature.

ACKNOWLEDGMENTS

The authors are grateful for Professor D. Schlom for suggestions and discussions. The work is supported by NSF under Grant Nos. of DMR-0122638 and DMR-0103354.

- ¹A. J. Bell and L. E. Cross, *Ferroelectrics* **59**, 197 (1984).
- ²N. A. Pertsev, A. G. Zembilgotov, and A. K. Tagantsev, *Phys. Rev. Lett.* **80**, 1988 (1998).
- ³V. G. Koukhar, N. A. Pertsev, and R. Waser, *Phys. Rev. B* **64**, 214103 (2001).
- ⁴D. A. Tenne *et al.*, *Phys. Rev. B* **69**, 174101 (2004).
- ⁵K. J. Choi *et al.*, *Science* **306**, 1005 (2004).
- ⁶Y. Yoneda, T. Okabe, K. Sakaue, H. Terauchi, H. Kasatani, and K. Deguchi, *J. Appl. Phys.* **83**, 2458 (1998).
- ⁷W. J. Merz, *Phys. Rev.* **91**, 513 (1953).
- ⁸W. J. Merz, *Phys. Rev.* **76**, 1221 (1949).
- ⁹C. J. Johnson, *Appl. Phys. Lett.* **7**, 221 (1965).
- ¹⁰S. H. Wemple, M. Didomenico, and I. Camlibel, *J. Phys. Chem. Solids* **29**, 1797 (1968).
- ¹¹F. Jona and G. Shirane, *Ferroelectric Crystals* (Pergamon, Oxford, New York, 1962).
- ¹²A. F. Devonshire, *Philos. Mag.* **40**, 1040 (1949).
- ¹³M. E. Drougard, R. Landauer, and D. R. Young, *Phys. Rev.* **98**, 1010 (1955).
- ¹⁴H. H. Wieder, *Phys. Rev.* **99**, 1161 (1955).
- ¹⁵D. Berlincourt and H. Jaffe, *Phys. Rev.* **111**, 143 (1958).
- ¹⁶A. Schaefer, H. Schmitt, and A. Dorr, *Ferroelectrics* **69**, 253 (1986).
- ¹⁷M. Zgonik *et al.*, *Phys. Rev. B* **50**, 5941 (1994).
- ¹⁸O. Nakao, K. Tomomatsu, S. Ajimura, A. Kurosaka, and H. Tominaga, *Appl. Phys. Lett.* **61**, 1730 (1992).
- ¹⁹S. Wada *et al.*, *Jpn. J. Appl. Phys., Part 1* **38**, 5505 (1999).
- ²⁰S. E. Park, S. Wada, L. E. Cross, and T. R. Shrout, *J. Appl. Phys.* **86**, 2746 (1999).
- ²¹A. J. Bell, *J. Appl. Phys.* **89**, 3907 (2001).
- ²²O. E. Fesenko and V. S. Popov, *Ferroelectrics* **37**, 729 (1981).
- ²³S. Wada and T. Tsurumi, *Br. Ceram. Trans.* **103**, 93 (2004).
- ²⁴T. Yamada, *J. Appl. Phys.* **43**, 328 (1972).

APPENDIX 13

A random-field model for polarization reversal in $\text{Pb}(\text{Yb}_{1/2}\text{Nb}_{1/2})\text{O}_3\text{-PbTiO}_3$ single crystals

Shujun Zhang,^{a)} Shashank Priya, Eugene Furman, Thomas R. Shrout, and Clive A. Randall

Material Research Institute, MRL Building, Pennsylvania State University, University Park, Pennsylvania 16802-4801

(Received 31 October 2001; accepted for publication 13 February 2002)

Polarization switching and dielectric temperature behavior have been investigated in $0.55\text{Pb}(\text{Yb}_{1/2}\text{Nb}_{1/2})\text{O}_3\text{-}0.45\text{PbTiO}_3$ (PYN-PT) single crystals. These compositions are of interest owing to their unusually high Curie temperature and high coercive fields. The dielectric permittivity was determined as function of temperature and the polarization was measured as a function of applied field for different drive frequencies. Analysis of the experimental results with a random-field model was found to show similar trends to recent reports for the $\text{Pb}(\text{Mg}_{1/3}\text{Nb}_{2/3})\text{O}_3$ relaxor materials. The frequency dispersion of the maximum in dielectric spectra, T_{max} , was also analyzed with the Vogel-Fulcher relation yielding a high freezing temperature of 577 K. Polarization behavior was found to follow a stretched exponential time dependence and a fractal dimension of ~ 2.2 was obtained. It is proposed that the polar cluster state in PYN-PT single crystals do not freeze in random orientations but rather arrange locally in preferred configurations. The fraction of the clusters decreases under increasing external field drive, resulting in the formation of the percolated network at higher fields. © 2002 American Institute of Physics. [DOI: 10.1063/1.1467399]

I. INTRODUCTION

The lead based complex perovskite ferroelectric single crystals are promising candidates for piezoelectric transducers because of their excellent dielectric and piezoelectric properties close to the morphotropic phase boundary (MPB) but with compositions in the rhombohedral phase field.¹⁻⁵ Longitudinal electromechanical coupling (k_{33}) values as high as $\sim 94\%$ and piezoelectric coefficients (d_{33}) ~ 2500 pC/N have been reported for $\langle 001 \rangle$ oriented crystals of $\text{Pb}(\text{Zn}_{1/3}\text{Nb}_{2/3})\text{O}_3\text{-PbTiO}_3$ (PZN-PT)⁶ and $\text{Pb}(\text{Mg}_{1/3}\text{Nb}_{2/3})\text{O}_3\text{-PbTiO}_3$ (PMN-PT),⁷ making these compositions attractive for both actuator and ultrasonic transducer applications. The magnitudes of piezoelectric and electromechanical properties are much greater than those of the conventional $\text{Pb}(\text{Zr},\text{Ti})\text{O}_3$ (PZT) ceramics, which are widely used in commercial piezoelectric devices. The implementation of the PZN-PT and PMN-PT piezocrystals in practical devices may be limited by their low Curie temperature (T_c) (150–170 °C) near the MPB compositions. PZT has a Curie temperature ranging from 200 °C–350 °C depending on its doping, however, at present it is extremely difficult to obtain PZT single crystals large enough to apply to piezoelectric devices.⁸ Naturally, the ideal choice would be a single crystal, which has a high piezoelectric and electromechanical coupling coefficient like that of PZN-PT and PMN-PT and a high T_c similar to that of PZT. The Curie temperature T_c is desired to obtain low temperature dependent properties near room temperature. Substantial efforts have been made to develop ferroelectric single crystals with high T_c and piezoelectric properties. $\text{Pb}(\text{In}_{1/2}\text{Nb}_{1/2})\text{O}_3\text{-PbTiO}_3$ single crystals

were reported to have a T_c of about 260 °C with longitudinal electromechanical coupling coefficient in the rectangular bar mode k'_{33} of about 77%.^{9,10} Recently, the growth and characterization of a new solid solution system based on $\text{Pb}(\text{Yb}_{1/2}\text{Nb}_{1/2})\text{O}_3\text{-PbTiO}_3$ (PYN-PT) has been reported.^{11,12} The T_c near MPB (~ 0.46 PT) in this system is around 337 °C and piezoelectric coefficients as high as 2500 pC/N can be obtained.

In this article, we extend our studies to explain the underlying mechanisms responsible for the observed properties. PYN-PT crystals close to MPB with 45% PT were chosen in this study. Dielectric measurements as a function of temperature for various frequencies shows dispersion around T_c , typically associated with ferroelectric relaxorlike behavior. Consequently, an in-depth study was undertaken to characterize this relaxation behavior. Relaxors are believed to exhibit highly nonlinear properties due to a dynamical microscopic polarization existing above a freezing temperature. However, the polarization can be put in a metastable state through the establishment of a longer range cooperation under the application of an applied electric field.¹³⁻¹⁵ Recently, relaxor behavior has been suggested to be a consequence of quenched random fields due to the defects, chemical inhomogeneous, and ordering, which is frozen-in from the high temperature processing.^{16,17} The concentration of these defects is sufficient to cause breaks in the translational symmetry of the lattice, and thereby limit the development of long-range polar order without the application of an external field to override those internal random fields.¹⁸ The random interaction between the clusters results in polarization freezing and glasslike characteristics on reduction of the thermal energy.^{16,17} Analysis of the excess polarization obtained from the polarization-electric field (P - E) hysteresis loops can be

^{a)}Electronic mail: soz1@psu.edu

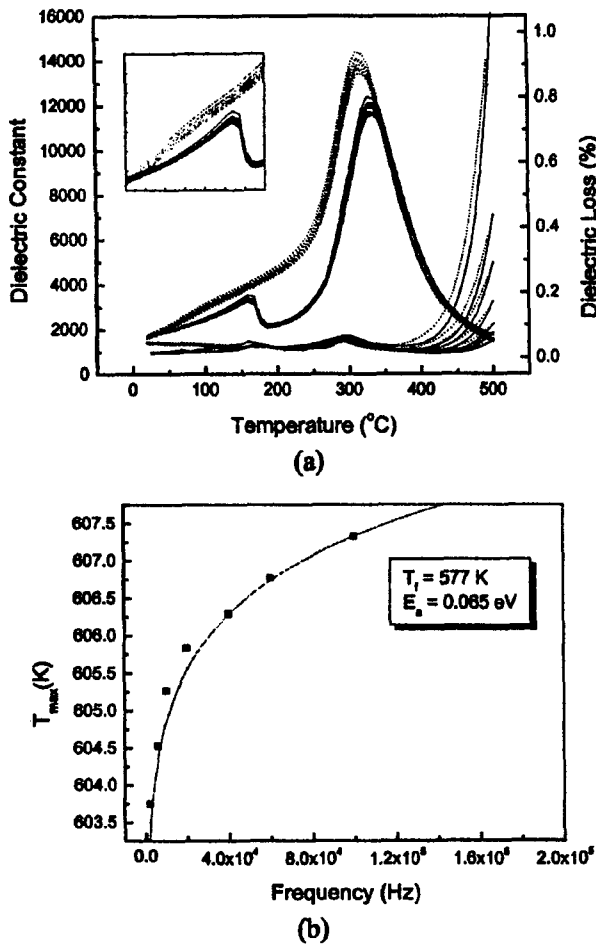


FIG. 1. Determination of the freezing temperature in the system PYN-PT for $x=0.45$. (a) Dielectric constant and dielectric loss as a function of temperature at 2, 6, 10, 20, 40, 60, and 100 kHz with heating (solid line) and cooling (dot line) processes. (b) T_{max} as a function of frequency. The line is analysis of this data with Eq. (1) using the Levenberg-Marquadt nonlinear analysis program.

used to establish the relaxation rates and fractal dimensionality of the polar clusters. It is noteworthy that in an investigation in PZN-PT crystals by Yu and Randall direct evidence of fractal domain behavior was observed under various electrical field applications.¹⁹

The objective of this article is to use techniques that have been applied to PZN-PT and PMN-PT materials to contrast the PYN-PT relaxor under the analysis of random-field models.

II. EXPERIMENT

High quality rhombohedral single crystals of PYN- x PT ($x=0.45$) were grown using the conventional high temperature solution method.¹¹ The samples used in this study were (001) oriented and had a dimension of $2.5 \times 2.5 \times 0.4$ mm³. High temperature dielectric behavior was determined, from room temperature to 500 °C, using a multifrequency LCR meter (HP 4284A). The data was recorded using a General Purpose Interface Bus (GP-IB) interface. Polarization-electric field hysteresis loops at high fields were measured by

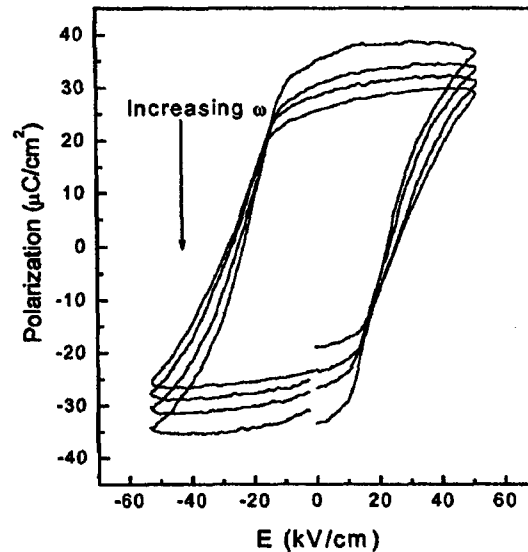


FIG. 2. Polarization-electric field hysteresis loops measured at frequencies 0.1, 1, 10, and 100 Hz, at the maximum applied electric field level of 50 kV/cm.

using a modified Sawyer-Tower circuit driven by a lock-in amplifier (Stanford Research Systems, Model SR830). High electric fields were applied via a Trek 609C-6 high voltage dc amplifier.

III. RESULTS AND DISCUSSION

A. Temperature dependence of dielectric constant

Figure 1(a) shows the dielectric constant and dielectric loss of a poled (001) oriented PYN-0.45PT single crystal as a function of the temperature. The data in the figure is shown for frequencies 2, 6, 10, 20, 40, 60, and 100 kHz with increasing and subsequently decreasing temperature (the dotted line data represents cooling and the solid line data corresponds to the heating). Two peaks are clearly shown in the heating process around ~ 160 (T_r) and ~ 325 °C (T_c). The first dielectric anomaly is believed to result from the breaking of the metastable macrodomain structure and formation of the microdomains on the scale of the local defect structure.²⁰ This transition is irreversible in the absence of an external electric field. This behavior indicates that in the absence of an external electric field, the polar regions are dynamic and contribute to the dielectric relaxation. Correspondingly, the dielectric loss has two peaks with increasing temperature. The dielectric constant in the low temperature region of 25 °C $< T < 100$ °C was found to be independent of the frequency, and the magnitude rises from 1700 to 2400. [This part is enlarged and inserted in Fig. 1(a)]. This shows that temperature dependence of dielectric behavior is relatively low for ferroelectric piezoelectrics, $\partial\epsilon/\partial T=9/\text{°C}$, it is significantly low compared to the MPB composition of 0.7PMN-0.3PT ($\partial\epsilon/\partial T=445/\text{°C}$ in the range of $[25, T_r]$).²¹ Thus, in PYN-0.45PT, we have nearly temperature independent properties in the vicinity of the room temperature. In the temperature range of $T_r < T < T_c$, frequency dependent permittivity becomes evident. On a subsequent cooling process,

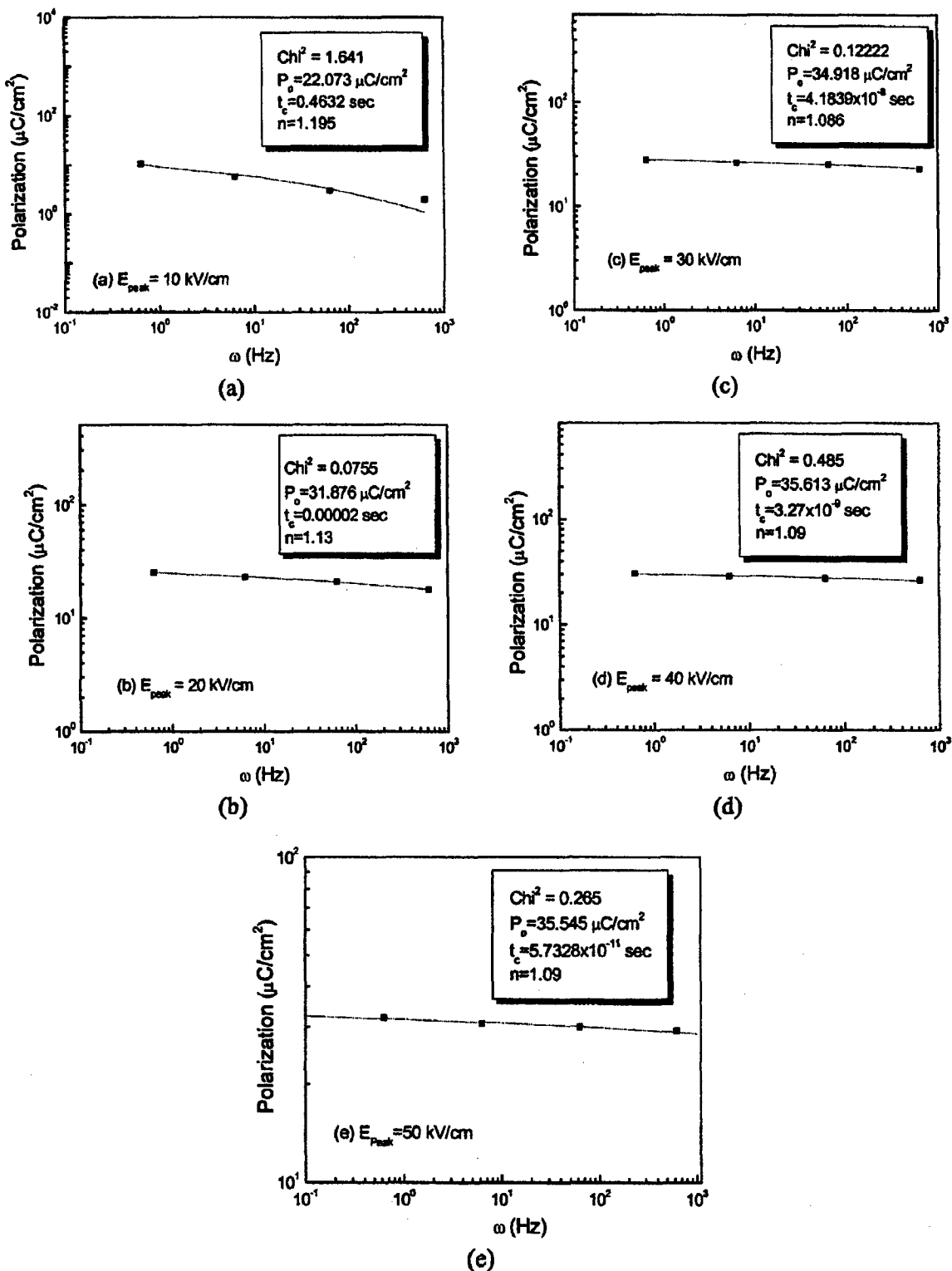


FIG. 3. Plot of remanent polarization determined from the hysteresis loops at various maximum applied electric as a function of the frequency (a) 10, (b) 20, (c) 30, (d) 40, and (e) 50 kV/cm. The data in these figures was analyzed using Eq. (2) and the fit parameters are shown in the plot.

strong ferroelectric relaxor characteristics were observed, with no secondary transformation at lower temperature T_r . A notable feature in Fig. 1(a) is the dispersion in the dielectric constant around T_c and a diffused phase transition similar to

that found in perovskite based relaxor solid solutions. The frequency dependence of the dielectric constant is weak and the shift in the T_c is $\sim 4.5^\circ\text{C}$ for the range of frequencies used in the measurement.

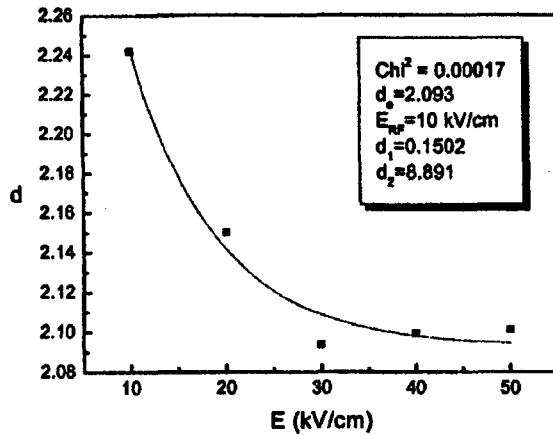


FIG. 4. Plot of fractal dimensionality as a function of the applied electric field.

Previously, it has been established that a relaxor ferroelectric is a polar-glassy system which has thermally activated polarization fluctuations above a static freezing temperature.¹⁶ The Vogel-Fulcher relationship can be used to determine the freezing temperature in ferroelectric relaxor materials.²² Figure 1(b) shows T_{max} as a function of the frequency. The data in this figure was analyzed using the Vogel-Fulcher relation

$$f = f_0 \exp[-E_a/k(T_{max} - T_f)], \quad (1)$$

where T_f is the static freezing temperature, E_a is the activation energy, and f_0 is the preexponential onset frequency (typically $\sim 10^{12}$ Hz), yielding a freezing temperature (T_f) of ~ 577 K and the activation energy E_a of 0.065 eV. The freezing temperature of PYN-0.45PT is much higher than that of the PMN-0.3PT single crystals, typically found to be ~ 370 K.²¹ The close fitting of the data in Fig. 1(b) suggests that the relaxor behavior in the PYN-PT system is analogous to a dipolar glass. Note the ratio T_f/T_{max} can be related to extent of interactions between the clusters.²² Further insight into the existence of the glassy state can be obtained from the time dependence of the polarization, and is discussed below.

B. Dynamics of polarization relaxation

Polarization switching occurs through stabilization and growth of micropolar clusters in the relaxorlike materials.²³ The process follows irreversible thermodynamic models, which takes into account the thermostatic and thermoelastic contributions of the first and second order of lattice defects. In the presence of quenched disorder, the polarization switching process can deviate significantly from equilibrium conditions. The fundamentals of these concepts have been discussed by Imry and Ma.²⁴ Under electrical drive conditions greater than that of the coercive field, a breakdown of the long-range ferroelectric order occurs, which results in the formation of the polar clusters. The functional form which has been used to analyze the relaxation in random-field magnetic and glassy systems is a stretched exponential, so in the ferroelectric case, we expect a similar form, namely:^{17,24,25}

$$P_r(\omega) = P_0 \exp[-(1/\omega t_c)^{1-n}], \quad (2)$$

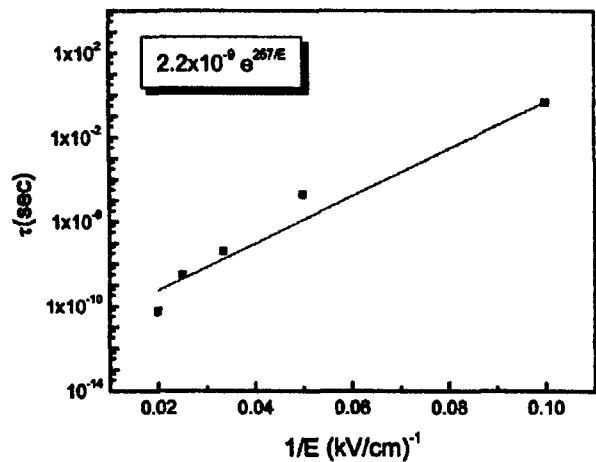


FIG. 5. Plot of the characteristic time constant as a function of the applied electric field.

where P_r is remanent polarization, ω is a drive angular frequency, t_c is a characteristic relaxation time, and n is an exponent. Figure 2 shows typical polarization hysteresis loops of PYN-0.45PT in the $\langle 001 \rangle$ direction, determined at 0.1, 1, 10, and 100 Hz at the maximum electric field level of 50 kV/cm. Similar data was taken for the maximum applied electric field levels of 10, 20, 30, and 40 kV/cm. The remanent polarization determined from the hysteresis loops at various maximum applied electric fields was plotted as function of the frequency and is shown in Figs. 3(a)–3(e). The data was analyzed using Eq. (2) and the fitted parameters are shown in the respective plots. Good correlations between the experimental data and the model can be seen in these figures.

C. Fractal dimensionality

The exponent n in Eq. (2) can be correlated to the dimensionality of the fractal cluster order using the relationship proposed by Huse *et al.*²⁶ as

$$n = (d-2)/(d-1). \quad (3)$$

The value of d calculated using Eq. (3) from the data in Figs. 3(a)–3(e) is ~ 2 and is plotted in Fig. 4 as function of the applied E field. The magnitude of d shows a systematic decrease with the E field. The data in Fig. 4 was fitted using an empirical relation of the form

$$d = d_0 + d_1 \exp[-(E - E_{RF})/d_2], \quad (4)$$

where d_0 is the initial value of d under low level fields, E_{RF} is the random field, d_1 is the exponential amplitude prefactor, and d_2 is the exponential relaxation constant. The analysis yielded values of $d_0 = 2.09$, $E_{RF} = 10$ kV/cm, $d_1 = 0.15$, and $d_2 = 8.89$ kV/cm. The empirical fitting to an exponential decaying function can be interpreted as that fraction of the polar clusters and can be reversed in various external drives. The fractal dimensionality is associated with the growth of the clusters and a network formation of these clusters that can undergo percolation at high fields.

TABLE I. Comparison of the important random-field parameters in PYN-0.45PT to PMN-0.3PT ceramic.

Crystal	n	d	t_0 (s)	E_0 (kV/cm)	E_{RF} (kV/cm)	T_f	d_0	d_1	d_2
PYN-0.45PT (crystal)	1.09 (40 kV/cm)	2.2	2.2×10^{-9}	257	10	577 K	2.09	0.15	8.89
PMN-0.3PT (ceramic) (Ref. 27)	0.1554 (1 kV/cm)	2	2.5×10^{-12}	138	1.61	366.1 K (Ref. 21) (crystal)	2.18	0.0265	0.305

D. Relaxation time constant

A characteristic time constant, determined from the analysis of experimental data shown in Figs. 3(a)–3(e), by using Eq. (2), is shown in Fig. 5. The data was analyzed by using the modified Arrhenius equation given as

$$t_c = t_0 \exp(-E_0/E), \quad (5)$$

where t_0 is the time required for cluster nucleation and E_0 is an activation field. The analysis yielded values of $t_0 \sim 2.2 \times 10^{-9}$ s and an activation field of 257 kV/cm. The value of E_0 is slightly higher than that reported previously by analysis of the frequency dependence of the coercive field. In general, a value for E_0 of ~ 100 kV/cm is obtained, which is approximately half of the magnitude obtained by the analysis of the polarization dependence for $E > E_c$ in the PYN-PT system.

A comparison of the random-field parameters in a PYN-0.45PT single crystal to PMN-0.3PT ceramic²⁷ is given in Table I.

IV. CONCLUSIONS

This article reported the presence of the polar glassy state in high T_c PYN-PT single crystals. Polarization reversal and frequency dependent T_{max} obeys the trends of the random-field model. A correlation between the experimental data and models indicates the presence of a high concentration of quenched disorder in the PYN-0.45PT system. High temperature growth of the crystals followed by quenching results in freezing of the high temperature thermodynamic equilibrium defects. Randomness and disorder are created by mixed interactions and competition leading to cooperative freezing process. At temperatures around T_f , many of these random polar defects arrange themselves in locally correlated clusters and domains, which participate in the switching process as a whole. The results of this article demonstrate the usefulness of the random-field approach in deterministically understanding the relaxation behavior of the high Curie temperature piezocrystals, and indicate the importance to build up a large database across the perovskite relaxors to aid the design of new piezoelectric crystals.

ACKNOWLEDGMENTS

This research was supported by the ONR and DARPA. The authors express their appreciations to Ru Xia for the crystal processing.

- ¹S. E. Park and T. R. Shrout, *J. Mater. Res.* **1**, 20 (1997).
- ²S. E. Park and T. R. Shrout, *Jpn. J. Appl. Phys., Part 1* **36**, 1154 (1997).
- ³T. R. Shrout, Z. P. Change, N. Kim, and S. Markgraf, *Ferroelectr. Lett. Sect. 12*, 63 (1990).
- ⁴S. Shimanuki, S. Saito, and Y. Yamashita, *Jpn. J. Appl. Phys., Part 1* **37**, 3382 (1998).
- ⁵M. Dong and Z.-G. Ye, *J. Cryst. Growth* **209**, 81 (2000).
- ⁶S. E. Park and T. R. Shrout, *J. Appl. Phys.* **82**, 1804 (1997).
- ⁷H. S. Luo, G. S. Xu, and Z. W. Yin, *Jpn. J. Appl. Phys., Part 1* **39**, 5581 (2000).
- ⁸K. Harada, S. Shimanuki, T. Kobayashi, S. Saitoh, and Y. Yamashita, *J. Am. Ceram. Soc.* **81**, 2785 (1998).
- ⁹N. Yasuda, H. Ohwa, M. Kume, and Y. Yamashita, *Jpn. J. Appl. Phys., Part 2* **39**, L66 (2000).
- ¹⁰N. Yasuda, H. Ohwa, M. Kume, and Y. Yamashita, *Jpn. J. Appl. Phys., Part 1* **39**, 5586 (2000).
- ¹¹S. J. Zhang, P. W. Rehrig, C. A. Randall, and T. R. Shrout, *J. Cryst. Growth* **234**, 415 (2002).
- ¹²S. J. Zhang, S. Rhee, C. A. Randall, and T. R. Shrout, *Jpn. J. Appl. Phys., Part 1* **41**, 2A (2002).
- ¹³G. Smolenskii and A. Agronovska, *Sov. Phys. Solid State* **1**, 1429 (1960).
- ¹⁴A. Glass, *J. Appl. Phys.* **40**, 4699 (1969).
- ¹⁵W. Pan, W. Gu, D. Taylor, and L. E. Cross, *Jpn. J. Appl. Phys., Part 1* **28**, 653 (1989).
- ¹⁶D. Viehland, S. Jang, L. E. Cross, and M. Wuttig, *Philos. Mag. B* **64**, 335 (1991).
- ¹⁷D. Viehland, M. Wuttig, and L. E. Cross, *Ferroelectrics* **120**, 71 (1991).
- ¹⁸A. Tan, J. F. Li, and D. Viehland, *Philos. Mag. B* **76**, 59 (1997).
- ¹⁹H. X. Yu and C. A. Randall, *J. Appl. Phys.* **86**, 5733 (1999).
- ²⁰X. Yao, Z. L. Chen, and L. E. Cross, *J. Appl. Phys.* **54**, 3399 (1983).
- ²¹D. Viehland, J. Powers, and L. E. Cross, *Appl. Phys. Lett.* **78**, 3508 (2001).
- ²²D. Viehland, S. Jang, L. E. Cross, and M. Wuttig, *J. Appl. Phys.* **68**, 2916 (1990).
- ²³W. Cao and J. Krumbansl, *Phys. Rev. B* **42**, 4334 (1990).
- ²⁴Y. Imry and S. Ma, *Phys. Rev. Lett.* **35**, 1399 (1975).
- ²⁵W. Kleemann, *Int. J. Mod. Phys.* **7**, 2469 (1993).
- ²⁶D. Huse, C. Henley, and D. Fishere, *Phys. Rev. Lett.* **55**, 2924 (1985).
- ²⁷D. Viehland and Y. H. Chen, *J. Appl. Phys.* **88**, 6696 (2000).